The effect of solids residence time on phosphorus uptake in co-precipitation systems targeting low phosphorus concentrations

by

Daniela Conidi

A thesis
presented to the University of Waterloo
in fulfillment of the
thesis requirement for the degree of
Doctor of Philosophy
in
Civil Engineering

Waterloo, Ontario, Canada, 2015

Author's Declaration

I hereby declare that I am the sole author of this thesis. This is a true copy of the thesis, including any required final revisions, as accepted by my examiners.

I understand that my thesis may be electronically available to the public.

Abstract

Chemical phosphorus (P) removal is generally considered to be necessary when attempting to achieve ultra low P concentrations (i.e. < 50 μg/L) in wastewater treatment. However, the impact of aging of chemical solids (i.e. hydrous ferric oxides (HFO)) and thereby solids residence times (SRT) typical of conventional wastewater treatment processes on P removal is not well understood. This study characterized the uptake of P in co-precipitation systems under varying influent P concentrations and methods of P addition (i.e. steady state versus transient dosing); identified the impact of SRT on P removal, HFO floc structure, equilibrium adsorption of P to HFO and on the dynamics of P removal under steady state and transient conditions; and described the dynamic behaviour of P sorption onto HFO floc by the development of a model.

The study employed lab scale continuous flow sequencing batch reactor (SBR) pilots that received the discharge of a flash mix tank. The pilots were fed with a synthetic natural water and operated over a range of SRTs (i.e. 2.8-26.6 days). Operation at different influent P concentrations and methods of P addition (i.e. steady state vs. transient dosing) was evaluated. Batch sorption testing with solids from the SBRs was also conducted.

Under steady state operating conditions the majority of P removal occurred in the flash tank (94% with 3.4 mg influent P/L; 83% with 6.4 mg influent P/L) with an additional smaller fraction of removal in the SBRs (additional 3.3 – 4.8% removal with 3.4 mg influent P/L; 5.5 - 8.8% with 6.4 mg influent P/L). Soluble P uptake was higher at SRTs ≤ 7.4 days with 3.4 mg influent P/L and SRTs ≤ 14.3 days with 6.4 mg influent P/L. The floc morphology (i.e. open vs. compact floc structure) in the flash solids was found to be different from that of the SBR aged solids using SEM analysis. Particle size distributions were found to be the same in all systems supporting the hypothesis that changes in floc morphology were more responsible for differences in P removal than floc size.

Batch sorption studies indicated that fresh HFO had a higher sorption capacity in comparison to aged (2.8, 7.4, 10.8 and 22.8 day) HFO. P desorption from HFO solids was found to be negligible supporting chemisorption as the mechanism of P adsorption. P adsorption onto HFO solids was determined to be best described by the Freundlich isotherm. An equilibrium model was found to adequately describe P adsorption onto HFO solids of different ages. Modelling showed that fresh HFO contributed more to P sorption than aged HFO in each SBR implying that the fresh flash solids were more responsible for the observed P uptake in the SBRs in comparison to the aged SBR solids.

Transient studies showed that P removal in the SBRs and batch sorption tests was characterized by an initial fast period of removal followed by a period of slower removal until pseudo-equilibrium was reached. A model was developed to describe the dynamic behaviour of P sorption onto three different solid types (i.e. steady state dosed SBR solids, transient dosed SBR solids, and preformed batch solids). Overall, the calibrated model was found to provide a good description of P removal in the SBRs and batch testing. The model was able to reflect the different process conditions (i.e. mixing) in experiments conducted in the SBRs and the batch tests. This was reflected in the estimated values of the rate coefficients obtained from the batch tests and the SBRs. It was found that the same rate coefficient could be used to describe P adsorption onto HFO floc of different ages (i.e. 2.8-26.6 days).

Acknowledgements

I am grateful to the many people who have provided me with guidance and support over the course of my thesis and to those who have positively influence my academic and professional path. I would especially like to thank the following people:

To my supervisor Dr. Wayne Parker for his invaluable support and guidance in the completion of this thesis and during my time as an undergraduate and graduate student. His passion and knowledge with respect to engineering and wastewater research have been a source of inspiration. I am extremely grateful for having had the opportunity to work with him for so many years and for his commitment to my work, his encouragement, his patience, his professional advice and his tireless effort editing my thesis.

To the members of my committee Dr. Glen Daigger, Dr. Peter Huck, Dr. Bill Annable, and Dr. Scott Smith for reviewing my thesis and providing valuable feedback.

To Dr. Peter Dold, Dr. Rich Jones, Mark Fairlamb and Dr. Christopher Bye at EnviroSim for their support and constructive feedback throughout the course of my research. To Dr. Scott Smith for his help, knowledge, and support with analyzing P at ultra low levels, helping me understand the "nitty gritty" chemistry work and in coding Matlab.

To Dr. Peter Seto for allowing me to set up shop at the former Wastewater Technology Centre in Burlington. To Sam Dith, Scott Dunlop, Stephen Lee, Quinton Rochfort, Ruxandra Birsan, and Kyle Waldner for providing tremendous help, knowledge and assistance over the course of my experimental phase. To Jennifer Fu, Kathryn Kerker, Adam Szczerba and Frederick Chu for their assistance in reactor operation, sampling and analysis. To the inorganic lab at Environment Canada for providing analytical services. To the WATLab at the University of Waterloo, especially Dr. Nina Heinig for her assistance in running SEM analyses.

To Dr. Anne-Emmanuelle Stricker who supervised me though two coop work terms during her postdoctoral work giving me my first crash course in wastewater. Anne's passion for research was one of the inspirations for my pursuit of graduate studies. I hold my work terms with her as invaluable experiences.

To my parents, sister and family for their love, patience, understanding and unparalleled support in putting up with me over the course of my thesis. To Sam, Christina, Katie, Marian, Laura, Qirong and Ruxandra for their friendship, moral support and encouragement during this whole process.

Table of Contents

List of Figures

List of Tables

Nomenclature

[ ]	Concentration (mM)
1/n	Freundlich constant
$1/n_1$	Freundlich constant representing High HFO
$1/n_2$	Freundlich constant representing Low HFO
$1/n_3$	Freundlich constant representing Old HFO
ε	Molar absorptivity constant at a given wavelength ($M^{-1}cm^{-1}$)
ℓ	Path length used to measure absorbance (cm)
a	Constant relating to the initial velocity of the reaction (Elovich Equation)
A	Light absorbance
ABD	Area based diameter (μm)
ANOVA	Analysis of variance
ASF	Active site factor
b	Langmuir constant relating to the net enthalpy of adsorption
b_a	Constant relating to the activation energy for adsorption
Bio-P	Biological phosphorus
BOD	Biochemical oxygen demand
c	Concentration (M)
C	Predicted concentration of analyte (mg/L TSS, Fe or TP)
C_{flash}	Measured concentration of analyte in flash tank effluent (mg/L TSS, Fe or TP)
C_s	Concentration of chemical solid/floc (i.e. HFO) (mg/L)
CI	Confidence interval
COD	Chemical oxygen demand
D	Intercept constant representing boundary layer thickness (mg/g)
ESD	Equivalent spherical diameter (μm)
f_1	Fraction of High HFO
f_2	Fraction of Low HFO
f_3	Fraction of Old HFO
Fe	Iron; or iron concentration (mg/L)
G	Velocity gradient/mixing intensity (s^{-1})
HFO	Hydrous ferric oxides

High HFO	Class of HFO containing high specific surface area for sorption
HRT	Hydraulic residence time (hours)
IQR	Interquartile range
j	Time step
k	Rate coefficient (1/time)
k_1	Rate constant of pseudo-first order adsorption ($minutes^{-1}$)
k_2	Rate constant of pseudo-second order adsorption (g/minute.mg)
k_d	Intra-particle diffusion rate constant ($mg/m.minute^{1/2}$)
K	Freundlich constant representing the sorption capacity at a specific solution-phase concentration
K_1	Freundlich constant representing the High HFO
K_2	Freundlich constant representing the Low HFO
K_3	Freundlich constant representing the Old HFO
K_{sp}	Phosphorus capacity switching function constant (mg P/L)
K_{sq}	Adsorptive capacity switching function constant (mg P/mg solids)
Low HFO	Class of HFO containing less accessible binding sites
M_1	Mass of High HFO solids (mg TSS)
M_2	Mass of Low HFO solids (mg TSS)
M_3	Mass of Old HFO solids (mg TSS)
Me	Metal
MLSS	Mixed liquor suspended solids
M_p	Daily solids production (mg)
M_s	Mass of solids in the system (mg)
M_t	Total mass of HFO solids in batch adsorption tests (mg TSS)
n	Inverse of the Freundlich constant 1/n
Old HFO	Class of HFO containing no active surface sites
P	Phosphorus; or soluble P concentration (mg P/L)
P_a	Concentration of adsorbed phosphate (mg P/L)
P_b	Background concentration of soluble P in SBRs (mg P/L)
P_e	Soluble P concentration at equilibrium in batch sorption tests (mg P/L)
P_f	Final soluble P concentration (μg P/L steady state data; mg P/L transient data)

P_{flash}	Soluble P concentration in flash tank effluent (µg P/L steady state data; mg P/L transient data)
P_i	Initial soluble P concentration (µg P/L steady state data; mg P/L transient data)
P_{liquid}	Concentration of P associated with the liquid phase (mg/L)
$P_{liquid,f}$	Final concentration of P in the liquid phase (mg/L)
$P_{liquid,i}$	Initial concentration of P in the liquid phase (mg/L)
P_o	Initial soluble P concentrations in batch sorption tests (mg P/L)
P_r	Soluble P removed per gram HFO solids (µg P/mg HFO)
P_{solid}	Concentration of P associated with the solid phase (mg/L)
$P_{solid,f}$	Final concentration of P associated with the solids (mg/L)
$P_{solid,i}$	Initial concentration of P associated with the solid phase (mg/L)
q	Mass of adsorbate taken up per unit solid mass (mg/mg)
q_e	Amount of adsorption of P onto the HFO at equilibrium (mg P/mg HFO)
$q_{e,exp}$	Experimental qe
$q_{e,cal}$	Calculated qe
q_i	Initial sorbed phase concentration (mg P/mg HFO)
q_{max}	Maximum adsorption capacity (mg P/mg solids)
Q_{feed}	Daily flow of feed from the flash tank into the SBRs (L/d)
RMSE	Root mean square error
r_p	Rate of P removal (mg/L/min)
rpm	Revolutions per minute
SBR	Sequencing batch reactor
SCM	Surface complexation model
SE	Standard error
SEM	Scanning electron microscope
SRT	Solids residence time (days)
SRT_o	Previous days SRT (days)
SS	Steady state
STD	Standard deviation
t	Time (minutes)
TP	Total phosphorus; total phosphorus concentration (mg/L)

TP_{flash}	Total phosphorus concentration in flash tank (mg/L)
Trans	Transient
TSS	Total suspended solids; total suspended solids concentration (mg/L)
V	Volume of SBRs (L)
$V_{flashfeed}$	Volume of feed from the flash tank entering the SBRs (L)
WWTP	Wastewater treatment plant
X_1	Mass of P sorbed to High HFO (mg P)
X_2	Mass of P sorbed to Low HFO (mg P)
X_3	Mass of P sorbed to Old HFO (mg P)
X_t	Total mass of P sorbed (mg P)

CHAPTER 1

1. INTRODUCTION

1.1 Problem Statement

Evidence of nutrient enrichment in lakes, estuaries, rivers and streams has focused federal environmental agencies towards implementing and enforcing enhanced water quality standards. These numerical standards require some wastewater treatment plants (WWTPs) to produce effluent with nutrient concentrations below those typically accepted as the limits of technology (i.e. 10 and 50 ug/L total phosphorus) (Gu et al., 2009; Levesque et al., 2010; and Neethling et al., 2007). In order to reliably achieve low effluent phosphorus (P) concentrations (i.e. < 50 ug/L), chemical P removal through the use of metal salts is usually required (Jenkins and Hermanowicz, 1991; Levesque et al., 2010; Benisch et al., 2013; Johnson et al., 2005; Johnson and Daigger, 2009). Chemical P removal with ferric (Fe) chloride is the topic of this research. The mechanisms of chemical P removal with ferric chloride are mainly characterized by rapid precipitation of hydrous ferric oxides (HFO) occurring simultaneously with co-precipitation, followed by a slower kinetic removal as a result of chemisorption (Szabó et al., 2006). The resulting soluble P concentration has been found to be dependent on the pH, Fe dosing, mixing and aging conditions as well as water chemistry.

A number of models that characterize the interactions between P and metal salts have been reported (Ferguson and King, 1977; Luedecke et al., 1989; Briggs, 1996; WEF, 1998; Smith et al., 2008; and Hauduc et al., 2013). The developed models have improved the ability to predict residual orthophosphate (PO_4^{3-}) concentrations when extremely low P concentrations are targeted. However, they do not address the impacts of aging and solids residence time on removal kinetics. The model limitations stem from the lack of information on the effects of aging of chemical precipitates and the role of solids contact times at solids residence times typical of wastewater solids on P removal (Benisch et al., 2013). In particular there is limited dynamic information related to the impact of aging on the rates at which P adsorbs. There is also limited information on the kinetics of removal.

It was hypothesized that:

- The age of floc present in co-precipitation systems will affect the uptake of PO_4^{3-} since aging of the HFO floc will affect the availability of active sites and hence may affect removal by adsorption mechanisms (Smith et al., 2008).
- The rates of adsorption of PO_4^{3-} to HFO floc may impact the soluble PO_4^{3-} concentration that can be achieved in a system.

The research involved a combination of experimental studies and model development and application that was conducted to test these hypotheses.

1.2 Objectives and Scope

The objective of this research was to enhance modelling of P removal under ultra-low concentrations by addressing transients and aging. This was achieved through the following means:

- Characterizing PO_4^{3-} uptake in co-precipitation systems when extremely low P concentrations (i.e. < 50 μg/L) were targeted.
- Evaluating the impact of SRT on steady state P removal in sequencing batch reactor systems.
- Obtaining insight into the effects of SRT on floc structure.
- Characterizing the impact of SRT on equilibrium adsorption of P to HFO floc.
- Evaluating the impact of SRT on the dynamics of P removal under steady state and transient conditions.
- Proposing a model to describe the overall dynamic behaviour of P sorption onto HFO floc.

This research was carried out using a lab scale continuous flow sequencing batch reactor pilot located at Environment Canada's Wastewater Technology Centre (Burlington, Ontario). The SBRs were fed with a synthetic natural water and operated at different SRTs to span the range of SRTs typically employed for wastewater treatment.

1.3 Significance

The knowledge acquired in this study improves our understanding of the mechanisms responsible for P removal when ultra-low P concentrations are required. The results provide insights into approaches which might be employed to minimize the consumption of chemicals while achieving very low effluent P concentrations. Ultimately, this research will help wastewater treatment plants to reliably produce a higher quality effluent at lower cost. The results include the enhancement of models for predicting the performance of P removal systems particularly in terms of understanding solids aging and dynamics.

1.4 Thesis Structure

This thesis consists of six chapters and five appendices. Chapter 1 briefly introduces chemical P removal, and the hypotheses, objectives and significance of the study. Chapter 2 presents background on chemical P removal including the mechanisms of removal and the existing models that characterize the interactions between P and metal salts for predicting residual P concentrations. Chapter 3 presents the methodology employed and the results of the steady state operation of the SBRs under high and low influent P concentrations characterizing P removal and floc structure. Chapter 4 presents the methodology employed and the results of batch sorption studies characterizing the impact of SRT on phosphate adsorption. A mathematical model is presented in this chapter which describes the sorption behaviour of P onto HFO floc of different ages. Chapter 5 presents the methodology employed and the results of dynamic studies characterizing the time varying responses of chemical P removal under different process conditions (i.e. during the steady state and transient operation of the SBRs and in batch tests with preformed solids). A mathematical model is presented in this chapter which describes the overall dynamic behaviour of P sorption onto HFO flocs. Finally the conclusions and recommendations for future work are presented in Chapter 6.

CHAPTER 2

2. LITERATURE REVIEW

2.1 Phosphorus Occurrence and Regulation

Phosphorus (P) is an essential nutrient for the growth of biological organisms (Metcalf & Eddy, 2003). P is found in nucleic acids (DNA and RNA), phospholipids, and adenosine triphosphate (ATP) and is vital for both cellular energetics and structure (WEF, 1998; Jones, 2002; Vadstein, 2000). P naturally cycles through the environment by biogeochemical interactions with rocks, soils, plants, animals, bacteria, and aqueous environments (ELC, 2002). Excessive P loading as a result of industrialization and commercialization can disturb natural cycling and lead to eutrophication in surface waters. The main sources of P in surface waters are from fertilizer runoff; sewage seepage; commercial and household cleaning products; domestic, municipal and industrial waste discharges; and natural mineral deposits (Metcalf & Eddy, 2003; WEF, 1998; ELC, 2002).

To protect sensitive ecosystems from eutrophication precautions must be taken to control P loadings into surface waters. The allowable concentrations of nutrients in controlled effluent discharges from treatment facilities are determined based on volume of discharge and an assessment of the assimilative capacity of the receiving water. Evidence of nutrient enrichment in lakes, estuaries, rivers and streams is refocusing the wastewater community to produce effluents with ultra low P concentrations.

There has been extensive work conducted in both Canada and the U.S. to ban or reduce P in laundry and dishwasher detergents (DFO, 2010; Washington State Department of Ecology, 2010; OAG, 2007). Federal environmental agencies are also moving towards implementing and enforcing enhanced water quality standards. In Canada, the government has recently established national standards for wastewater treatment: the Wastewater Systems Effluent Regulations (SOR/2012-139) (Minister of Justice, 2012). In the United States, the Environmental Protection Agency (EPA) has been working in collaboration with most state environmental agencies since the late 1990s to develop and adopt numerical nutrient water

quality standards (Levesque et al., 2010). The majority of the regulatory work is focused on areas where extremely low total phosphorus (TP) limits are required. In the US these areas include: Chesapeake Bay, the Everglades, Gulf of Mexico, Pacific Northwest and Puget Sound (WERF, 2008). In Canada nutrient standards are being established in the Lake Simcoe watershed under the Lake Simcoe Protection Act, 2008 (XCG, 2010). Gu et al. (2009), Levesque et al. (2010) and Neethling et al. (2007) report that these numerical standards require some wastewater treatment plants (WWTPs) to produce effluent with nutrient concentrations below those typically accepted as the limits of technology (i.e. 10 and 50 μg/L TP). Examples of these low effluent limits are illustrated in Table 2-1.

Table 2-1: Current Low Effluent TP Limits

Treatment Plant	Location	TP Limit	Reference
Spokane County Regional Water Reclamation Facility	Washington, DC	50 μg/L	(Johnson et al, 2012)
West Camden Sewage Treatment Plant	New South Wales, Australia	40 μg/L	(Takács et al., 2011)
Lakeshore Water Pollution Control Plant	Innisfil, Ontario	< 100 μg/L	(Benisch et al., 2013)
City of Las Vegas' Waster Pollution Control Facility	Las Vegas, NV	9-20 μg/L	(Gu et al., 2009)
City of Coeur D'Alene WWTP	Coeur D'Alene, Idaho	< 50 μg/L	(Falk et al., 2012)

In 2007, the Water Environment Research Foundation (WERF) created the Nutrient Removal Challenge Program which is working to develop the science and technology needed to address the needs of regulators and dischargers facing ultra low limits (Neethling et al., 2010). In order to improve technology for P removal to low levels, it is important for practitioners to know and understand the forms of P that contribute to TP concentrations (Neethling et al., 2007).

2.1.1 Phosphorus Speciation in Aqueous Environments

In aqueous environments P usually exists as orthophosphate, organic phosphorus, or polyphosphates. Orthophosphate occurs as salts and esters of phosphoric acid (e.g. PO_4^{3-}, HPO_4^{2}, $H_2PO_4^{-}$, and H_3PO_4) (Metcalf & Eddy, 2003; WEF, 1998). At equilibrium HPO_4^{2-} and $H_2PO_4^{-}$ are the dominant forms encountered in the circumneutral pH range typical of

wastewater treatment processes. Organic phosphorus is mostly formed through biological processes (Standard Methods, 2005) and represents P included in intracellular molecules and P associated with cell decay and debris (Gu et al., 2009). Some types of organic phosphorus such as pharmaceuticals are man made (Levesque et al., 2010). Polyphosphates are synthetic compounds consisting of condensed orthophosphates (WEF, 1998). Neethling et al. (2008) further speciated P into chemical and adsorbed forms which represent P associated with metal precipitates and metal hydroxides as shown in Table 2-2.

Table 2-2: Phosphorus Species in Water (Neethling et al., 2008)

Category	Species	Solid/ Liquid	Comment
Orthophosphate	PO_4^{3-}, HPO_4^{2-}, $H_2PO_4^-$, H_3PO_4	Liquid	Weak acid, most dominant form, reactive
Polyphosphates/ Condensed phosphate	Pyrophosphate, tripolyphosphate, metaphosphate	Liquid	Complex large molecule. Precipitate in condensed form or hydrolysis to orthophosphate. Hydrolysis rates high in presence of microorganisms (sludge).
Organic phosphorus	Cell material, intracellular phosphate, intracellular granules	Solid or Soluble	Linked to biological growth, enhanced biological phosphorus removal, etc. Phosphorus in organic compounds.
Chemical phosphorus	Phosphorus precipitants, typically Fe, Al, Ca, struvite, etc.	Solid	Particle size important. Reactions slower and could change with time.
Adsorbed phosphorus	Adsorption to sorbent or to metal hydroxides, form complex	Solid	Could be considered a chemical phosphorus species.

2.1.2 Phosphorus Speciation in Analytical Environments

Analytical classifications typically group the various forms of P into soluble, and particulate, as well as in terms of their reactivity to acid and heat (Gu et al., 2009; Neethling et al., 2007). Soluble or filterable P is typically defined as the portion of P that passes through a 0.45 μm filter (WEF, 1998; Standard Methods, 2005). Particulate phosphates are those typically associated with sediments, precipitates, and biological sludges (Standard Methods, 2005). The different forms of P are converted to dissolved orthophosphate through a digestion step and

then analyzed using colorimetric methods. Table 2-3 classifies the fractions of P based on analytical determinations.

Table 2-3: Definition of phosphorus fractions based on standard methods (Gu et al., 2009)

Term	Definition by measurement method
Total phosphorus (TP)	Total digested P without filtration
Total soluble phosphorus (sTP)	Total digested P of filtrate (0.45μm)
Total particulate phosphorus (pTP)	The difference between TP and sTP, pTP=Tp-sTP
Total acid-hydrolyzable phosphorus (tAHP)	Total acid-hydrolyzable P without filtration
Soluble acid-hydrolyzable phosphorus (sAHP)	Acid-hydrolyzable P of filtrate
Particulate acid-hydrolyzable phosphorus (pAHP)	Calculated as pAHP = tAHP - sAHP
Total reactive phosphorus (tRP)	Total reactive P based on colorimetric method without filtration (mostly orthophosphate)
Soluble reactive phosphorus (sRP)	Reactive P of filtrate
Particulate reactive phosphorus (pRP)	Calculated as pRP=tRP-sRP
Total organic phosphorus (tOP)	Calculated as tOP=TP-tAHP
Dissolved organic phosphorus (DOP)	Calculated as DOP=sTP-sAHP
Particulate organic phosphorus (pOP)	Calculated as pOP=tOP-DOP

As summarized in Standard Methods (2005): reactive P refers to phosphates that respond to colorimetric tests without sample hydrolysis or digestion including orthophosphate and small fractions of polyphosphates which are hydrolyzed unavoidably, acid-hydrolyzable P refers to dissolved and particulate polyphosphates and some phosphates from organic compounds that are converted to dissolved orthophosphate though hydrolysis with heated acid, and organic P refers to the phosphates that are converted to orthophosphate by oxidation destruction. Organic P is typically calculated based on other measurements since no clear method of measurement exists (Neethling et al., 2008).

2.1.3 Methods of Phosphorus Analysis

Spectrophotometric techniques are the most often used for orthophosphate analysis. Analysis methods are typically based on combining phosphate samples with ammonium molybdate and then reducing this solution with ascorbic acid in the presence of potassium antimonyl tartrate to

form a blue colour complex (Spivakov et al., 1999). Absorbance of light by the blue complex is measured at 650 or 880 nm using spectroscopy (Standard Methods, 2005). The concentration of P is proportional to the light absorbance (A) of the colour measured as illustrated by Beer's Law (Equation 2-1):

$$A = \varepsilon \ell c \qquad \text{(Equation 2-1)}$$

where ε is the molar absorptivity constant at a given wavelength ($M^{-1}cm^{-1}$), ℓ is the path length used to measure absorbance (cm), and c is concentration (M).

The ascorbic acid method was designed to analyze P concentrations in the range of 0.01 to 6 mg/L (Standard Methods, 2005). In order to achieve low TP in treated effluents, the effluent soluble P concentrations often approach detection limits (0.01 mg P/L or less) (Takács et al., 2006a). Work has only recently been started to test the theory and optimize the methods of low level orthophosphate determination (Levesque et al., 2010; Gilmore, 2009). Theoretically, the standard methods for the determination of orthophosphate can be used with longer path lengths (refer to ℓ in Equation 2-1) for absorbance to measure lower concentrations (Standard Methods, 2005; Gilmore, 2009). Gilmore (2009) optimized standard methods for determination of P for path lengths longer than 1 cm. The ascorbic acid method (Standard Methods 4500-P.E.) was modified for a 10 cm path length to use a colour forming reagent volume 30% of the volume recommended by the Standard Methods (from 1.6 mL to 0.5 mL) and an increased colour development time of 1-3 hours which increases sensitivity and reproducibility (Gilmore, 2009). Eleuterio and Neethling (2009) confirmed the ascorbic method as a reliable technique to measure orthophosphate at low levels.

Issues surround the definition of soluble P since colloidal particles are known to pass through a 0.45µm filter increasing P concentrations and affecting the reproducibility of low level analysis (Neethling et al., 2007). Colloids have also been reported to build up on the surface of the filter decreasing phosphorous concentrations (Gilmore, 2009). Gilmore (2009) developed a filtration protocol after testing the impact of sample volume, filter types, and flow rate on low level P analysis results. The filtration protocol developed with synthetic samples using ultra pure water and pH 4 used a 47 mm Millipore filter, a filter flow rate of 250 ml/hr (since slow rates

highlight colloidal tendencies to associate with filters), and a 10 mL filtrate volume (Gilmore, 2009).

2.2 Phosphorus Removal in Wastewater Treatment Systems

In a wastewater treatment system P exists in many forms. Secretion by cells or cell death and disintegration discharges soluble organic phosphates; particulate organic phosphates are associated with cell debris material and can be precipitated out and removed with the sludge (Levesque et al., 2010; Gu et al., 2011). Organic P can also be broken down into biodegradable and nonbiodegradable fractions (Gu et al., 2011). Soluble biodegradable organic P can be hydrolyzed to orthophosphate during treatment while soluble non-biodegradable organic P will pass through the WWTP becoming the refractory portion in the final effluent (Neethling et al., 2007; Gu et al., 2009). In general, hydrolysis converts particulate P to soluble species (Takács et al., 2006a). Biological synthesis, bio-P uptake and chemical precipitation convert soluble P into particulate forms (Takács et al., 2006a). Since P is not volatile, removal mechanisms aim to convert all soluble and colloidal forms of P to a particulate, settleable form (Takács et al., 2006a) which can be removed by solids-liquid separation. The solid-liquid separation technique becomes an important factor in ensuring that particulate bound P is removed.

Chemical P removal is the most commonly used practice and involves precipitating and/or co-precipitating P with coagulant (typically metal salts). Biological P (Bio-P) removal involves uptake of P by poly-phosphorus accumulating organisms. These removal mechanisms can be incorporated individually, in combination or simultaneously. However, when conventional sedimentation, biological wastewater treatment and/or bio-P processes cannot consistently and reliably reach ultra low effluent P criteria chemical precipitation becomes a necessary addition (Jenkins and Hermanowicz, 1991; Levesque et al., 2010; Benisch et al., 2013; Johnson et al., 2005; Johnson and Daigger, 2009). Chemical P removal is the focus of this research.

Chemical P removal relies on effective coagulation and flocculation processes. A coagulant is added at a well mixed location and acts to destabilize colloidal particles (Metcalf & Eddy, 2003). Coagulation is typically characterized by intense mixing to ensure the chemical is properly distributed within the solution. Coagulation is followed by flocculation which

promotes particle growth or floc formation as a result of particle collision (Metcalf & Eddy, 2003) at slower mixing intensity. The floc formed, as well as the P species associated with the floc, is then removed through solid/liquid separation techniques such as sedimentation or filtration (Metcalf & Eddy, 2003). For conventional activated sludge WEF (1998) reports the P content in suspended solid dry mass as 20-25 mg P/g VSS (2-2.5%). In comparison, for chemical P removal the P content in the suspended solid dry mass varies between 40 and 100 mg P/mg SS (4-10%) (WEF, 1998).

Chemical addition for P removal can be employed in the primary, secondary and tertiary stages of a wastewater treatment plant (Jenkins and Hermanowicz, 1991). The addition of chemicals to raw wastewater in the primary sedimentation process is termed pre-precipitation (Jenkins and Hermanowicz, 1991). Addition of chemical to the secondary process is termed simultaneous or co-precipitation (Jenkins and Hermanowicz, 1991; Metcalf & Eddy, 2003). Chemicals can be added at various locations including the primary effluent, the aeration basin, or the effluent from the aeration basin before secondary sedimentation (Jenkins and Hermanowicz, 1991). Addition of chemicals to tertiary treatment processes is termed post-precipitation (Jenkins and Hermanowicz, 1991). Multiple dosing locations can be employed with combined advantages but slightly increased cost (Jenkins and Hermanowicz, 1991). Although chemical P removal is an appealing process to use due to its ease of operation and implementation, the drawbacks include increased sludge production and operational and maintenance costs (WEF, 1998). Table 2-4 summarizes observations associated with dosing at the various locations.

Calcium (Ca(II)), aluminum (Al(III)) and iron (either Fe(III) or Fe(II)) are the most commonly employed coagulants (WEF, 1998; Metcalf & Eddy, 2003). Aluminum and iron salts include alum ($Al_2(SO_4)_{3.18}H_2O$), sodium aluminate ($NaAlO_2$), ferric chloride ($FeCl_3$), ferric sulfate ($Fe_2(SO_4)_3$), ferrous chloride ($FeCl_2$), and ferrous sulfate ($FeSO_4$), respectively (Jenkins and Hermanowicz, 1991). Iron in the ferrous form is available as pickle liquor, a byproduct from steel manufacturing, which is oxidized to ferric iron (Jenkins and Hermanowicz, 1991). Fe(III) formed from the oxidation of Fe(II) has been reported to be a more efficient scavenger for phosphate than Fe(III) addition (Jenkins, 1971). Szabó et al. (2008) reported that Al(III) and

Fe(III) containing coagulants had similar efficiencies (on a molar basis) for phosphate removal in model and real wastewaters.

Table 2-4: Significance of dosing location (adapted from Metcalf & Eddy, 2003; Jenkins and Hermanowicz, 1991; Jenkins, 1971)

Process	Result
Pre-precipitation (Primary)	Precipitates removed along with primary sludge Enhances BOD and TSS removal efficiency Employs efficient chemical use Reduces P loadings on downstream processes May require addition of polymer to aid in flocculation
Simultaneous/ Co-precipitation (Secondary)	P involved in precipitation, adsorption, exchange, and agglomeration and removed along with sludge Less efficient chemical use Creates additional inert solids MLSS Phosphate carryover in effluent TSS Improved settling characteristics of activated sludge Lower effluent BOD
Post-precipitation (Tertiary)	Precipitates removed by additional solid separation techniques i.e. filtration Can meet stringent standards Significant increased cost

Calcium is typically added in the form of lime ($Ca(OH)_2$) (Metcalf & Eddy 2003). Lime reacts with the natural bicarbonate alkalinity to precipitate $CaCO_3$ and therefore the quantity required for P removal is dependent on the alkalinity of the wastewater (Metcalf & Eddy, 2003). The pH is increased to a value ≥10 for calcium to react to precipitate phosphate and therefore this method is not used as a simultaneous process (Jenkins and Hermanowicz, 1991; WEF, 1998). Due to the operational difficulty in handling lime, the increase in the mass of sludge produced compared with metal salts, the slow growth of calcium phosphate solids, lime is not used as frequently as the other coagulants (Jenkins and Hermanowicz, 1991; WEF, 1998; Jenkins, 1971).

Chemical selection is based on various factors including cost, influent P levels, wastewater suspended solids, alkalinity consumption, quantities of sludge generated and sludge handling

facilities and disposal methods, safety, availability, reliability, and compatibility with other treatment processes (Jenkins and Hermanowicz, 1991; Metcalf & Eddy, 2003). Precipitation with ferric chloride is the focus of this research.

2.3 Mechanisms of Chemical P Removal

Understanding and modelling the mechanisms involved in attaining extremely low P concentrations with iron has been the focus of a number of reports (Smith et al., 2008a; Szabó et al., 2008; Newcombe et al., 2008b; Takács et al., 2011; Weng et al., 2012; Mao et al., 2012; Hauduc et al., 2013). However as described by Takács et al. (2011) the mechanisms of P and ferric interaction are still not fully understood and this can result in inefficient design (i.e. single-point dosage, low mixing, inefficient flocculation) and increased costs (i.e. chemical overdose, excess sludge production, uncertainty of existing P removal capacity before a shock load event, suboptimal dosing strategy). A detailed understanding of the mechanisms of P removal and models describing chemical interactions are required to effectively design P removal systems.

Szabó et al., (2006) proposed the mechanisms of chemical P removal as co-precipitation and adsorption. The addition of ferric salts to wastewater results in the formation and rapid precipitation of HFO floc (Smith et al., 2008a). When PO_4^{3-} is present it will initially co-precipitate during the rapid HFO precipitation while subsequent uptake is slower and due to adsorption/complexation reactions on the surface of the HFO floc (Smith et al., 2008a; Szabó et al., 2008). These complexation reactions are a result of iron and P sharing an oxygen atom (Smith et al., 2008a) as shown in Equation (2-2):

$$\equiv FeOOH(s) + HOPO_3(aq) = \equiv FeOOPO_3 + H_2O \qquad \text{(Equation 2-2)}$$

The exact reaction depends on the number of iron atoms sharing each oxygen atom (Smith et al., 2008a) as Geelhoed et al. (1997) indicated that oxygen surface groups may be coordinated with one, two or three Fe atoms. The availability of reactive oxygen atoms or “surface sites” is dependent on pH, mixing and aging.

The majority of P removal occurs during the initial fast reaction under sufficient mixing conditions (classified as instantaneous “equilibrium” removal); however the slower long term

removal (classified as slow "kinetic" removal) has been reported to be significant in achieving low effluent P concentrations (Szabó et al., 2006; Szabó et al., 2008). These rates of removal can influence coagulant dosing as it was found that the same residual P concentration (1.8 mg/L) was reached with a Fe:P molar ratio of 1.0 after 10 minutes and with a Fe:P molar ratio of 0.7 after 30 minutes (Szabó et al., 2008).

Continuous flow experiments by Szabó et al. (2008) verified the benefits of maintaining chemical floc in contact with the process flow to achieve additional P removal. The results showed that systems with longer solids residence time (SRT) and hydraulic residence time (HRT) could provide more efficient P removal than those with short SRT in cases of similar mixing. This phenomenon was reported to result from longer contact time between phosphate ions and metal hydroxide particles which can partially mitigate the effect of inefficient mixing in simultaneous P removal systems (Szabó et al., 2008).

The results of Szabó et al. (2008) can help explain trends in removal that have been observed when different dosing locations in the treatment process are employed. For pre and post precipitation processes that have short HRTs, co-precipitation was identified as the dominant removal mechanism. In these situations, mixing efficiency is more important in ensuring many opportunities for collisions between metal and phosphate ions (Szabó et al., 2008) and hence good removal. However, for simultaneous precipitation, the efficiency of co-precipitation is lower since there is less intensive mixing. Significant adsorption can take place due to the SRT of the system (Szabó et al., 2008). Increased contact time can also be achieved by recycling solids through the system (Szabó et al., 2008).

2.4 Factors Influencing Chemical P Removal Mechanisms

As mentioned previously, various factors can influence the residual P concentration achievable during chemical precipitation. These factors include: initial P concentration; metal dose and type; wastewater composition (including ion composition and organic content); pH; alkalinity; the identity, stability, and growth kinetics of inorganic precipitates (including reaction time); temperature and hydrodynamic regime (mixing) during precipitation; age of flocs; and solid separation (Jenkins et al., 1971; Jenkins and Hermanowicz, 1991; Szabó et al., 2008; Weng et

al., 2012). The effects of pH, dose, mixing, wastewater composition, aging, and removal kinetics are discussed below.

2.4.1 Effects of pH

The reactions of phosphate and the metals that are typically employed for phosphate removal have been found to be pH dependent. pH dependence in surface complexation reactions arises as a result of proton competition for surface oxygen and phosphate oxygen (Smith et al., 2008a). Several studies (Mao et al., 2012; Caravelli et al., 2012; Caravelli et al., 2010; Smith et al., 2008a; Smith et al., 2008b; Szabó et al., 2008; WEF, 1998; Gillberg et al., 1996) outline the effect of pH on P removal. P removal is reported to be limited at very low and very high pH values. At low pH (< 4), precipitation of metal hydroxides is limited (Szabó et al., 2008; Caravelli et al., 2010) and mostly soluble P complexes form (Szabó et al., 2008). At high pH (7-10) the surface of the metal hydroxide is mostly negatively charged and soluble iron hydroxides start to form (NIST, 2001). At pH greater than 10, phosphate forms precipitates with magnesium and calcium ions (Szabó et al., 2008).

It is known that co-precipitation and adsorption of phosphate ions on ferric hydroxide flocs occurs around neutral pH values (Pierri et al., 2000). However, the extent of adsorption is reduced with increasing pH as a result of competition between hydroxyl and phosphate ions for iron (III) ions (Lijklema, 1980). Mao et al. (2012) also observed lower P removal by HFO with increasing pH. The optimal pH range for phosphate removal was reported by Smith et al. (2008b) to be between 4 and 6 with moderate removal between pH 8 and 9. Szabó et al. (2008) reported the highest efficiency to be between pH 5.5 and 7. Caravelli et al. (2012) confirmed this range by reporting maximum efficiency at pH values between 5 and 7 (>98%) and reported lower efficiency at pH 8 (95%). Earlier studies by Caravelli et al. (2010) found that the efficiency of P precipitation in the presence of biomass was similar for pH values between 5 and 8 (98%) and was less effective at pH 9. Based on the literature findings there is no general consensus for the optimal pH range for removal. However, in the circumneutral pH range typical for wastewater treatment it is assumed that effective removal is provided.

2.4.2 Effects of Coagulant Dose

In practice, metal dosages are generally established on the basis of bench-scale and full-scale testing since existing models do not take into account competing reactions (Metcalf & Eddy, 2003). When low residual P concentrations (<0.1 mg P/L) are desired, the literature indicates that metal (Me) doses need to exceed the stoichiometric 1 mole Me/mole P ratio (Szabó et al., 2008). With metal doses above 1.5 to 2.0 of the initial P concentration (i.e. Me_{dose}/P_{ini} >1.5-2.0) (with initial soluble P concentrations between 0.5 and 6 mg/L) experiments by Szabó et al. (2008) were able to achieve an 80-98% soluble P removal efficiency. Systems with higher SRTs require increased iron doses (Johnson et al., 2012). A 10 to 12 day SRT system required a dose of 2 moles Fe/mol influent P to reach 50 μg/L effluent TP while at a 10 to 18 day SRT a dose of 2.8 moles Fe/mol influent P (almost 50% increase) was required (Johnson et al., 2012).

Although the concentrations of residual soluble PO_4^{3-} decrease with increased metal dose, higher coagulant doses have diminishing returns in terms of the concentration of P removed (Szabó et al., 2008). At higher iron concentrations, iron particles are suspected to interact with each other instead of with phosphate molecules (Smith et al., 2008a). The high iron dosing experiments carried out by Smith et al. (2008a) were conducted with molar doses up to 100 moles Fe/mole P. Wastewater treatment plants typically employ doses that are only two to four times the stoichiometric ratio when low level effluent P is targeted (Takács et al., 2006a). Therefore, in the range of doses employed in practice the effects of high iron doses should not be seen.

Takács et al. (2011) and Johnson et al. (2012) reported that optimizing the initial mixing intensity upon metal salt addition and the contact time provided after the initial rapid mixing can greatly reduce the amount of metal salt required for P removal. Multipoint dosing can also minimize dose requirements since the metal salts have multiple stages of contact with P (Johnson et al., 2012; Benisch et al., 2013). Benisch et al. (2013) report that dosing ratios can be misleading when examining total plant performance since mixing, aging and contact time affect iron efficiency.

2.4.3 Effects of Mixing

Mixing is a key factor in the coagulation and flocculation processes. Many studies have shown the importance of providing sufficient mixing for efficient P removal (Lijklema, 1980; Sagberg et al., 2006; Szabó et al., 2008, Smith et al., 2008a; Takács et al., 2011; Johnson et al., 2012). Szabó et al. (2008) conducted experiments with pre-polymerized metal salts instead of freshly formed salts to simulate situations with insufficient mixing where metal hydroxides will form in the absence of P. Removal with pre-polymerized salts was found to be less efficient thereby indicating the importance of rapid mixing to ensuring a high probability of phosphate ions contacting with ferric ions (Szabó et al., 2008). Similar experiments were conducted by Lijklema (1980) on the effects of the reversal of reagent addition on P adsorption. It was found that P adsorption was higher in experiments where the coagulant was added to a P solution and lower when P was added to freshly formed hydroxide. The less efficient adsorption was attributed to the formation of polymers resulting in a reduced number of singly coordinated hydroxyl groups (Lijklema, 1980). Therefore, sufficient mixing provides a higher probability for contact between P molecules and HFO floc attributing to increased co-precipitation and adsorption.

Szabó et al. (2008) characterized P removal efficiency as a function of mixing intensity. Mixing intensity was expressed in terms of revolutions per minute (rpm) and a velocity gradient (G). Mixing with a G value of 425 s^{-1} (350 rpm) was found to provide close to 90% P removal within 10-20 minutes, while coagulant addition during low mixing intensity (20 rpm, G=6 s^{-1}) impaired removal (Szabó et al., 2008). Achieving a G value of 425 s^{-1} in a wastewater treatment process is typically not desired since the high shear will break apart flocs. However, treatment plants that have been recently designed and upgraded to meet ultra low TP limits including the Spokane County Regional Water Reclamation Facility (Washington, USA) and the West Camden Sewage Treatment Plant (New South Wales, Australia) have been able to innovatively integrate high mixing intensities to optimize removal (Johnson et al., 2012; Takács et al., 2011). The Spokane County Facility uses a primary rapid mixer (G value of 400 s^{-1}) upstream of the aerated grit basin and a rapid mix tank (400 s^{-1} G) prior to the membrane system to provide the necessary mixing and contact time (Johnson et al., 2012). The West Camden Facility uses a high shear mixing box prior to tertiary clarifiers (Takács et al., 2011).

In addition to the reduction in chemical use provided by the above mixing designs additional reduction in chemical requirements was achieved by recycling metal hydroxide floc to the biological treatment process.

2.4.4 Effects of Recycling and Aging

In activated sludge processes, liquid/solid separation is typically achieved by gravity settling, filtration, or floatation (Metcalf & Eddy, 2003). The resulting solids stream is either returned to the front of the biological treatment process or further treated through sludge handling techniques for ultimate reuse or disposal. Recycling solids through the biological treatment process provides additional solids retention time allowing for further interaction between the liquid and solid phases. Jenkins et al. (1971) recognized that it is possible to recycle precipitated solids in the treatment process to achieve increased phosphate removal. Recycling tertiary solids has been found to enhance P removal and decrease metal dosing requirements (Takács et al., 2006b; Newcombe et al., 2008a; Takács et al., 2011; Falk et al., 2012; Johnson et al., 2012).

Based on the work of Smith et al. (2008a) and Szabó et al. (2008) recycling solids in the treatment process and thus aging these solids is believed to influence the long term slow P removal reactions or adsorption mechanisms. When metal hydroxyl flocs are recycled to the head of a treatment process the time in which the precipitates remain in contact with P (contact time) is equivalent to the solids retention time or the age of solids in the process (Johnson et al., 2012). This process of aging is expected to change the morphology of the precipitates i.e. size and structure. The transition from amorphous hydroxide floc to crystalline structures with floc aging is expected to impact on phosphate adsorption. According to Dzombak and Morel (1990) the chemical and physical properties of HFO aged less than 24 hours are characterized by higher surface area and higher levels of cation and anion adsorption while aging decreases adsorptive capacity.

Smith et al. (2008a) conducted experiments (using electron microscope images) and dye adsorption techniques to determine the effects of aging on the availability of surface sites in HFO floc. Experiments were conducted with fresh, 4 day old and 2 year old HFO. Surface sites

were determined to be readily available in fresh HFO since their structure is very open (leading to increased removal); however as HFOs age, the structure became larger and denser limiting the surface area for binding and decreasing the number of active sites. Reduced P removal as a result of aging was also reported by Mao et al., (2012), Szabó et al., (2008) and Lijklema (1980). Freshly formed HFO (aged 1 minute) were reported to achieve approximately 60% P removal while HFO aged 30 minutes before coming in contact with P only removed 30-35% of the original P (Szabó et al., 2008). Mao et al. (2012) studied HFO that was aged 1 minute, 8.5 hours and 24 hours while Lijklema (1980) studied HFO aged 1 hour and 24 hours. The extent of aging studied was limited to time frames which are not reflective of typical solid residence times in a wastewater treatment system. Further research is required to determine the influence of typical SRTs on chemical P removal.

Kang et al. (2003) compared the use of amorphous (ferrihydrite) versus crystalline (goethite and hematite) iron oxide particles as adsorbents for P removal from secondary wastewater effluents (surface areas: 200-300 m^2/g (ferrihydrite), 20 m^2/g (goethite), and 20-25 m^2/g (hematite)). The results showed greater P removal using ferrihydrite followed by smaller removals using goethite and then hematite. Particle size analysis indicated that the three particle types had almost the same size distribution with an average diameter of 3.5μm (Kang et al., 2003). However SEM analysis indicated that the structure of the particles differed suggesting that the surface structure related to morphology was more responsible for P removal than particle size (Kang et al., 2003). Hence it would appear that the impact of solids morphology cannot be ignored when studying the impacts of solids age on adsorption.

The observation of enhanced P removal via recycling and aging (Szabó et al., 2008) contradicts the results that aging reduces active surface sites and limits P removal (Smith et al., 2008a). It is hypothesized that not all of the solids inventory which is created by iron addition is saturated with respect to P. Hence, in real wastewater systems that are transient in nature, there is additional sorption capacity available to take up P during periods of high P loading. Further research is required to determine to what extent aging affects adsorption mechanisms.

2.4.5 Effects of Water Chemistry

Most fundamental studies on chemical P removal have employed simple water matrices (i.e. hydrogen (H), iron (Fe) and P). In order to improve the ability of models to predict chemical phosphorus removal in wastewater matrices, an understanding of the effects of more complex water chemistry is required. Wastewater constituents such as alkalinity, soluble and total COD and total suspended solids (TSS) concentrations, and the presence of cation species have all been reported to influence chemical P removal. The extent of their influence is described below.

2.4.5.1 Alkalinity

Alkalinity represents the pH buffering capacity of a wastewater and in natural waters is typically a function of the carbonate, bicarbonate, and hydroxide concentrations (Standard Methods, 2005). Szabó et al., (2008) conducted jar test experiments in the same pH range (without pH control) with alkalinities in the range of 0-600 mg $CaCO_3$/L. Higher alkalinity resulted in slightly higher residual soluble P concentrations; however, this phenomenon could not be explained. It was hypothesized that the formation of metal hydroxides occurs more quickly in higher alkalinity waters because the hydrogen ion capturing capacity is higher creating a kinetic advantage for fast precipitation of metal hydroxides and a lower probability for co-precipitation of phosphate and metal hydroxides (Szabó et al., 2008). It was also hypothesized that competition could exist between the bicarbonate (HCO_3^-) ions and phosphate (HPO_4^{2-}) ions for active sites (Szabó et al., 2008). These results contradicted those of Newcombe et al. (2008b) and Kang et al. (2003) where changes in alkalinity (i.e. from 0-350 mg/L and 0-400 mg/L as $CaCO_3$, respectively) had a minimal effect on P removal. Further research on the effect of alkalinity on chemical P removal is required.

2.4.5.2 Organics, Biomass and Total Suspended Solids

The presence of organic matter has been shown to decrease chemical P removal (Szabó et al., 2008; Mao et al., 2012; Weng et al., 2013). Experiments by Mao et al. (2012) found that the presence of citrate (50, 100, 200uM) reduced P adsorption onto fresh HFO. Through modeling and experiments, Weng et al. (2013) showed that an increase of dissolved organic carbon from 0.5 to 50 mg/L lead to a greater than 50% decrease of P adsorption onto crystalline iron oxides

under normal soil conditions. In wastewater treatment systems, organic matter is indirectly measured by the chemical oxygen demand (COD) concentration while total suspended solids (TSS) represents the amount of suspended inorganic and organic compounds (Metcalf & Eddy 2003). Szabó et al. (2008) found that increasing COD and TSS concentrations led to less efficient chemical P removal. The mechanism responsible for decreased removal was hypothesized to be due to carboxylic and phenolic groups on the organic matter competing with phosphate for binding sites on the surface of the metal hydroxides (Szabó et al., 2008). The individual effects of COD and TSS could not be determined as high COD concentrations occur with higher TSS concentrations in wastewater systems.

Caravelli et al. (2012) studied the effect of biomass concentration (3.0 ± 0.3 gTSS/L, volatile fraction 0.86) on chemical P removal. The presence of biomass was found to not significantly affect removal for pH values between 5 and 6, however for higher pH values (7-8) the presence of biomass significantly ($p<0.05$) improved P removal. Higher removal was attributed to sweep flocculation favoring the retention of phosphate anions under the alkaline conditions tested (Caravelli et al., 2012). Despite biomass being composed of organic compounds and suspended solids the improvement in removal was attributed to the floc properties. Further research is required to determine if biomass concentrations reduces P removal due to competition mechanisms.

2.4.5.3 Water Hardness

Water hardness is associated with the presence of Mg^{2+} and Ca^{2+} ions in water. Gilmore (2009) conducted experiments to compare the effect of hard and soft water (presence of calcium and magnesium) on P removal. Experiments performed in hard water reached lower residual PO_4^{3-} concentrations than experiments in soft water and hence it was concluded that calcium and magnesium ions aid in the removal process. Differences in residual P due to water hardness were more prominent after a few hours of mixing indicating that the effect of Ca^{2+} and Mg^{2+} ions was more significant for adsorption processes than co-precipitation process (Gilmore, 2009). Weng et al. (2013) found that the presence of Ca^{2+} enhanced P adsorption at pH > 5 while the effect of Mg^{2+} was insignificant. The addition of Ca^{2+} to experiments by Kang et al. (2003) exploring P removal with iron oxides in secondary effluent did not improve removal. It

was hypothesized that Ca^{2+} interacted with organic matter present in the secondary effluent (Kang et al., 2003).

There is relatively little reported research on the interactions of Ca^{2+} and Mg^{2+} with HFO during chemical phosphorus removal; however interactions between Ca^{2+}, Mg^{2+} and PO_4^{3-} are better documented. P is known to interact with cations to form mixed cation phosphates (i.e. magnesium (Mg^{2+}), calcium (Ca^{2+}), iron, or aluminum phosphates, or hydroxyphosphates) (Smith et al., 2008a). Mg^{2+} forms slightly stronger complexes than Ca^{2+} while complexes of Al(III) and Fe(III) are much stronger (Jenkins et al., 1971). Interaction with these metal ions and cations are mostly a function of pH. P forms dissolved complexes with Ca^{2+} and Mg^{2+} in the alkaline pH region thereby increasing phosphate solubility (Jenkins et al., 1971). Jenkins et al. (1971) showed that for a $Ca\text{-}PO_4\text{-}CO_3\text{-}H^+\text{-}H_2O$ system precipitation of calcium carbonate (calcite) competed with calcium phosphate (hydroxyapatite) precipitation between pH 9 and 10.5, but hydroxyapatite precipitation by itself was responsible for low P residuals between pH 7.5 and 8.5 and above pH 10.5. The presence of Mg^{2+} effects Ca^{2+} interactions with P causing precipitation of beta-tricalcium phosphate rather than apatite and the precipitation of a magnesium calcium carbonate rather than calcite (Jenkins et al., 1971). This increases P solubility at pH values below 9, but decreases solubility at higher pH values (Jenkins et al., 1971). At pH values of 10.5 or higher, $Mg(OH)_2$ precipitates (Jenkins et al., 1971). In general, research is still needed to understand chemical P removal under more complex water matrices and with interactions of other anions and cations.

2.5 Modelling Chemical P Removal

Several models have been developed to characterize the interactions between P and metal salts. The models by Ferguson and King (1977), Luedecke et al. (1989), Briggs (1996), WEF (1998), Smith et al. (2008a) and Hauduc et al. (2013) are summarized in Table 2-5. Table 2-5 also summarizes the existing model used in Envirosim's simulation software BioWin for predicting effluent P concentrations.

Table 2-5: Summary of Chemical Precipitation Models

Description	Assumptions	Modelling Process	Limitations
Ferguson and King (1977) Type: Empirical Coagulant: Aluminum Removal Mechanisms: Co-precipitation (Dosing into secondary effluent)	Steady-state (i.e. no changes in concentration with respect to time) Instantaneous chemical reactions Complete solids separation Aluminum phosphate ($Al_{1.4}PO_4(OH)_{1.2}(s)$) precipitates before aluminum hydroxide The molar ratio of Al:P in the precipitate is constant at all pH values Mass balances and chemical equilibria can be applied Considers soluble forms of aluminum phosphate and aluminum hydroxide to bring residual concentrations into good agreement with jar test data from engineering literature (Briggs, 1996)	The final pH of the wastewater is predicted based on initial pH, chemical dose and buffer capacity/alkalinity. Precipitation calculations are divided into three regions: Zone I: Al:P < 1.4 Removal is determined stoichiometrically until a residual of 1mg P/L (pH between 5.2 and 6.9). Zone II: Al:P ≈ 1.4 Removal is less than that predicted by stoichiometry, residuals are based on aluminum phosphate solubility (minimum residual P = 10^{-6}M at pH 5.2-6.0). Zone III: Al:P > 1.4 Both aluminum phosphate and aluminum hydroxide precipitate, residuals are based on assuming equilibria between both solids and the solution for a given pH. Any further increase in aluminum dose only changes pH and does not decrease P residual. The phosphate residual for Zone III is a boundary plotted on a concentration versus pH diagram.	Based on the solubility equilibria of a fictitious precipitate i.e. $Al_{1.4}PO_4(OH)_{1.2}(s)$ Does not account for total P or removal of precipitated solids only describes ortho-P precipitation Solubility products are empirically derived
Luedecke et al., (1989) Type: Empirical Coagulant: Ferric	Steady-state $Fe_{2.5}PO_4(OH)_{4.5}$ is the stoichiometry for the ferric phosphate precipitate Mass balances and chemical equilibria can be applied	Calculations are divided into four regions: 1. No precipitation Doses are below the calculated minimum required to start precipitating ferric phosphate precipitate 2. $Fe_{2.5}PO_4(OH)_{4.5}$ (s) precipitation Residuals are based on mass balances for iron and phosphorus and equilibrium between the iron phosphorus precipitate and the solution. 3. FeOOH(s) precipitation	Model was established with phosphate removal objectives of 80% targeting a 2 mg/L effluent concentration (Jenkins, 1971) Based on empirically derived solubility products

Luedecke et al., (1989) (continued) Removal Mechanisms: Simultaneous precipitation Adsorption		Occurs when the initial P concentration is less than the equilibrium P concentration when both solids are present, and the iron dose is greater than equilibrium 4. co-precipitation of $Fe_{2.5}PO_4(OH)_{4.5}$ (s) and FeOOH(s) Residuals are calculated assuming equilibrium between both solids and the solution at given pH. Any increase or decrease in dose results only in a change in the concentration of the iron precipitate. Once the amount of precipitate is determined the P equilibrium concentration is adjusted for adsorbed P. Concentration of adsorbed phosphate is a function of an adsorption coefficient, and the total amount of adsorbent which is equal to the sum of both precipitates adjusted for the number of available OH groups	Based on solubility equilibria of a fictitious precipitate The adsorption coefficient is adjusted to each experimental condition in a broad range indicating that the adsorption process is not described correctly Hauduc et al. (2013).
Briggs (1996) Type: Empirical/theoretical Coagulant: Ferric and aluminum Removal Mechanisms: Co-precipitation (dosing into secondary effluent) Dissociation Hydrolysis Adsorption Biological nutrient requirements	Dynamic system behaviour (i.e. accounts for variability in concentration with respect to time) Equilibrium attained instantaneously for precipitation See assumptions associated with Ferguson and King (1977) and Luedeke et al (1989).	Considers reactions at the point of metal addition, and rate processes within the aeration tank. Precipitation reactions developed on principles of Ferguson and King (1977) and Luedeke et al. (1989) Precipitates behave as inert solids in the aeration tank and dissociate/precipitate when soluble concentrations are reduced below or increase above minimum equilibrium concentrations (<0.3-0.5mg/L) respectively. The resultant increase/decrease in concentration is determined stoichiometrically. The model accounts for solubilization of particulate biodegradable organic P into soluble biodegradable organic P which in turn is hydrolyzed into ortho-P. Adsorption of P is modeled based on the Elovich equation but with incorporation of switching functions for the phosphorus residual and maximum adsorption capacity. Adsorbed P is also released during dissociation.	Inability to simulate effluent solids concentrations can impact effluent P concentrations See limitations associated with Ferguson and King (1977) and Luedeke et al. (1989).

WEF Model (1998) Type: Empirical Coagulant: Ferric coagulant Removal Mechanisms: Co-precipitation	Steady-state $Fe_{1.6}H_2PO_4(OH)_{3.8}$ is the stoichiometry for the ferric phosphate precipitate Mass balances and chemical equilibria can be applied Saturation with respect to two solid phases (Smith et al., 2008b).	Stoichiometric reactions for chemical P removal are used to estimate iron dose until residual of 1mg P/L. Around 1 mg/L reactions equilibrium controlled and competing reactions start to dominate. To achieve P levels below 1 mg/L excess metal salt dosing is required since predictions based on stoichiometry are no longer accurate. Metal hydroxide is formed in addition to metal phosphate precipitate. Model predicts a minimum of 35ug PO_4^{3-}/L at optimum pH 6.95 Takács, 2006b) Takács et al. (2006b) recalibrated the WEF model by combining it with equilibrium based pH calculations to be able to determine the ionic strength of the solution allowing for calculation of pH, iron doses, and sludge production. The recalibrated model has broader pH range of removal and predicts a minimum residual of 7ug PO_4^3/L at pH 6.5. However, the minimum residual is fixed by assumption at 7ug/L which causes the model to over predict phosphate removal. Titrations were performed (Tackács et al., 2006a) to determine best-fit values for dissociation and solubility constants so that P removal could be described using actual, real components that form in aqueous media as oppose to empirical components in the original model. Results indicated that no pure phosphate precipitation occurs above pH 5, pure ferric phosphate precipitates below pH 3.5 only, a mixture of ferric phosphate and hydroxide with increasing molar ratios precipitates between pH 3.5 and 4.5, and pure ferric hydroxide precipitates above pH 4.5.	As presented by Smith et al. (2008b): Dose dependence is not shown since (1) saturation with respect to two solid phases is assumed and hydrous ferric phosphate is always present in equilibrium with the solution and (2) varying Fe/P ratios are ignored pH dependence was narrow compared to measure data Residual P only a function of pH and predictions are generally under predicted Supersaturation might not be achieved in wastewater treatment The chemical species proposed $Fe_{1.6}H_2PO_4(OH)_{3.8}$ has been verified not to exist
Smith et al., (2008a) Type: Mechanistic (Gilmore et al., 2009)	Geochemical principles for P adsorption with crystalline goethite can be applied to amorphous hydrous ferric oxides (HFO)	Smith et al., (2008a) applied geochemical principles to Fe and P interactions to develop a P complexation model. This model is used in conjunction with chemical equilibrium modeling to more realistically describe low level P experimental data.	Model was created using a simple water, iron, P system and does not account for the effects of variable water chemistry.

Smith et al., (2008a) (continued) <u>Coagulant:</u> Ferric <u>Removal Mechanisms</u>: Co-precipitation Adsorption Surface Complexation		Addition of acidic $FeCl_3$ to water or wastewater, with pH between 6 and 8, results in its neutralization and the simultaneous precipitation of HFOs. P is removed by precipitation of $FePO_4$ at pH 4 or lower, co-precipitation of phosphate into the HFO structure, or adsorption onto existing HFO flocs due to complexation reactions on the HFO surface The surface complexation model (SCM) is broken down into two parts as described in full in (Smith et al., 2008a). The first part involves chemical equilibrium calculations to determine the amount of HFO and $FePO_4$ that precipitates. Once the amount of HFO is determined the second part of the model allows P to complex with the HFO surface through the use of the ASF (Smith et al., 2008a) Improved prediction of the behaviour of phosphorus when low level removal is targeted.	The model is not able to perform SCM calculations for low doses (less than 0.6mgFe/L). The model is not able to describe the kinetic behaviour of P removal i.e. fast followed by slow removal observed by Szabó et al. (2008) or the influence of HFO aging (Hauduc et al., 2013)
Hauduc et al., (2013) <u>Type:</u> Mechanistic/Empirical <u>Coagulant:</u> Ferric <u>Removal Mechanisms:</u> Co-precipitation Adsorption Surface Complexation	Dynamic system behaviour All reactions can be kinetically modeled. Chemical equilibrium dissociation processes can be modeled dynamically with very fast rate kinetics as described in Musvoto et al. (2000) See assumptions associated with Smith et al. (2008a)	The physico-chemical aspect of the model was developed using kinetic rate expressions to describe: chemical equilibrium dissociation (i.e. water dissociation, carbonate, and phosphate acid-base systems), chemical ion pairing (i.e. for Fe and Ca), physical mineral precipitation (i.e. precipitation of HFO or $FePO_4$), and chemical surface complexation onto HFO (i.e. chemical surface complexation and aging). The hydrous-ferric oxide aspect of the model includes the following modifications to the model by Smith et al. (2008a): • addition of kinetic rates towards equilibrium • definition of two populations of HFO: fresh HFO with a high ASF and older HFO with a low ASF (formation of each fraction of HFO is dependent on mixing intensity)	The kinetics of P removal are poorly described HFO aging was calibrated to experimental data with a maximum age of 30 minutes and does not account for solid ages typical of wastewater treatment. The effects of pH, TSS and COD were not investigated. Poor description of kinetics and behaviour at

Hauduc et al., (2013) (continued)		• expression of surface complexation species in terms of Fe concentration and calculation of proton or P contents based on stoichiometry and ASF • introduction of two processes of HFO aging: fresh HFO ages to older HFO with low ASF, and low HFO ages to old HFO with no reactive sites.	high Fe/P doses
BioWin (EnviroSim, 2007) Type: Empirical/Theoretical Coagulant: Ferric, Aluminum Removal Mechanisms: Co-precipitation Biological Nutrient Requirements	Steady-state and dynamic behaviour The P content or requirements for biomass is 0.022 mg P/ mg COD The P nutrient half saturation coefficient is 0.001 mgP/L, which is used to slow the growth of biomass when there is no P available as a nutrient.	Effluent P predictions are based on: the weak acid-base system; nutrient and energy-storage requirements for various microorganisms; and formation of insoluble precipitates with magnesium, calcium, as well as iron and aluminum ions if present (EnviroSim, 2007). The chemical precipitation model uses an equilibrium approach to describe ferric precipitation. Metal addition results in the formation of insoluble phosphate/hydroxo complex ($Fe_{1.6}H_2PO_4OH_{3.8}$), a soluble metal-phosphate complex ($FeH_2PO_4^{2+}$), and any residual metal will be mostly bound in metal hydroxide precipitate ($Fe(OH)_3$) (EnviroSim, 2007). The distribution and residual concentrations of components involved is pH and dose dependent. The best achievable soluble PO_4 concentration when the solution is in equilibrium with the composite product $Fe_{1.6}H_2PO_4OH_{3.8}$ is 0.01 mgP/L with iron dosing at pH 7 (EnviroSim, 2007). The default molar ratio of the precipitate is 1.6mmolFe/mmol P under low doses and optimal pH. However, the actual (observed) ratio will depend on pH, as well as the formation of other ferric phosphate and hydroxide components (EnviroSim, 2007). Magnesium and calcium precipitates including struvite ($MgNH_4PO4{\bullet}6H_2O$), and hydroxy-dicalcium-phosphate (HDP, $Ca_2HPO_4(OH)_2$) are also accounted for when calculating residual P (EnviroSim, 2007).	The chemical species proposed $Fe_{1.6}H_2PO_4(OH)_{3.8}$ has been verified not to exist (Smith et al., 2008b) Adsorption and desorption mechanisms are not considered

The chemical equilibrium models by Ferguson and King (1977), Luedecke et al. (1989) and WEF (1998) described in Table 2-5, have been traditionally used to model chemical P removal (de Haas et al., 2001). In these models, P removal mechanisms include co-precipitation or co-precipitation and adsorption reactions. A similar modelling process was used in all three models. The precipitation reactions employed were defined for two predominant regions: a region at high effluent P concentration where the required metal dose can be determined stoichiometrically (i.e. constant Fe/P at a controlled pH), and an equilibrium region at low effluent P concentrations where significantly higher metal doses are required and both metal hydroxyl phosphate and metal hydroxide form (i.e. Fe/P increases at controlled pH) (Jenkins and Hermanowicz, 1991).

The limitations associated with these traditional chemical equilibrium models are also summarized in Table 2.5. Major criticisms surround the use of non-realistic equilibrium constants and species (Smith et al., 2008b) and fictitious precipitates to describe precipitation in the particular system(s) tested (Briggs, 1996). Another limitation involves the description of the precipitation of pure ferric phosphate ($FePO_4$). Smith et al. (2008b) along with Takács (2006a) have shown that $FePO_4$ only precipitates at acidic pH values (at or below 4) and thus models based on $FePO_4$ precipitation are not suitable to describe chemical P removal (Szabó et al. (2008). Equilibrium models also fail to account for the kinetics of the precipitation process (Caravelli et al., 2010). As described by Caravelli et al. (2010) precipitation/dissolution reactions take longer to reach thermodynamic equilibrium than aqueous phase reactions such as acid/base equilibria.

Briggs (1996) and EnviroSim (2007) have reported models that describe dynamic system behaviour (i.e. account for changes in concentration with respect to time) and allow calibration to site specific situations (Table 2-5). As summarized in Table 2-5, chemical P removal has been described in these models by rate limited co-precipitation, dissociation, hydrolysis, adsorption, and incorporation into biological growth (Briggs, 1996). These models consider the interactions of the different fractions of P in a wastewater treatment system aeration basin. However, since the chemical equilibrium aspects of the models are based on the equilibrium

models of Ferguson and King (1977), Luedecke et al. (1989) and WEF (1998) limitations surround the use of fictitious precipitates as mentioned above.

Inadequacies also surround the use of kinetics in the models by Briggs (1996) and EnviroSim (2007). Holtan et al. (1988) identified that a limitation of existing kinetic models was that most researchers applied rate expressions that are most commonly used when dealing with solutions. As a result, the concentration terms imply that any molecule or ion of the reactant is capable of reacting which is not the case in solid-liquid system when only the atoms or ions on the surface layer are available to react (Holtan et al., 1988). Therefore Holtan et al. (1988) suggest that a factor describing the concentration of reactive surface sites should be included in kinetic expressions.

Smith et al. (2008a) reported a model (Table 2-5) that employs geochemical principles in conjunction with chemical equilibrium modelling to describe ferric and P interactions. This surface complexation model (SCM) was based on interactions between amorphous hydrous ferric oxides (HFO) and P (i.e. adsorption and co-precipitation). The geochemical principles built on studies of phosphate interactions with goethite, a crystalline iron oxide (Geelhoed et al., 1997). Smith and Ferris (2001) demonstrated that interactions with amorphous hydrous ferric oxides are similar to those with goethite. The model uses an active site factor (ASF) to describe the availability of reactive oxygen atoms or "surface sites" for P complexation before, after, and during precipitation. The value of the ASF was found to be a function of dosing, mixing, pH and aging conditions (Smith et al., 2008a).

The advantages of the SCM model include the fact that it is based on recognized chemical species as compared to the equilibrium or kinetic models and that it includes surface geochemical interactions, which are ignored in previous equilibrium and kinetic models (Smith et al., 2008b). As mentioned in Table 2-5 the model is better suited to predict behaviour in systems when low effluent P limits are targeted. Limitations however include that the model was developed using a simple hydrogen-iron-P system and that the model does not account for influences of variable water chemistry. The model is also not able to describe the kinetic behavior of P removal observed by Szabó et al. (2008) i.e. the initial fast removal followed by

slow removal and the influence of HFO aging (loss of active surface sites) (Hauduc et al., 2013).

The most recent model described in Table 2-5, developed by Hauduc et al. (2013), builds on the model by Smith et al. (2008a) to dynamically describe chemical P removal in wastewater. The model combines chemical equilibrium, physical precipitation and co-precipitation reactions as well as sorption and aging (surface consolidation) processes. All process reactions are described using kinetic rate expressions. The aging aspect of the model described by Hauduc et al. (2013) and Takács et al. (2011) is one of the main modifications to the model by Smith et al. (2008a). Further details on the aging process from Hauduc et al. (2013) and Takács et al. (2011) are described as follows:

- Iron dosing results in the formation of two fractions of HFO (i.e. high HFO and low HFO) as a function of the mixing intensity provided.
- High HFO is formed under high intensity mixing and is characterized by an open structure and a high specific surface area for sorption.
- In contrast, low HFO is formed under low intensity mixing and has a more compact structure and less accessible binding sites.
- Addition of P to High HFO is considered an equilibrium precipitation process and results in fast co-precipitation/sorption leading to saturation of the surface sites.
- The addition of P to low HFO results in a slower reaction where a smaller fraction of P is precipitated and is described with a kinetic adsorption model.
- P bound on each fraction of HFO becomes mechanically entrapped into the HFO structure and does not contribute to any further reaction.
- Unbound HFO simultaneously undergoes aging (surface consolidation).
- High HFO ages to low HFO and low HFO ages to a third fraction of solids termed old HFO which contain no active surface sites.
- Old HFO also accounts for the mechanically entrapped phosphates.

Therefore, the model provides additional insight/hypothesis into the mechanisms of chemical P removal previously described by Szabó et al. (2006, 2008) and Smith et al. (2008a).

As summarized in Table 2-5, limitations of the dynamic physico-chemical model reported by Hauduc et al. (2013) include the inability to accurately describe the sequence of fast followed by slow removal kinetics of P observed by Szabó et al. (2008), and poor descriptions of removal behaviour at high Fe/P doses. Hauduc et al. (2013) indicated that kinetic limitations may be due to an inadequate description of phosphate diffusion into less accessible binding sites. The model is also limited in its description of aging. The model was calibrated to experimental data from Szabó et al. (2008) where pre-polymerized HFOs were aged between 1 and 30 minutes which is not a typical timeframe for wastewater solids residence times.

On the basis of the literature reviewed it was found that although model development has increased the ability to predict residual PO_4^{3-} concentrations when extremely low P concentrations are targeted, models are still not able to correctly describe removal kinetics and the impacts of aging and solids residence time. Further, the models have not been evaluated with respect to predicting chemical P removal behaviour in complex waters where organics and other species may interfere with removal mechanisms. Improving the ability of the models to describe these mechanisms will lead to more consistent effluent P levels at reduced dosage rates and chemical sludge production resulting in savings in chemical and sludge treatment costs (Takács et al., 2006b).

2.6 P Adsorption Modelling

As summarized in Sections 2.3 co-precipitation and adsorption have been identified as prominent mechanisms of chemical P removal. Adsorption of P onto the surface of crystalline oxides such as goethite (α-FeOOH) has been characterized (Weng et al., 2012; Kang et al., 2003; Rietra et al., 2001; Li and Stanforth, 2000; Geelhoed et al., 1997). Surface complexation models have been used to provide a quantitative description of the adsorption of anions and cations onto the surface of iron oxides (Mao et al., 2012; Davis and Leckie, 1980; Golberg, 1985; Stumm et al., 1970; Dzombak and Morel, 1990; Hiemstra and Riemsdijk, 1996). This prior work focused on the use of crystalline oxides that have well-defined particle size and specific surface areas (Lijklema, 1980). Hence these studies are often only used as a starting point for understanding the mechanisms of removal via adsorption onto amorphous precipitates in wastewater. In comparison, experiments conducted with fresh HFO are confounded by aging

effects making quantitative interpretation more difficult (Lijklema, 1980; Smith et al., 2008a; Mao et al., 2012).

The literature reveals two types of adsorption: physical adsorption and chemisorption. Physical adsorption is reversible and results in a small decrease in system energy upon adsorption whereas chemisorption is partly or completely irreversible and is associated with a large decrease in energy (Berkheiser et al. 1980). Chemisorption includes adsorption through surface ligand exchange and adsorption by incorporation into the adsorbent structure (Holtan et al., 1988). Most studies suggest that the mechanism of P adsorption on chemical solids is chemisorption where phosphate ions replace hydroxide ions (Briggs, 1996) as illustrated in Equation (2-3):

$$2C_s + P \rightarrow 2C_sP_a + H_2O + OH^- \qquad \text{(Equation 2-3)}$$

where C_s is the chemical solid/floc, P is the soluble ortho-phosphate, and P_a is the adsorbed ortho-phosphate. Experiments conducted by Lijklema (1980), support high-affinity adsorption on the positive sites of the hydroxide complex resulting in complete neutralization at very low concentrations of P in solution. The results of Luedecke et al. (1989) support this view since the adsorptive capacity of the solid precipitates was strongly correlated to the number of hydroxide groups available for exchange with P (Briggs, 1996). Holtan et al. (1988) indicated that in addition to exchange with hydroxo groups, sorption of phosphate can also occur by ligand exchange with aquo-, or ol-groups. In practice, chemisorption of phosphate (the amount of hydroxide ions replaced by phosphate ions) can be determined by measuring the amount of acid required to keep the pH constant in batch adsorption tests (Lijklema, 1980).

Equilibrium sorption behaviour is typically described mathematically by fitting residual P results to an isotherm. In soil sorption systems, the Langmuir, Freundlich and Temkin isotherms have been most widely used (Holtan et al., 1988). However, the particles involved in soil sorption studies have definitive shapes, sizes, and surface area whereas iron hydroxide is amorphous. Application of these isotherms to experimental data should be done critically to ensure that an accurate representation of the amorphous nature of the precipitate is provided. There is no consensus on which type of isotherm best describes adsorption behaviour. Newcombe et al. (2008b) used the Langmuir isotherm to characterize P adsorption onto

amorphous HFO and HFO coated sand while Kang et al. (2003) used the Freundlich isotherm to describe the adsorption of P onto ferrihydrite ($Fe_5HO_8 \cdot 4H_2O$), hematite (α-Fe_2O_3) and goethite. Lijklema (1980) conducted adsorption experiments with freshly precipitated iron (III) hydroxide. The adsorption isotherms were shown to fit Equation (2-4) (Lijklema, 1980) which has similarities to the Freundlich isotherm (Briggs, 1996):

$$\frac{[P_a]}{[Fe]} = 0.298 - 0.0316pH + 0.201[P]^{1/2} \qquad \text{(Equation 2-4)}$$

where P_a, Fe, and P are the adsorbed phosphate concentration, iron dose, and soluble phosphate concentration respectively in mmolar units. Equation (2-4) was determined through experimentation that involved the addition of various concentrations of phosphate to a solution of fresh precipitate with a 15 minute equilibration time. When the dosing was conducted in the reverse order and fresh precipitate was added to solutions of phosphate, Equation (2-4) was found to under predict P removal (Smith et al, 2008b). Since the sorption process is described as a slow kinetic process occurring over several hours/days (Szabó et al., 2006; Szabó et al., 2008) limitations also exist in applying Equation (2-4) to data obtained over a longer equilibration time.

There are relatively few models that describe the kinetics of P adsorption onto solids. Mao et al. (2012) showed that the adsorption of dissolved P onto fresh HFO was initially rapid reaching pseudo-equilibrium in the first hour. Further removal of P occurred over several days (Lijklema, 1980). The Elovich type equation (Hingston, 1981) as illustrated in Equation (2-5) is most typically used and shows an initial fast period of adsorption followed by a slower adsorption period (Briggs, 1996):

$$\frac{dq}{dt} = a\exp(-b_a q) \qquad \text{(Equation 2-5)}$$

where q is the mass of adsorbate taken up per unit solid mass, a is a constant relating to the initial velocity of the reaction, and b_a is a constant relating to the activation energy for adsorption. Zeng et al. (2004) showed that the Elovich equation provided satisfactory fitting of the kinetic data of P adsorption onto iron oxide tailings. These findings were consistent with the P sorption kinetics observed by Sparks (1989) and Chein and Clayton (1980) in soils.

The Elovich equation may oversimplify modeling since the maximum adsorption capacity is not taken into account indicating that adsorption will occur infinitely even as P residuals approach zero (Briggs, 1996). Briggs (1996) modified Equation (2-5) by applying switching functions that accounted for the phosphorus residuals and the maximum adsorption capacity (Equation 2-6):

$$\frac{dP_a}{dt} = aC_s \exp\left(-b_a \frac{P_a}{C_s}\right)\left(\frac{P}{K_{SP}+P}\right)\left(\frac{q_{\max}-q}{K_{Sq}+(q_{\max}-q)}\right) \qquad \text{(Equation 2-6)}$$

where P_a = adsorbed phosphate (mg P/L),

C_s = chemical solids concentration (mg/L),

P = soluble ortho-phosphate concentration (mg P/L),

q_{max} = maximum adsorption capacity (mg P/mg solids),

K_{Sq} = adsorptive capacity switching function constant (mg P/mg solids), and

K_{SP} = phosphorus switching function constant (mg P/L).

Equation (2-6) shows that: as the residual soluble P concentration decreases, the rate of adsorption decreases becoming zero when the residual soluble P concentration is zero; and as the amount of P adsorbed approaches the maximum adsorption capacity, the phosphate adsorption rate will be reduced to zero (Briggs, 1996). Equation (2-6) provides a mechanistic model for P adsorption with more applicability to real systems.

In addition to the simple Elovich equation, first-order, second-order, power function, intraparticle diffusion, and parabolic diffusion models have been used to describe P adsorption behaviour (Yu et al., 2012; Zeng et al., 2004). Table 2-6 summarizes the various kinetic equations. The kinetic models presented in Table 2-6 along with the simple Elovich equation are empirical. Application of these models is limited to fitting of experimental results with minimal application to real systems. Further research into the application of sorption kinetics into real wastewater systems which are transient and dynamic in nature is required to better describe P sorption behaviour.

Table 2-6: Kinetic Models (adapted from Yu et al., 2012 and Zeng et al., 2004)

Model Name	Model Equation
First Order	$\log(q_{e,exp} - q) = logq_{e,cal} - \frac{k_1 t}{2.303}$
Second Order	$\frac{t}{q} = \frac{1}{k_2 q_{e,cal^2}} + \frac{t}{q_{e,cal}}$
Intra-particle diffusion	$q = k_d t^{0.5} + D$
Power function	$q = at^{b_a}$
Parabolic Diffusion	$\frac{q}{t} = a + \frac{b_a}{t^{1/2}}$

2.7 Summary and Research Gaps

The literature review has indicated that some form of chemical P removal is required to achieve low effluent P concentrations. The mechanisms of P removal with ferric chloride are mainly characterized by rapid equilibrium precipitation of HFOs occurring simultaneously with co-precipitation, followed by a slower kinetic removal as a result of chemisorption (Szabó et al., 2006). The pH, Fe dosing, mixing and aging conditions as well as water chemistry dictate the extent to which these mechanisms will perform. Several models have been developed to describe chemical P removal. Model development has increased the ability to predict residual PO_4^{3-} concentrations under transient and dynamic conditions typical of wastewater treatment process; however current models are unable to accurately describe all of the mechanisms and effects responsible for P removal when striving for ultra low concentrations. Model limitations stem from the lack of information on the effects of aging of chemical precipitates and the role of solids contact times and solids residence times typical of wastewater solids on P removal (Benisch et al., 2013). In particular there is limited dynamic information relating to the issues of aging and how soluble P reacts, i.e. the rates at which it adsorbs. There is also limited information on the kinetics of removal. Therefore, this research aims at characterizing the impact of solids residence time on P removal (including the rates of adsorption) and the kinetics of P removal under steady state and transient conditions.

CHAPTER 3

3. THE EFFECT OF SOLIDS RESIDENCE TIME ON PHOSPHORUS REMOVAL

3.1 Overview

The impacts of floc aging on P removal in timeframes typical of solids residence times (SRT) employed in activated sludge have not been determined. The objective of this work was to characterize the impact of SRT on steady state P removal in wastewater treatment. Steady state samples were obtained from lab scale continuous flow sequencing batch reactors (SBRs) under high (6.4 mg P/L; 1.4 mol Fe/mol P) and low (3.4 mg P/L; 2.6 mol Fe/mol P) influent phosphate concentrations. In this chapter residual P concentrations, particle size distribution and microscopy analyses were determined over a range of SRTs (2.8-22.8 days under low influent P concentrations; 3.1-26.6 days under high influent P concentrations). The results showed that the majority of P removal (94% under low influent P concentrations; 83% under high influent P concentrations) occurred immediately after Fe addition with an additional but smaller fraction of removal in the SBRs (3.3 – 4.8% under low influent P concentrations; 5.5 - 8.8% under high influent P concentrations). Soluble P uptake did not increase above an SRT of approximately 7.4 days under low influent P concentrations and 14.3 days under high influent P concentrations. The amount of sorbed P (μg P/mg TSS) decreased with SRT, providing evidence that aging changed floc morphology. Floc size was found to have no distinguishable influence on P removal. However, changes in floc morphology with SRT were consistent with P removal trends.

3.2 Introduction

Concerns regarding effluent discharges into sensitive receiving water bodies have resulted in very low orthophosphate (PO_4^{3-}) limits (<10 μg-P/L) for a number of locations (Takács et al., 2006a). Currently, these limits can only be achieved with some level of chemical P removal through the use of metal salts. The removal of PO_4^{3-} with ferric chloride was the topic of this research.

Characterization and modelling of the physical and chemical processes involved in attaining extremely low P concentrations with hydrous ferric oxides (HFO) has been the focus of recent research (Smith et al., 2008a; Szabó et al., 2008; Newcombe et al., 2008b; Weng et al., 2012; Mao et al., 2012; Hauduc et al., 2013). The addition of ferric salts to water has been reported to result in the formation and rapid precipitation of HFO floc (Smith et al., 2008a). PO_4^{3-} initially co-precipitates during the rapid HFO formation while subsequent uptake is slower and due to adsorption/complexation reactions on the surface of the HFO floc (Smith et al., 2008a; Szabó et al., 2008). These complexation reactions involve iron and P sharing an oxygen atom (Smith et al., 2008a). The availability of reactive oxygen atoms or "surface sites" has been found to depend on mixing and aging. The majority of removal occurs during the initial fast reaction; however the slower long term removal is significant in achieving low effluent concentrations (Szabó et al., 2008).

Recycling solids through the wastewater treatment process provides additional solids retention time allowing for "slow" interactions between the liquid and solid phases. Research has shown that recycling solids enhances P removal and decreases metal dosing requirements (Takács et al., 2006b; Szabó et al., 2008; Newcombe et al., 2008a; Takács et al., 2011; Falk et al., 2012). Szabó et al., (2008) found that systems with a longer hydraulic residence time (HRT) and solids residence time (SRT) provided increased PO_4^{3-} uptake.

The recycling of solids in wastewater treatment has been found to lead to floc aging. The process of aging is expected to change the morphology of HFO precipitates. Smith et al. (2008a) determined that the availability of surface sites decreases as a result of HFOs becoming more crystalline with age thus limiting the surface area for P binding. Aging therefore affects the slow P removal reactions or adsorption mechanisms (Smith et al., 2008a; Szabó et al., 2008). Reduced P removal with aged pre-polymerized HFO was reported by Mao et al. (2012), Szabó et al., (2008) and Lijklema (1980). The aging described in these studies was over short time frames not typical of solid residence times (SRTs) observed in wastewater treatment processes. Therefore, a better understanding of the aging of chemical solids and the role of solids contact time and SRT on chemical use and achievable P limits is still required (Benisch et al., 2013). Ideally this will lead to relationships that quantitatively describe the

influence of SRT on PO_4^{3-} sorption in continuous co-precipitation systems under conditions that are typical of wastewater treatment processes.

The objective of this work was to characterize the impact of SRT on steady state P removal as well as to obtain an improved insight into the effects of SRT on floc structure and hence the relationship between floc properties and P removal. Steady state samples were obtained from lab scale continuous flow sequencing batch reactors (SBRs) using synthetic natural water under high and low influent phosphate concentrations.

3.3 Materials and Methods

3.3.1 Experimental Set-up

Steady state experiments were conducted in four (reactor A, B, C and D) continuously operating SBRs located at Environment Canada's Wastewater Technology Centre (Burlington, Ontario). A schematic of the lab scale system is shown in Figure 3-1.

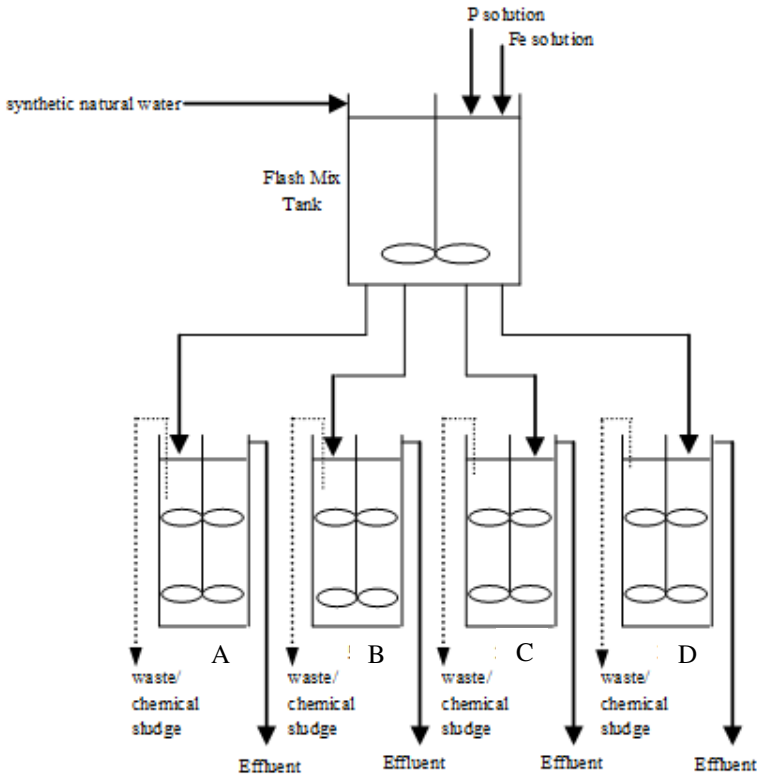

Figure 3-1: Simplified Process Schematic

The flash mix tank was fed with a synthetic natural water adapted from a recipe by Environment Canada (1990). The recipe (Table 3-1) was modified to provide an alkalinity typical of wastewater and to include phosphate. A volume of stock phosphate solution was introduced into the flash mix tank via a fluid metering (FMI) pump. Stock phosphate solution (1 g PO_4^{3-}/L) was prepared by dissolving KH_2PO_4 in Milli-Q water. The pilot was operated under a low influent P loading for 2 years and under a high influent P loading for approximately 50 days. All chemicals used were reagent grade or better. All solutions were prepared with ultra pure water (Milli-Q, 18 MΩ).

Table 3-1: Synthetic natural water recipe

Constituent	Concentration (mg/L)
sodium bicarbonate ($NaHCO_3$)	384
calcium sulfate di-hydrate ($CaSO_4.2H_2O$)	120
magnesium sulfate ($MgSO_4$)	120
potassium chloride (KCl)	8
phosphate (PO_4^{3-})	High Influent Concentration: 6.4 mg P/L Low Influent Concentration: 3.4 mg P/L
Alkalinity	268.2 ± 9.8 mg/L as $CaCO_3$
pH	7.6-8.0

The synthetic feed water in the flash tank was then dosed with ferric chloride (16.1 ± 1.8 mg-Fe/L) under rapid mixing and transferred into each of the SBRs. The iron dosing concentration was determined experimentally based on meeting effluent P concentrations in the range of 50 µg P/L under low influent P concentrations, while the mixing (rpm) corresponded to experiments performed by Szabó et al. (2008) and Gilmore (2009). The SBRs were equipped with pH control, aeration, and mechanical mixing and allowed to react (flocculate), waste, settle and decant. Table 3.2 summarizes the specific design parameters of the flash mix tank and the SBRs. Each SBR was operated at one of four target SRTs of 2 (A), 5 (B), 10 (C) and 30 (D) days. SRT was controlled by adjusting waste volumes weekly based on effluent and reactor solid concentrations, and by tracking the SRT dynamically (Takács et al., 2008).

Table 3-2: Process Design Parameters

Design Parameter	Flash Mix Tank
Volume (L)	12
Mixing (rpm)	350
Velocity Gradient (G) (s^{-1})	310
HRT	<2 minutes
Design Parameters	**SBRs**
Volume (L)	2.5
Feed Volume (L/cycle)	1.5
Decant Volume (L/cycle)	1.5
Mixing (rpm)	20
Airflow (mL/min)	> 80
Velocity Gradient (G) (s^{-1})	98
pH	6.9 ± 0.1 (adjustments made with 0.1 M NaOH and 0.1 M H_2SO_4)
SRT (d)	2, 5, 10 and 30
HRT (h)	10
SBR sequence times	Feed (2mins), React (4.5hrs), Settle (1.25hrs), Decant (13mins)
SBR cycle times	4 cycles/day (6 hours each)

3.3.2 Sample Collection and Preparation

Once steady state was achieved with respect to SRT the flash tank and SBRs were regularly sampled for analysis. Flash tank samples were collected after Fe dosing while the flash reactor contents were fed into each SBR. SBR samples were collected from the waste and effluent streams. Waste samples were taken at the end of the react phase while the solids were still in suspension. Effluent samples were collected during the decant phase. Table 3-3 summarizes the steady state sampling plan.

Soluble P, Fe, total P and microscopy samples required additional processing prior to analysis. Samples that were collected for soluble P analysis were filtered immediately through a 0.45 μm nitrocellulose membrane filter (Whatman Millipore). Fe samples were preserved to pH < 2 with nitric acid while total P samples were preserved to pH < 2 with sulfuric acid. Microscopy samples were 'washed' to remove salts from the aqueous solution. The washing procedure involved centrifuging the samples to separate the floc from the aqueous solution, draining the aqueous solution, and resuspending the flocs in Milli-Q water. The procedure was repeated three times and the final aqueous suspension was thinly spread onto silicon dioxide and dried at 105^{o}C until the water was evaporated.

Table 3-3: Steady state sampling plan

Analysis	Sample Location	Sampling Frequency	
		Low Influent P	High Influent P
Soluble P	Flash tank	Weekly	Daily
	SBR effluent	Weekly	Daily
Total suspended solids	Flash tank	Weekly	Weekly
	SBR waste	Weekly	Weekly
	SBR effluent	Bi-weekly	-
Fe	Flash tank	Intermittently	Intermittently
	SBR waste	Intermittently	Intermittently
	SBR effluent	Intermittently	Intermittently
Total P	Flash tank	Intermittently	Intermittently
	SBR waste	Intermittently	Intermittently
Particle Size Distribution	Flash tank	Intermittently	-
	SBR waste	Intermittently	-
Microscopy	Flash tank	Intermittently	-
	SBR waste	Intermittently	-

3.3.3 Sample Analysis

Soluble P concentrations were determined with the optimized ascorbic acid method (detection limit of 10 μg P/L) as presented by Gilmore et al. (2009). A UV-Vis spectrophotometer (UV-1700, Shimadzu Corporation, Kyoto, Japan) with a 10 cm path length was used. Concentrations above 0.1 mg/L were analyzed according to Standard Method 4500-P.E (Standard Methods, 2005) with a 1 cm path length. All glassware and plasticware were acid washed in a 10% v/v nitric acid solution overnight and rinsed with Milli-Q water. TSS concentrations were determined according to Standard Method 2540D (Standard Methods, 2005).

Fe and total P samples were analyzed by the Environment Canada, Wastewater Technology Centre Analytical Laboratory. Fe samples were digested with nitric acid according to Standard Method 3030E (Standard Methods, 2005). Fe concentrations were then determined by Inductively Coupled Plasma (ICP) using Standard Method 3120B (Standard Methods, 2005). P samples were digested and quantified by continuous flow analysis (CFA) using QuAAtro Applications Method Q-026-04 (Automated Ascorbic Acid Method 4500-P F; Standard Methods, 2005).

Flash tank and SBR waste samples that were collected under low influent P concentrations were characterized by particle size analysis and through microscopy to obtain information on floc characteristics. Particle size analysis was conducted using an automated imaging technique (FlowCAM VS Series Benchtop Model, Fluid Imaging Technologies, Yarmouth, Maine). The FlowCAM system counted, imaged, and analyzed particles in a continuous flow (Fluid Imaging Technologies, 2012). The fluorescence and laser light scatter of passing particles were monitored by a laser, photomultiplier tubes, and scatter detector monitor (Fluid Imaging Technologies, 2012). A camera captured raw images of the field of view at a user defined interval (Fluid Imaging Technologies, 2012). These images were processed by the computer, digital signal processor and trigger circuitry (Fluid Imaging Technologies, 2012). FlowCAM analysis provided information on particles with sizes between 2 μm to 2 mm. Particle size distribution measurements with FlowCAM were obtained using estimates of equivalent spherical diameter (ESD) and area based diameter (ABD). ESD was based on feret measurement which is a measure of the perpendicular distance between parallel tangents touching opposite sides of the particle (Fluid Imaging Technologies, 2012). Thirty six feret measurements were taken for each particle, one each 5^o between -90^o and $+90^o$, and averaged to obtain the ESD (Fluid Imaging Technologies, 2012). ABD is calculated by summing the number of pixels in the threshold (binary) grayscale image, multiplying by the area of a single pixel, converting to microns, and using the formula for the area of a circle to solve for the diameter (Fluid Imaging Technologies, 2012).

Morphology characteristics were obtained using both FlowCAM and SEM analyses. From FlowCAM, measures of particle compactness and transparency were collected. These parameters were expected to provide an indication of differences in particle density i.e. the more dense a particle the higher the compactness and the lower the transparency. Compactness and transparency were derived from the following formulas (Fluid Imaging Technologies, 2012):

$$Compactness = \frac{Perimeter^2}{4 \times \pi \times Area} \quad \text{(Equation 3-1)}$$

$$Transparency = 1 - \frac{ABD}{ESD} \quad \text{(Equation 3-2)}$$

Scanning Electron Microscopy (SEM) measurements were performed on a Zeiss FESEM Ultra Plus (with EDX/OIM) (Zeiss, Oberkochen, Germany). Samples were examined without using conductive coating.

3.3.4 Quality Control

All soluble P and TSS samples were collected and analyzed in duplicate to ensure quality control. The original stock phosphate solution and additional soluble P samples were analyzed independently (infrequently) by the Environment Canada, Wastewater Technology Centre Analytical Laboratory. Quality control of Fe and total P samples was evaluated by the Environment Canada, Wastewater Technology Centre Analytical Laboratory by including blank spikes and duplicates with each run.

3.3.5 Statistical Analysis

The distributions of the data sets were assessed with respect to normality using the Anderson-Darling test. Normal distributions were summarized in terms of the mean and 95% confidence interval (CI) of the mean (i.e. mean (lower 95% CI, upper 95% CI)). Non-normal distributions were summarized in terms of the median and 95% CI of the median (i.e. median (lower 95% CI, upper 95% CI)). In order to make statistical comparisons between results, non-normally distributed data were transformed into normally distributed data with a natural logarithm transformation (i.e. taking the natural logarithm of the data). The log transformed data were then used to make statistical comparisons using standard parametric analyses (Mathews, 2005).

Monte Carlo simulation was used to generate the confidence intervals for calculated parameters. Random samples (n=1000) were generated for the input parameters based on their underlying distributions (i.e. normal (mean, standard deviation)) (Sheehy and Martz, 2012). Non-normally distributed data were transformed into normally distributed data with a natural logarithm transformation and the mean and standard deviation of the transformed data were used to generate random samples. The random samples were transformed back into their non-normal distribution with the exponential function. The generated values were employed to calculate the desired parameters.

3.4 Results and Discussion

3.4.1 Floc Age

Since the age of the chemical solids was equivalent to the SRT in each reactor it was important that the SRT be accurately quantified. The target SRTs were 2, 5, 10 and 30 days in reactors A, B, C and D, respectively but it was anticipated that the actual values may have deviated from the targets. The SRT was tracked through the following dynamic calculation (Takács et al., 2008):

$$SRT = SRT_o + 1 - \left(SRT_o \times \frac{M_p}{M_s} \right) \quad \text{(Equation 3-3)}$$

where SRT is the dynamic SRT of the system accounting for the aging of existing solids and the addition of fresh solids (days), SRT_o is the previous days SRT (days), M_p is the daily solids production (i.e. the amount of fresh solids fed into the SBRs in mg), and M_s is the mass of solids in the system on the current day (mg). Flash tank TSS concentrations were used to determine daily solids production while SBR waste TSS concentrations were used to determine system mass. If the SBRs were not wasted on a particular day Equation (3-3) was simplified to Equation (3-4):

$$SRT = SRT_o + 1 \quad \text{(Equation 3-4)}$$

Table 3-4 summarizes the dynamically calculated SRT along with the measured TSS, Fe and Total P (TP) concentrations in each reactor under high and low influent P concentrations. The raw data for dynamic SRT, TSS, Fe and TP throughout the experimental steady state periods are shown in Appendix A.

Based on the results summarized in Table 3-4 the SRT appeared to have been maintained close to the desired 2, 5, 10 and 30 day values under both influent P conditions. However, upon comparing predicted concentrations of TSS, Fe and TP to the independently monitored concentrations of these analytes as a function of SRT and dosing condition (Figure 3-2) there appeared to be a discrepancy in the original SRT estimates. Predicted concentrations of each analyte (C) were determined by calculating the mass loading of TSS, Fe or TP in each reactor based on Flash concentrations and the target SRT values using Equation (3-5):

Table 3-4: Reactor TSS, Fe, TP and SRT. SRT calculated using dynamic SRT (Takács et al., 2008).

Sample	TSS (mg/L)	Fe (mg/L)	TP (mg/L)	SRT (d)
	Low Influent P Concentration			
Flash	31 (30, 32)[1]	16.1 (13.3, 19.0)	3.4 (2.35, 4.51)	-
A	242 (225, 258)[1]	96.8 (70.8, 122.8)	22.2 (17.7, 26.6)	2.26 (2.22, 2.30)[1]
B	461 (435, 487)	311.2 (192.7, 429.7)	64.3 (42.7, 85.8)	4.77 (4.72, 4.82)[1]
C	956 (903,1008)	402.8 (282.6, 523.0)	74.3 (52.7,95.8)	9.79 (9.73, 9.90)[1]
D	1747 (1670, 1824)	859.0 (704.5, 1013.5)	184.8 (106.9, 262.8)	29.15 (28.94, 29.28)[1]
	High Influent P Concentration			
Flash	35 (30, 41)	16.1 (13.3, 19.0)	6.4 (6.2, 6.6)	-
A	392 (213, 572)	82.5 (82.3, 82.6)[2]	27.3 (26.6, 28.1)[2]	2.9 (2.0, 3.4)[1]
B	652 (434, 871)	265[2]	75.8 (73.5, 78.1)[2]	4.6 (4.2, 5.2)[1]
C	1211 (862, 1561)	567[2]	179 (167, 191)[2]	9.4 (9.3, 9.5)
D	2681 (2523, 2840)	1000[2]	270 (260, 280)[2]	28.7 (28.3, 29.1)

* [1]values are non-normally distributed and reported as median, (95% lower CI, 95% upper CI)
[2]not enough information available to calculate statistics, values are reported as means and ranges

$$C = \frac{C_{flash} \times SRT \times Q_{feed}}{V} \qquad \text{(Equation 3-5)}$$

where C_{flash} is the measured concentration of the analyte in the flash tank effluent (mg/L), Q_{feed} is the daily flow of feed from the flash tank into the SBRs (L/d) and V is the volume of the SBRs (L). The discrepancy between the measured and predicted parameters (Figure 3-2) was especially pronounced with the target SRT of 30 days. In general, all three analytes followed the same overall trend where SRT appeared to be underestimated at the low range (SRT < 10 days) and overestimated at 30 days. This discrepancy may have been due to the nature of the abiotic precipitates used in the study and their deviations from real wastewater floc behaviour in terms of size and settling. SRT was therefore re-estimated for each parameter such that the measured values of TSS, Fe and TP matched the predicted values based on mass loading calculations (Equation 3-5). The best estimate of SRT was then determined by averaging the three different estimates obtained from each parameter. These revised estimates of SRT are provided in Table 3-5. From Table 3-5 it can be seen that the revised SRT estimates were higher than the targets in SBR A-C and lower than the target SRT of 30 days in SBR D. The estimates of the revised SRT were similar under low and high influent P concentrations for SBR A and B. However, revised SRT estimates differed between influent P concentrations in SBR C and D where estimates were higher under high influent P concentrations.

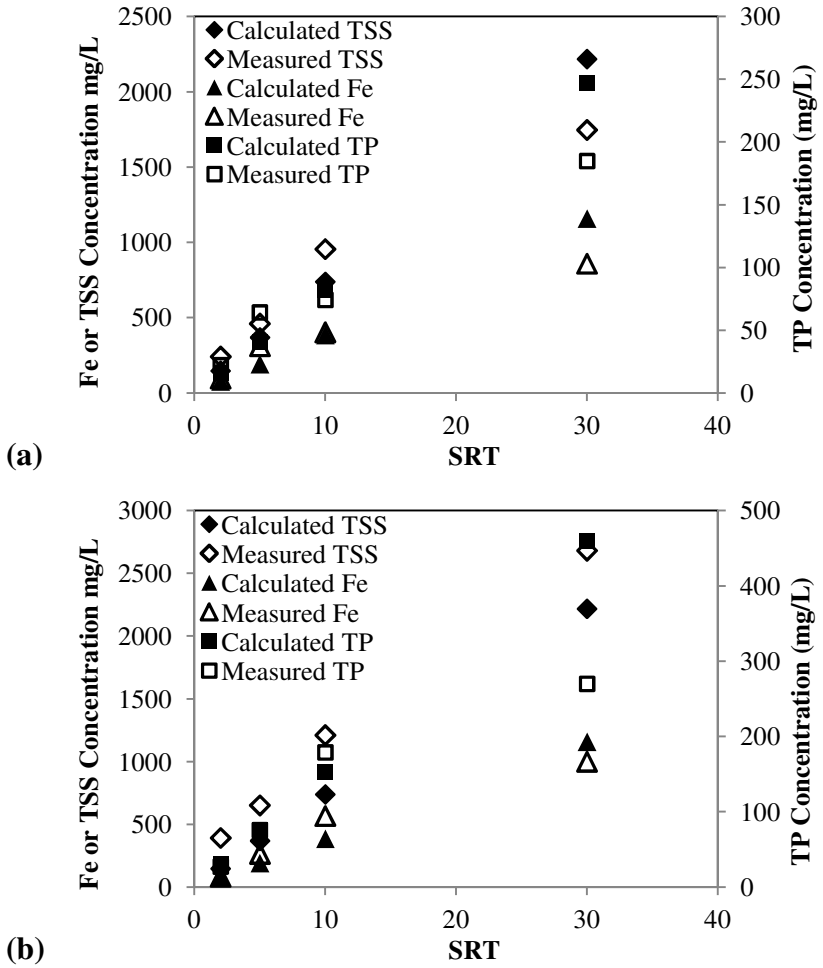

Figure 3-2: Measured vs. Calculated TSS, Fe and TP concentrations as a function of SRT under (a) low influent P concentrations and (b) high influent P concentrations.

Table 3-5: Revised estimates of SRT under low and high influent P concentrations.

Reactor	Target SRT (d)	Revised SRT (d)	
		Low Influent P	High Influent P
A	2	2.8	3.1
B	5	7.4	6.9
C	10	10.8	14.3
D	30	22.8	26.6

The inconsistencies between the measured and calculated estimates of TSS, Fe and TP (Figure 3-2) may have resulted from challenges associated with the analysis procedures. Underestimated values may have been a result of the inefficient capture of the desired

constituent. For example, some of the chemical solids produced may have been too small to be captured by the glass fibre filters used in the TSS analysis (Standard Methods, 2005) resulting in underestimated TSS values. Further research is required to determine if the analytical methods are sound for predicting results especially at high concentration ranges.

3.4.2 Phosphorus Removal

Considering wastewater treatment plants have been facing extremely low effluent P targets it was deemed important to determine the achievable P limits as a function of SRT. Figure 3-3 shows the soluble P concentrations observed in the flash tank and SBR effluents. The raw data for each experimental steady state period are shown in Appendix A. The distribution of soluble P was determined to be non-normal under low influent P concentrations and was summarized using the median and the 95% CI for the median while the mean and 95% CI for the mean were used to describe the normally distributed soluble P concentrations under high influent P concentrations (Figure 3-3). P removal (%) was determined from the influent P concentration.

From Figure 3-3 it can be seen that the 95% CIs for the median and mean soluble P concentrations in the flash mix tank are much wider than the estimates around the SBRs. Hence, flash samples contain higher variability. This variability was attributed to the instantaneous nature of HFO precipitation and PO_4^{3-} co-precipitation. Soluble P removal (i.e. % P Removal in Figure 3-3) was determined by comparing influent P concentrations to the effluent soluble P. Removal in the flash mix tank was 94% under low influent P concentrations and 83% under high influent P concentrations. The SBRs provided an additional 3.3 – 4.8% removal under low influent P concentrations and 5.5 - 8.8% under high influent P concentrations. The removals in each reactor were compared under high and low influent P concentrations using a 2-Sample T-Test. Low influent P conditions provided statistically higher ($p < 0.05$) removal efficiencies as compared to high influent P concentrations. This was attributed to the higher ratio of Fe dose to influent P concentration under low influent P concentrations, which increased removal efficiency (Szabó et al., 2008). Removal efficiencies were compared between reactors using ANOVA and Tukey testing.

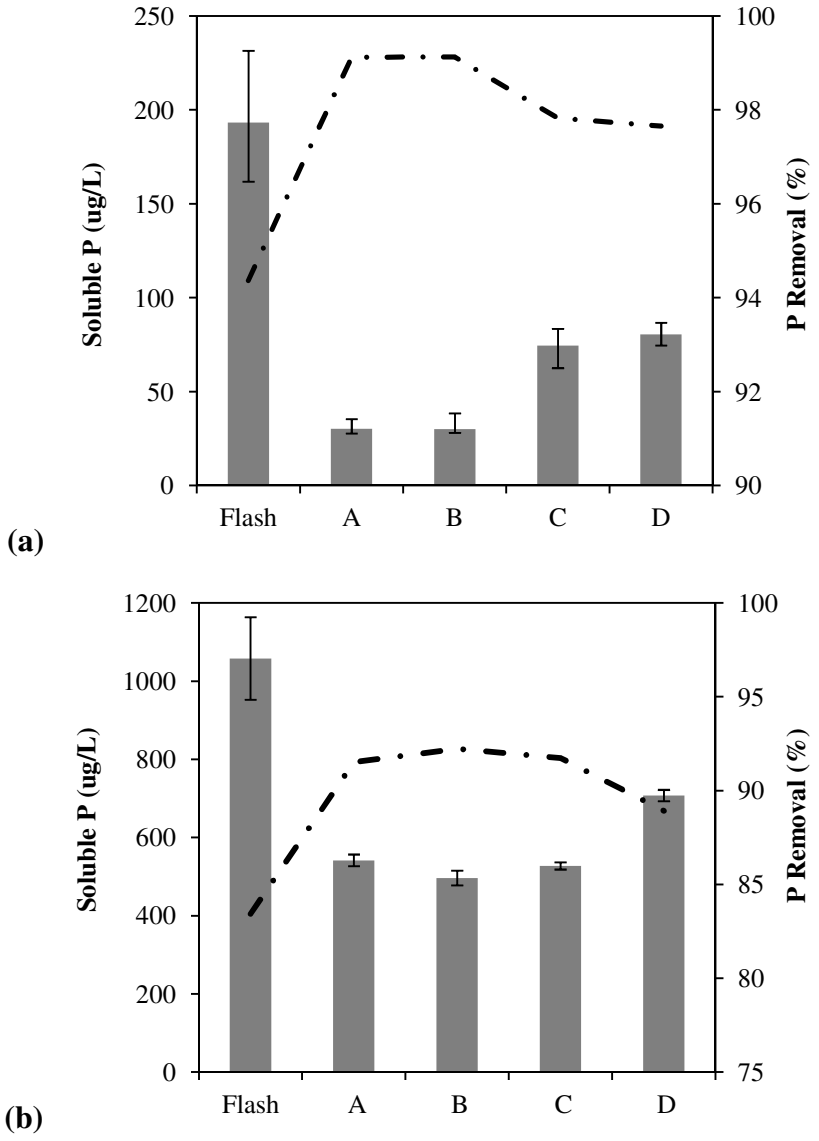

Figure 3-3: Effluent Soluble P Concentrations under (a) low and (b) high influent P concentrations. Boxes correspond to (a) median and (b) mean soluble P values. Solid lines provide 95% CI. Dashed lines represent % P removed from influent.

Under low influent P concentrations, reactor A (n = 63, SRT = 2.8 d) and B (n = 51, SRT = 7.4 d) provided statistically lower residual P concentrations ($p < 0.05$) than reactor C (n = 64, SRT = 10.8 d) and D (n = 62, SRT = 22.8 d). However, differences in removal between reactors A and B and between reactors C and D were not significant ($p > 0.05$). Therefore, under low influent P concentrations P removal was higher in the lower SRT systems (≤ 7.4 days) and decreased with SRT's greater than 7.4 days. Under high influent P concentrations, differences in removal between reactor A (n = 95, SRT = 3.1 d) and C (n = 93, SRT = 14.3) were not

significant ($p > 0.05$). However, reactor B (n = 97, SRT = 6.9 d) provided statistically higher P removal ($p < 0.05$) while removal in reactor D (n = 97, SRT = 26.6 d) was statistically lower. Therefore, under high influent P concentrations P removal was higher at SRTs ≤ 14.3 days and decreased at SRTs greater than 14.3 days.

The results illustrated in Figure 3-3 were consistent with the observations of Szabó et al., (2008) where the majority of P removal from the aqueous phase occurred instantaneously in the flash mix tank (94% under low influent P concentrations; 83% under high influent P concentrations) and further aging of solids provided additional (3.3 – 4.8% under low influent P concentrations; 5.5 - 8.8% under high influent P concentrations) removal from the initial P concentration. However, in contrast to the work of Szabó et al., (2008) removal was evaluated based on solids ages that were typical of SRTs in real wastewater systems. Szabó et al. (2006) attributed the mechanisms of chemical P removal to co-precipitation and adsorption. The initial fast removal was attributed to co-precipitation while adsorption/surface complexation continued as a slower reaction (Smith et al., 2008a; Szabó et al., 2008). However, under the experimental conditions of this study co-precipitation and adsorption could not be differentiated. Therefore, the reported values of P removal encompass both co-precipitated and surface sorbed P.

Since P removal in the SBRs only accounted for a small portion of the total percent P removed (Figure 3-3) the removal occurring in the SBRs were somewhat masked by the high removals in the flash mix tank. Therefore, the initial soluble P concentrations in each reactor at the beginning of the react cycle were calculated to provide insight into the removals within each SBR. The initial P concentration (P_i) was calculated by taking into consideration both the dilution of soluble P from the flash tank as the contents of the flash mix tank were added to each reactor and the background soluble P concentration remaining in the SBR after decanting:

$$P_i = \frac{P_{flash} \times V_{flashfeed}}{V} + P_f \qquad \text{(Equation 3-6)}$$

where P_{flash} is the soluble P concentration in the flash tank effluent (µg/L), $V_{flashfeed}$ is the volume of feed from the flash tank entering the SBRs (L), V is the volume in the SBRs (L) and P_f is the final soluble P concentration in the SBR (µg/L).

Table 3-6 summarizes the initial and final (i.e. effluent) soluble P concentrations from each of the four reactors along with the 95% CI for P_i and the % P removal. Monte Carlo simulation was used to generate the 95% CIs. From Table 3-6 it can be seen that under low initial P concentrations between 60 to 80% of the soluble P was removed in the SBR react cycle. The percent removal in reactors A and B were approximately 19-20% higher than in reactors C and D. Under high influent P concentrations between 47 to 56% of the soluble P was removed. The percent removal in reactors A, B and C were between 6.7-8.8% higher than in reactor D. P removal in the SBRs was believed to result from adsorption/surface complexation. However, it was not possible to directly evaluate the individual contributions of freshly generated solids and the aged solids to the observed removals. The use of sorption modelling to assess the sorption capabilities of the fresh and aged solids will be described subsequently in Chapter 4.

Table 3-6: Initial vs. final soluble P concentrations.

	Low Influent P Concentrations		
	P_i (µg/L)	**P_f (µg/L)**	**P Removal (%)**
Sample	**Median (95%CI)**	**Median (95%CI)**	
A	148 (144, 153)	30 (28, 35)	80
B	145 (144, 150)	30 (28, 38)	79
C	189 (184, 194)	74 (62, 83)	61
D	200 (195, 205)	80 (74, 87)	60
	High Influent P Concentrations		
	P_i (µg/L)	**P_f (µg/L)**	**P Removal (%)**
Sample	**Mean (95%CI)**	**Mean (95%CI)**	
A	1169 (1155, 1183)	542 (527, 556)	54
B	1122 (1108, 1136)	496 (477, 515)	56
C	1154 (1141, 1168)	527 (518, 536)	55
D	1335 (1321, 1350)	707 (692, 722)	47

Since P removal directly occurs as a result of the presence of HFO the removal based on the amount of HFO present in each reactor was estimated for comparison purposes. Table 3-7 shows the amount of soluble P removed per gram of HFO solids in each reactor. The data were calculated with Equation (3-7):

$$P_r = \frac{P_i - P_f}{C_s} \qquad \text{(Equation 3-7)}$$

where P_r is the soluble P removed per gram of HFO solids (µg P/mg HFO), P_i is the initial soluble P concentration in each reactor corresponding to the influent P concentration in the

flash tank and the soluble P concentration determined from (Equation 3-6) in the SBRs (µg/L), P_f is the final soluble P concentration in each reactor and C_s is the solids concentration in each reactor (mg/L HFO). A Monte Carlo simulation was used to calculate median and 95% CIs for P_r. The final distributions of P_r were determined to be non-normally distributed under both influent P concentrations.

Table 3-7: Soluble P removed as a function of HFO concentration.

	Low Influent P Concentrations			
	µg P/mg TSS x10^2		µg P/mg Fe x10^2	
Sample	**Median**	**95% CI**	**Median**	**95% CI**
Flash	10790	10490-11130	20330	19780-20870
A	47	46-49	121	117-127
B	25	24-27	38	36-39
C	12	12-13	29	27-30
D	7	6-7	13	12-13
	High Influent P Concentrations			
	µg P/mg TSS x10^2			
Sample	**Median**	**95% CI**		
Flash	15270	15060-15540		
A	152	145-159		
B	95	91-98		
C	51	49-53		
D	23	23-24		

In this analysis the amount of HFO solids in the SBRs was characterized on the basis of both TSS and Fe concentrations under low influent P concentrations. Since statistics could not be calculated for the Fe concentrations under high influent P concentrations calculations were limited to the use of TSS. There was some uncertainty as to which parameter (TSS or Fe) would provide a better estimate of the concentration of solids in the reactor for the purposes of normalization. TSS concentrations may be biased as the mass of TSS will increase with increasing P concentrations as a result of the added mass that P provides to the solids. The Fe concentrations were considered to provide a measure of the generated HFO since all of the dosed Fe was expected to precipitate into the HFO (i.e. residual soluble Fe concentrations are negligible). However, this estimate would be low since the contribution of hydroxide to HFO was ignored. For the purposes of this paper soluble P removal was compared using both TSS and Fe concentrations (Table 3-7). However, since the measurement of TSS concentrations was more frequent resulting in a larger array of data in comparison to the measurement of Fe

concentrations (Appendix A) subsequent characterizations of HFO solids will be represented by TSS.

From Table 3-7 it can be seen that the normalized P uptake was more than 100 times greater in the flash mix tank compared to the other reactors under both influent P concentrations and normalization to both TSS and Fe concentrations. In comparing the 95% CIs the amount of P removed decreased with SRT under both influent P concentrations and normalization to both TSS and Fe. These results follow the observations of Smith et al. (2008a) where decreased removals were deemed to result from a reduction in the number of reactive surface sites on aged HFO. The results support a hypothesis that P removal in the flash tank was the result of a different mechanism than that of the SBRs. Removal in the flash tank was attributed to co-precipitation during HFO formation and the subsequent surface sorption of P onto HFO floc whereas removal in the SBRs was attributed to surface sorption only. Therefore, the removal in the flash tank was much higher due to both mechanisms acting on P. Sorption modelling was employed to compare the surface sorption capabilities of the flash and SBR solids and will be discussed subsequently in Chapter 4.

3.4.3 Floc Characteristics

It was anticipated that varying the SRT of the SBRs would impact the physical and chemical properties of the floc (i.e. size and morphology). Through microscopy Smith et al. (2008a) showed that HFO aging resulted in the structure becoming larger and denser thus limiting the surface area and the number of available surface sites available for binding. Differences in floc morphology between amorphous and crystalline iron oxides have also been reported by Kang et al. (2003).

Particle size analysis was conducted using FlowCAM. Table 3-8 summarizes the distribution parameters obtained with FlowCAM for particle size i.e. mean, median and IQR of the ESD and ABD diameters (see Section 3.3.3 for description of ESD and ABD). Based on the estimates of central tendency (Table 3-8) it is evident that the distribution of particle diameters was positively skewed (mean > median). Therefore, the best estimates of central tendency and variability were deemed to be provided by the median and IQR. Based on the median and IQR

values it was apparent that the particle size distributions overlapped and therefore differences between reactors could not be delineated. Despite the fact that the differences in size could not be differentiated, the particle sizes (μm) were less than 10 μm. These results were consistent with the observations of Kang et al. (2003) where the particle size distribution of amorphous (ferrihydrite) and crystalline (goethite and hematite) iron oxide particles were similar with an average diameter of 3.5μm.

Table 3-8: Floc size distribution parameters. Estimates were obtained using FlowCAM under low P dosing conditions.

Sample	ESD Diameter (μm)			ABD Diameter (μm)			Sample Size
	Mean	Median	IQR	Mean	Median	IQR	
Flash	4.7	2.1	3.1	2.9	1.7	1.3	375639
A	6.1	2.9	5.9	4.2	2.2	3.5	3265971
B	7.2	3.2	7.4	5.0	2.3	4.6	4505502
C	4.6	2.4	4.4	3.5	2.0	2.8	3053118
D	5.1	2.7	4.9	3.8	2.2	3.4	8916765

Information on floc morphology was also obtained using FlowCAM and SEM analyses (Table 3-9 and Figure 3-4). Table 3-9 summarizes the morphology parameters of compactness and transparency obtained with the FlowCAM analysis (see Section 3.3.3 for description of compactness and transparency). The semi-quantitative measures of compactness and transparency were expected to provide an indication of particle density (Section 3.3.3). Based on the median and IQR values (Table 3-9) it was apparent that the estimates of compactness

Table 3-9: Morphology characteristics. Estimates were obtained using FlowCAM under low P dosing conditions.

Sample	Compactness[1]		Transparency[2]		Sample
	Median	IQR	Median	IQR	Size
Flash	1.8	1.1	0.2	0.3	375639
A	1.7	1.0	0.2	0.2	3265971
B	1.8	1.1	0.2	0.2	4505502
C	1.6	0.7	0.2	0.2	3053118
D	1.6	0.6	0.2	0.2	8916765

*[1] Compactness - The more convoluted the shape, the greater the value. Circle has a value of 1 (Fluid Imaging Technologies, 2012)

[2] Transparency - Varies from 0-1, 0=filled circle, values near 1 have elongated/irregular shape or many interior holes (Fluid Imaging Technologies, 2012)

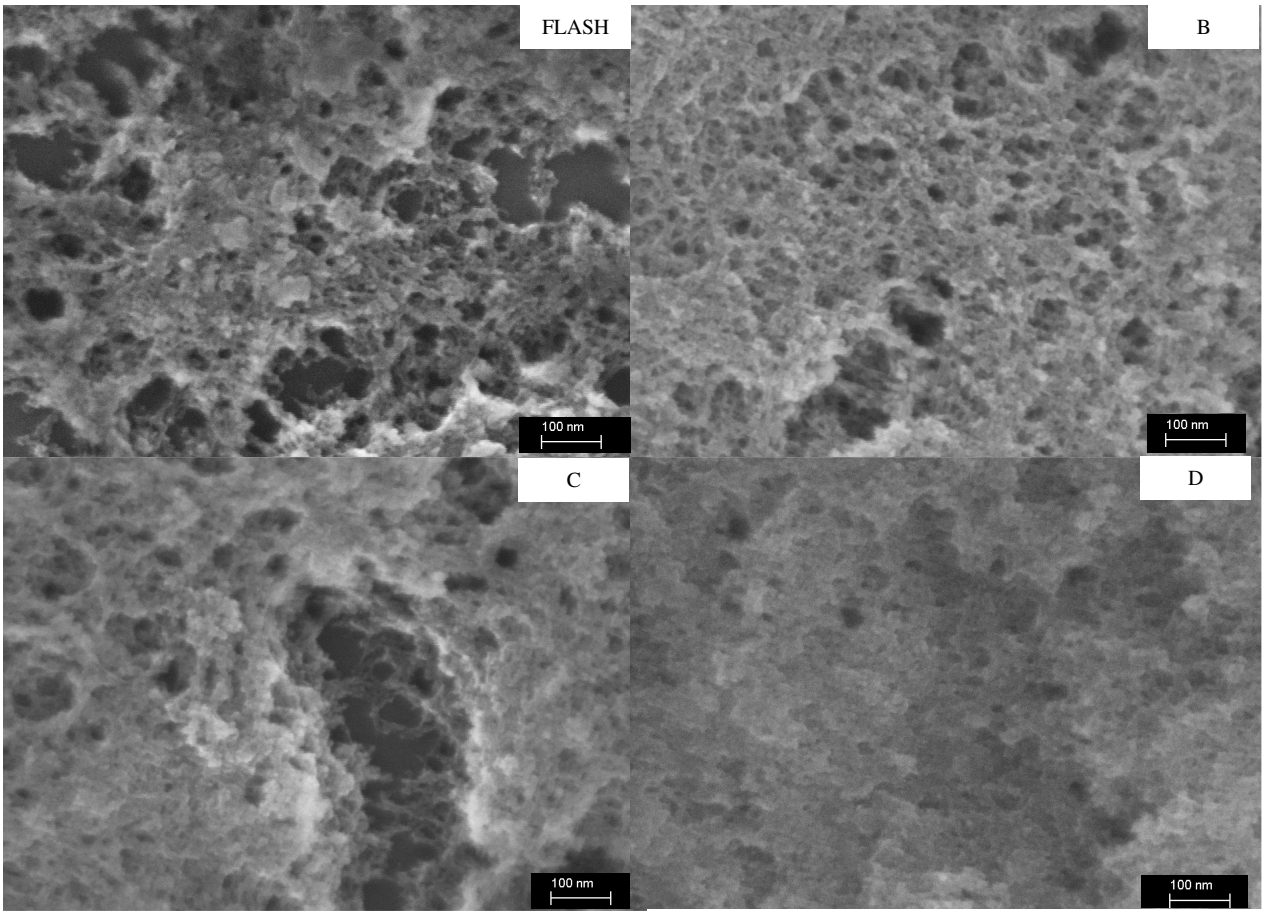

Figure 3-4: SEM images of floc structure. Measurements were obtained using SEM under low P dosing conditions. Magnification = 100 kX, EHT = 10 kV, WD = 8.8 mm (Flash), 9.1 mm (B), 8.9 mm (C), 9.0 mm (D).

and transparency overlapped and therefore differences between reactors could not be delineated. However, from the SEM images in Figure 3-4 it was concluded that the flash tank samples had a more open structure as compared to the aged samples. Increases in floc age appeared to create much more compact flocs. These results were consistent with the results found by Smith et al., (2008a) and Kang et al., (2003) where aging led to a decrease in surface area and available surface sites for binding. Although the aged flocs appeared more compact (Figure 3-4) no increase in particle size with age was evident (Table 3-8) as anticipated by the experimental results by Smith et al., (2008a). Increases in particle size would have the effect of reducing the surface area of the flocs and thus reducing P removal. Therefore, the results support a hypothesis that HFO morphology is more responsible for P removal than particle size (Kang et al., 2003).

Overall, the trends described by the P removal results and the HFO morphology characterizations were consistent. P removal was affected by the solids age (i.e. SRT). Aging as a function of SRT lead to the compaction of HFO flocs leading to a lower surface area and fewer surface sites for binding. As such, lower SRT systems were characterized by higher P removal while higher SRT systems were characterized by lower P removal. The extent of removal achieved as a function of SRT was dependent on the influent P concentration. Removal did not directly decrease with increasing SRT unless the results were normalized to the HFO concentration. Removals that were normalized to the HFO concentrations decreased with SRT as a direct result of the TSS concentration increasing with SRT.

It should be noted that although differences in floc structure supports the hypothesis that floc aging reduces the number of surface sites, differences in surface chemistry may also result in differences in P removal. However, based on the results provided in this Chapter there was no mechanistic evidence of the number or types of surface sites available on the HFO floc or how these sites changed with SRT. Further research is required to quantify these surface sites and determine how properties other than morphology contribute to the observed removal.

3.5 Conclusions

In this study the interactions between soluble P removal and SRT were explored and the following conclusions were arrived at:

- P removal (based on influent P concentrations) was statistically higher under low influent P concentrations.
- The majority of P removal occurred in the flash tank (94% under low influent P concentrations; 83% under high influent P concentrations) with an additional smaller fraction of removal in the SBRs (additional 3.3 – 4.8% removal under low influent P concentrations; 5.5 - 8.8% under high influent P concentrations).
- Soluble P uptake was higher in the lower SRT systems: ($\leq$ 7.4 days) under low influent P concentrations and SRTs $\leq$ 14.3 days under high influent P concentrations.
- P removals in the SBR react cycle (based on initial P concentrations in the SBR) were between 60-80% under low influent P concentrations and 47-56% under high influent P concentrations.

- The amount of sorbed P (μg P/mg TSS) decreased with SRT providing evidence that aging changed floc morphology.
- Differences in floc morphology (i.e. open vs. compact floc structure) between flash solids and SBR aged solids were evident. However, differences in particle size distributions could not be differentiated supporting the hypothesis that changes in floc morphology are more responsible for differences in P removal than floc size (Kang et al., 2003).

CHAPTER 4

4. THE EFFECT OF SOLIDS RESIDENCE TIME ON PHOSPHORUS ADSORPTION TO HYDROUS FERRIC OXIDE FLOC

4.1 Overview

The impact of SRT on phosphate adsorption to HFO floc was characterized and an equilibrium model that describes the sorption of P onto HFO floc of different ages was developed. The results showed that the fresh HFO had a higher sorption capacity in comparison to aged (2.8, 7.4, 10.8 and 22.8 days) HFO and contributed substantially to P removal at steady state. P adsorption onto HFO solids was determined to be best described by the Freundlich isotherm. P desorption from HFO solids was negligible supporting the hypothesis that chemisorption is the mechanism of P adsorption on HFO solids. A model that included the contribution of different classes of HFO solids (i.e. High, Low or Old) to adsorption was found to adequately describe P adsorption onto HFO solids of different ages. From the model it was determined that the fractions of High and Low HFO decreased with SRT, the fractions of Old HFO increased with SRT, the transformation of High HFO into Low HFO did not limit the overall production of Old HFO and the fresh HFO solids contributed more to P removal at steady state than the aged solids.

4.2 Introduction

Concerns over eutrophication in sensitive aquatic ecosystems has focused the wastewater community to produce effluents with ultra low P concentrations (i.e. <10 ug-P/L). In order to reliably meet these low effluent targets, chemical P removal with metal salts has been deemed to be necessary (Jenkins and Hermanowicz, 1991; Levesque et al., 2010; Benisch et al., 2013; Johnson et al., 2005; Johnson and Daigger, 2009). Removal of P with ferric chloride was the topic of this research.

A detailed understanding of the mechanisms of chemical P removal and models describing chemical interactions are required to effectively design P removal systems. Szabó et al., (2006) attributed the mechanisms of chemical P removal to co-precipitation and adsorption. The

addition of ferric salts to wastewater has been reported to result in the formation and rapid precipitation of HFO floc (Smith et al., 2008a). PO_4^{3-} initially co-precipitates during the rapid HFO formation while subsequent uptake is slower and due to adsorption/complexation reactions on the surface of the HFO floc (Smith et al., 2008a; Szabó et al., 2008). These complexation reactions involve iron and P sharing an oxygen atom (Smith et al., 2008a). The availability of reactive oxygen atoms or "surface sites" has been found to depend on pH, mixing and aging.

Recycling solids through the biological treatment process provides additional solids retention time allowing for "slow" interactions between the liquid and solid phases. Research has shown that recycling tertiary solids enhances P removal and decreases metal dosing requirements (Takács et al., 2006b; Newcombe et al., 2008a; Takács et al., 2011; Falk et al., 2012; Johnson et al., 2012). However, recycling solids has also been found to lead to floc aging. Aging is expected to change the morphology of the precipitates. The transition from amorphous hydroxide floc to crystalline structures with floc aging is expected to impact on phosphate adsorption. Dzombak and Morel (1990) showed that aging decreased the adsorptive capacity of HFO. These findings were confirmed through experiments by Smith et al. (2008a) where HFO aging lead to larger, denser structures which limited the surface area for binding and decreased the number of active surface sites. Reduced P removal as a result of aging has also been reported by Mao et al., (2012), Szabó et al., (2008) and Lijklema (1980). The aging described in these studies was over short time frames not typical of solid residence times (SRTs) observed in wastewater treatment processes. Therefore, a better understanding of the aging of chemical solids and the role of solids contact time and SRT on chemical use, achievable P limits, and adsorption mechanisms is required (Benisch et al., 2013).

Most studies have suggested that the mechanism of P adsorption on chemical solids is chemisorption where phosphate ions replace hydroxide ions (Briggs, 1996). Experimental results from Lijklema (1980) and Luedecke et al. (1989) have supported this view. Adsorption of P onto the surface of crystalline oxides such as goethite (α-FeOOH) has been well characterized (Weng et al., 2012; Kang et al., 2003; Rietra et al., 2001; Li and Stanforth, 2000; Geelhoed et al., 1997; Davis and Leckie, 1980; Golberg, 1985; Stumm et al., 1970; Dzombak

and Morel, 1990; Hiemstra and Riemsdijk, 1996). However, this prior work focused on the use of crystalline oxides that have well-defined particle size and specific surface areas (Lijklema, 1980). Hence these studies have only been used as a starting point for understanding the mechanisms of removal via adsorption onto amorphous precipitates in wastewater. In comparison, experiments conducted with fresh HFO were confounded by aging effects making quantitative interpretation more difficult (Lijklema, 1980; Smith et al., 2008a; Mao et al., 2012).

Further insight into the process of HFO aging was provided by Hauduc et al. (2013) and Takács et al. (2011) through the development of a model which combined chemical equilibrium, physical precipitation and co-precipitation reactions as well as sorption and aging (surface consolidation) processes. Figure 4-1 illustrates the model conceptually. From Figure

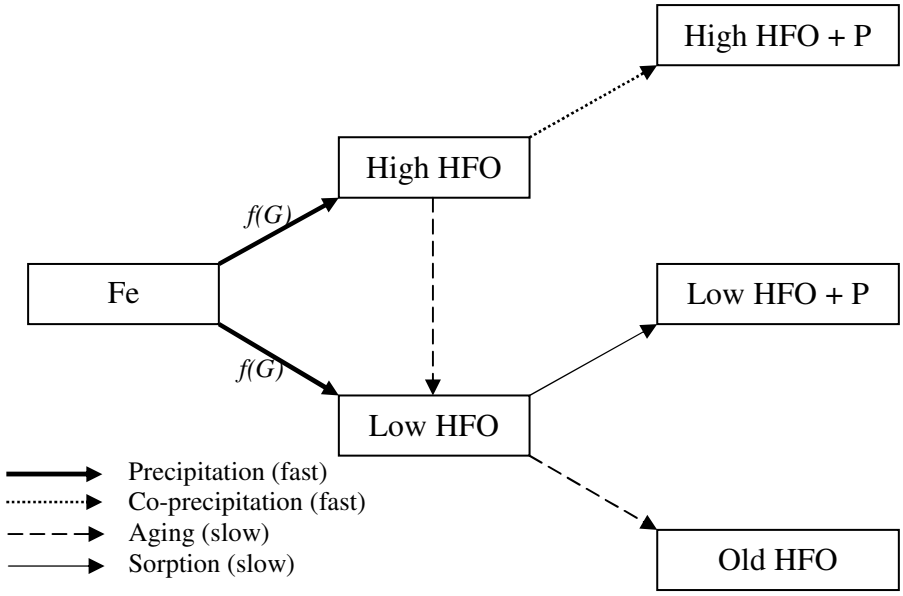

Figure 4-1: Schematic of equilibrium-kinetic chemical P model (Hauduc et al., 2013; Takács et al. 2011) (adapted from Takács et al., 2011)

4-1 it can be seen that iron dosing resulted in the formation of two fractions of HFO (i.e. high HFO and low HFO) as a function of the mixing intensity (G) provided. High HFO was formed under high intensity mixing and was characterized by an open structure and a high specific surface area for sorption. In contrast, low HFO were formed under low intensity mixing and had a more compact structure and less accessible binding sites. Addition of P to High HFO was

considered an equilibrium precipitation process resulting in fast co-precipitation/sorption leading to saturation of the surface sites. The addition of P to low HFO resulted in a slower reaction where a smaller fraction of P was precipitated and was described with a kinetic adsorption model. P bound on each fraction of HFO became mechanically entrapped into the HFO structure and did not contribute to any further reaction. Unbound HFO simultaneously aged (surface consolidation). High HFO aged to low HFO and low HFO aged to a third fraction of solids termed old HFO which contained no active surface sites. Old HFO also accounted for the mechanically entrapped phosphates. The effect of SRT on the aging of HFO and thus the fractionation of these three types of HFO solids has yet to be quantified.

The objective of this work was to characterize the impact of SRT on phosphate adsorption to HFO floc. Batch sorption experiments were carried out with steady state HFO samples obtained from lab scale continuous flow sequencing batch reactors (SBRs) using synthetic natural water. A model to describe the overall sorption behaviour of P onto HFO floc of different ages was applied to the data obtained.

4.3 Materials and Methods

4.3.1 Materials

HFO flocs were collected from a lab scale continuous flow sequencing batch reactor (SBR) pilot located at Environment Canada's Wastewater Technology Centre (Burlington, Ontario). The experimental set-up consisted of 4 SBRs (A-D) operating at one of four SRTs: 2.8 (A), 7.4 (B), 10.8 (C) or 22.8 (D) days. A schematic of the lab scale system is shown in Figure 4-2.

The SBRs were fed from a common flash mix tank that was fed with a synthetic natural water adapted from a recipe by Environment Canada (1990). The recipe (Table 4-1) was modified to provide an alkalinity typical of wastewater and to include phosphate. A volume of stock phosphate solution was introduced into the flash mix tank via a fluid metering (FMI) pump. Stock phosphate solution (1 g PO_4^{3-}/L) was prepared by dissolving KH_2PO_4 in Milli-Q water. All chemicals used were reagent grade or better. All solutions were prepared with ultra pure water (Milli-Q, 18 MΩ).

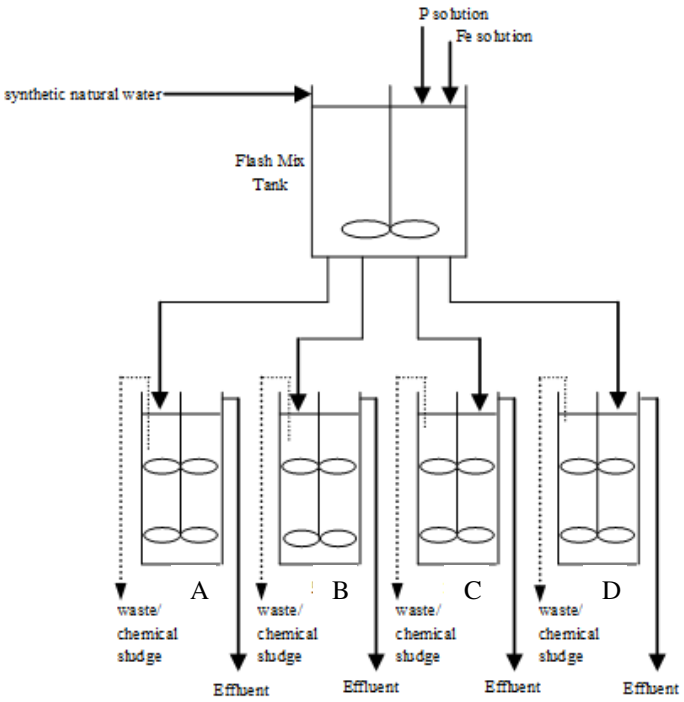

Figure 4-2: Simplified Process Schematic

Table 4-1: Synthetic natural water recipe

Constituent	Concentration (mg/L)
sodium bicarbonate ($NaHCO_3$)	384
calcium sulfate di-hydrate ($CaSO_4.2H_2O$)	120
magnesium sulfate ($MgSO_4$)	120
potassium chloride (KCl)	8
phosphate (PO_4^{3-})	Mean: 3.4 mg P/L, 95% CI: 2.35-4.51 mg P/L
Alkalinity	268.2 ± 9.8 mg/L as $CaCO_3$
pH	7.6-8.0

The synthetic feed water in the flash tank was dosed with a stock iron solution (Mean: 16.1 mg Fe/L; 95% CI 13.3-19.0 mg Fe/L) under rapid mixing and transferred into each of the SBRs. The stock iron solution (1 g Fe/L) was prepared by dissolving $FeCl_3 \cdot 6H_2O$ in Milli-Q water. The resulting Fe:P molar ratio was 2.6. The SBRs were equipped with pH control, aeration, and mechanical mixing and allowed to react (flocculate), waste, settle and decant. Table 4-2 summarizes the specific design parameters of the flash mix tank and the SBRs. SRT was controlled by adjusting the waste volumes weekly based on effluent and reactor solid concentrations, on the basis of the dynamic SRT model described by Takács et al. (2008).

Table 4-2: Process Design Parameters

Design Parameter	**Flash Mix Tank**
Volume (L)	12
Mixing (rpm)	350
Velocity Gradient (G) (s^{-1})	310
HRT	<2 minutes
Design Parameters	**SBRs**
Volume (L)	2.5
Feed Volume (L/cycle)	1.5
Decant Volume (L/cycle)	1.5
Mixing (rpm)	20
Airflow (mL/min)	> 80
pH	6.9 ± 0.1 adjustments made with 0.1 M NaOH and 0.1 M H_2SO_4
SRT (d)	2.8, 7.4, 10.8 and 22.8
HRT (h)	10
SBR sequence times	Feed (2mins), React (4.5hrs), Settle (1.25hrs), Decant (13mins)
SBR cycle times	4 cycles/day (6 hours each)

4.3.2 Sampling and Sample Preparation

Once steady state with respect to SRT was achieved in the reactors, HFO floc were collected for adsorption testing. HFO sampling involved taking a grab sample from the SBR during the react phase or from the flash mix tank while its contents were draining into the SBRs. The samples that were quantified for soluble P analysis were filtered immediately through a 0.45 μm nitrocellulose membrane filter (Whatman Millipore).

4.3.3 Adsorption Procedure

Batch adsorption experiments were carried out in a temperature controlled benchtop shaker (MaxQ™ 4000 Benchtop Orbital Shaker, Thermo Scientific) at 20°C. A volume of sample containing HFO was added to a polyethylene container and the pH was adjusted to 6.9. A pH controller was used to maintain the pH at 6.9 ± 0.03 throughout the experiment through addition of either 0.1 M H_2SO_4 or 0.1 M NaOH. The rate of stirring was consistent at 150 rpm, which was determined to provide just enough mixing to keep the flocs in suspension. At time 0, a volume of the P stock solution was dosed into the batch adsorption vessel. Table 4-3 lists all the P dosing concentrations tested for each type of HFO sample along with the HFO sample properties. Samples were taken for P analysis after a 24 hour equilibration time that has been

reported to achieve equilibrium in phosphate adsorption studies (Li and Stanforth, 2000). Data confirming the 24 hour equilibrium time will be shown in a subsequent chapter. The drawn samples were filtered immediately through a 0.45 μm nitrocellulose membrane filter (Whatman Millipore) and analyzed for soluble P.

Table 4-3: Summary of P Dosing and HFO sample properties

Sample	P Spikes (mg/L)	HFO Sample TSS (mg/L)
Flash	60, 40, 16, 4, 4, 3, 3, 2, 2, 1.6, 1.6, 1.6, 1.6, 1, 1, 0.5, 0.5	29 ± 7
A	64, 64, 60, 40, 16, 16, 4, 4, 2.5, 2.5, 1, 1, 1, 0.5, 0.5, 0.5, 0.5	251 ± 55
B	96, 96, 32, 16, 8, 8, 6, 6, 4, 4, 2, 2, 0.5, 0.5	465 ± 86
C	96, 96, 60, 32, 32, 16, 8, 8, 6, 6, 2, 2, 1, 1	968 ± 165
D	250, 96, 96, 32, 32, 12, 8, 8, 4	1854 ± 249

4.3.4 Desorption Procedure

Batch desorption tests were conducted to determine if P adsorption onto HFO was reversible. The desorption experiments were carried out in a temperature controlled benchtop shaker (MaxQ™ 4000 Benchtop Orbital Shaker, Thermo Scientific) at 20°C. The synthetic natural water (Table 4-1) without P was used as the aqueous medium. A volume of synthetic water was added to a polyethylene container and the pH was adjusted to 6.9. A pH controller was used to maintain the pH at 6.9 ± 0.03 throughout the experiment with additions of 0.1 M H_2SO_4 and 0.1 M NaOH. The rate of stirring was maintained at 150 rpm. At time 0, a volume of sample containing HFO was added to the desorption vessel. Samples were taken for P analysis after a 24 hour equilibration time. The drawn samples were filtered immediately through a 0.45 μm nitrocellulose membrane filter (Whatman Millipore) and analyzed for soluble P.

4.3.5 Sample Analysis

HFO samples were analyzed for soluble P and TSS prior to adsorption testing. All soluble P and TSS samples were collected and analyzed in duplicate. Soluble P concentrations were determined with the optimized ascorbic acid method (detection limit of 10 μg P/L) (Gilmore et al., 2009). A UV-Vis spectrophotometer (UV-1700, Shimadzu Corporation, Kyoto, Japan) with a 10 cm path length was used. Concentrations above 0.1 mg/L were analyzed according to Standard Method 4500-P.E (Standard Methods, 2005) with a 1 cm path length. All glassware

and plastic ware used were acid washed in a 10% v/v nitric acid solution overnight and rinsed with Milli-Q water. TSS concentrations were determined according to Standard Method 2540D (Standard Methods, 2005).

4.4 Results and Discussion

4.4.1 Adsorption Results

Equilibrium sorption behaviour is typically described mathematically by fitting soluble P results to a sorption capacity isotherm. The amount of adsorption or mass of P sorbed per mass of HFO solids was calculated with Equation (4-1):

$$q_e = \frac{P_o - P_e}{C_s} \qquad \text{(Equation 4-1)}$$

where q_e is the amount of adsorption of P onto the HFO at equilibrium (mg P/mg HFO), P_o is the initial soluble P concentration in the HFO sample including the dosed P and the background concentrations (mg P/L), P_e is the concentration of soluble P at equilibrium (mg P/L), and C_s is the concentration of HFO solids in the sample (mg TSS/L). Figure 4-3 shows the equilibrium sorption data for each reactor. The observed equilibrium sorption data will be discussed first while subsequent discussion will address the sorption isotherms. The raw sorption data are shown in Appendix B.

The characterization of the amount of P adsorption onto each type of HFO solid was expected to provide insight into the effects of solids age on adsorption. It is evident that the amount of adsorption onto the flash solids was much higher than that on the SBR solids (Figure 4-3). For example, with a P_e concentration of 10 mg P/L Figure 4-3 shows that the relative amounts of adsorption (q_e) were approximately 0.25 mg P/mg TSS onto the flash solids and from 0.02 to 0.04 mg P/mg TSS onto the SBR solids (i.e. A-D). In Figure 4-3 the amount of P adsorbed onto the flash solids plateaued around 0.25 mg P/mg TSS while the adsorption of P onto the SBR solids leveled off between 0.04-0.06 mg P/mg TSS. These results support the theory that aging limits surface sites available for binding and thus limits the sorption capacity of the solids (Dzombak and Morel, 1990; Smith et al., 2008a). The reduced P removal as a result of aging was in agreement with the experimental results reported by Mao et al., (2012), Szabó et

al., (2008) and Lijklema (1980). However the aging described in this study was over timeframes that were more typical of those associated with the solids in wastewater treatment.

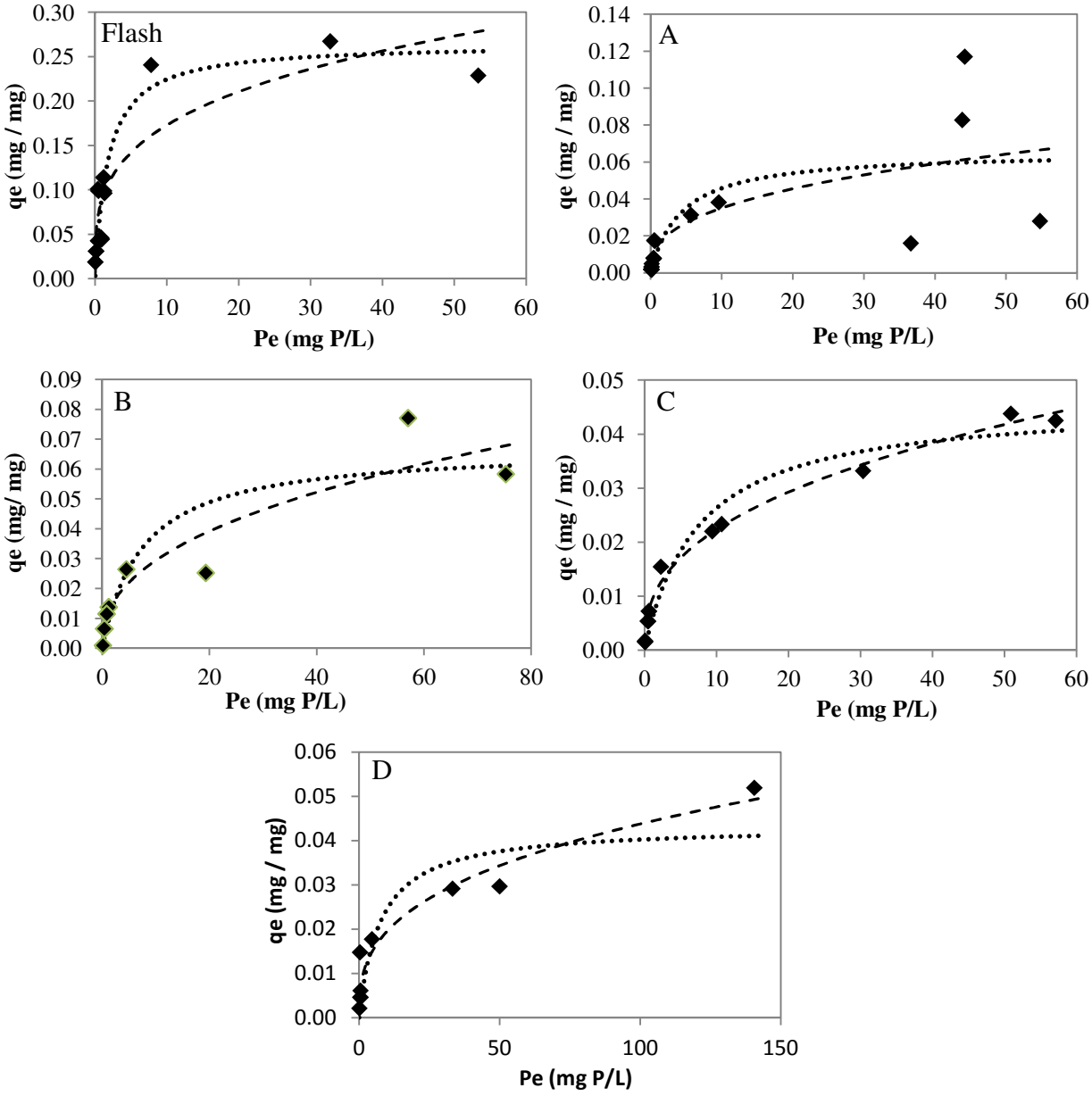

Figure 4-3: Observed equilibrium sorption data and isotherms. ♦ mg P/mg TSS - - Freundlich isotherm ·· Langmuir isotherm

It should be noted that the responses presented in Figure 4-3 were created assuming that the HFO solids had no prior P adsorbed on the surface (i.e. adsorption started at zero). This

approach facilitated the fitting of conventional isotherms (i.e. Freundlich and Langmuir). However, since the HFO samples were taken from each reactor after P addition it was assumed that an initial concentration of sorbed P existed on the HFO surfaces. Based on the experimental conditions, prior removal as a result of co-precipitation or adsorption could not be differentiated and thus the starting adsorbed concentration of HFO could not be accurately defined. Therefore, the responses reflect the additional sorption capacity (i.e. in addition to the P removed via sorption after P dosing). In practice, these results would reflect the additional sorption capacity available from HFO precipitates that were recycled through a wastewater treatment process.

Modelling the P uptake is an important tool to aid in the design of P removal systems. The observed equilibrium data were employed to fit the Langmuir (Equation 4-2) and Freundlich (Equation 4-3) isotherms using non-linear regression:

$$q_e = \frac{q_{\max} b P_e}{1 + b P_e} \qquad \text{(Equation 4-2)}$$

$$q_e = K P_e^{1/n} \qquad \text{(Equation 4-3)}$$

where q_{max} is the maximum adsorption capacity (mg P/mg solids), b is a constant relating to the net enthalpy of adsorption (Weber and DiGiano, 1996), K is a constant which indicates the sorption capacity at a specific solution-phase concentration (Weber and DiGiano, 1996), and 1/n is a constant representing a joint measure of the cumulative magnitude and diversity of energies associated with a particular adsorption reaction (Weber and DiGiano, 1996). Figure 4-3 illustrates the fit of each isotherm while Table 4-4 summarizes the parameter estimates along with the standard error (SE) and the 95% confidence interval (CI).

From Table 4-4 it can be seen that the magnitude of the parameter estimates for q_{max} and K in the flash tank were higher than the estimates of these parameters for the SBRs. This confirmed that adsorption was much higher in the flash tank in comparison to the SBRs. However, the values of q_{max} and K between the SBRs could not be differentiated due to overlapping 95% CIs. Further, the values of the Freundlich constant 1/n in the flash and SBR samples were indistinguishable based on CIs. The parameter estimates of b were higher in the flash sample

Table 4-4: Summary of estimated Langmuir and Freundlich parameter values.

	Langmuir Isotherm Values x10^3					
Sample	**q_{max}**	**SE**	**95% CI**	**b**	**SE**	**95% CI**
Flash	260	20	220, 310	560	120	310, 810
A	65	16	32, 99	230	280	-360, 830
B	67	9	48, 87	130	68	-14, 280
C	46	4	38, 54	130	38	50, 220
D	43	7	27, 60	130	100	-110, 380
	Freundlich Isotherm Values x10^3					
	K	**SE**	**95% CI**	**1/n**	**SE**	**95% CI**
Flash	90	10	69, 110	280	36	210, 360
A	15	7	-1, 30	380	140	77, 680
B	11	2	6, 16	410	52	300, 530
C	9	0.5	8, 10	390	15	360, 420
D	9	0.2	5, 13	350	46	240, 460

and in SBR A indicating a higher enthalpy of adsorption (Weber and DiGiano, 1996), but the values could not be differentiated between the remaining SBRs. These results were not consistent with the effluent results presented in Chapter 3. In Chapter 3, differences in effluent quality in the SBRs were statistically apparent at different SRTs. In addition, the SBR parameter estimates of q_{max} and K (Table 4-4) showed a trend similar to the effluent data (i.e. higher removal with SBR A and B). However, due to the uncertainty in the data the statistical methods did not differentiate between the SBRs. The differing conclusions may be attributed to the larger sample size of the effluent data in comparison to the sorption data. Pooling the sorption data and using the data simultaneously to model P sorption will be assessed subsequently (see Section 4.5) to determine if the pooled data can describe the expected changes in sorption behaviour with SRT.

In the analysis of the fit of the two different models, smaller values of the SE for the estimates were deemed to indicate that the model better fit the data. The SEs for the Freundlich parameter estimates were lower than the SEs for the Langmuir isotherm parameter estimates for each sample. Therefore, the Freundlich isotherm was suspected to better describe the observed adsorption responses. However, the magnitude of the SE values obtained with the Langmuir and Freundlich models were similar and hence, the practicality of using the SE for determining the best fit was limited. The residuals from the nonlinear regression were analyzed and found to be similar for both isotherms. The preferred model was therefore

selected on the basis of practical considerations of the usefulness of the model parameters and support from the literature. Although the Langmuir isotherm gives the ability to compare solids based on q_{max}, a clear plateau was not observed in the SBR samples (Figure 4-3). Similar to q_{max}, the Freundlich K term can also be used to quantify the extent of sorption and to make comparisons between different reactors (Weber and DiGiano, 1996). Further support for the use of the Freundlich isotherm was obtained from the literature. Kang et al. (2003) used the Freundlich isotherm to describe the adsorption of P onto ferrihydrite ($Fe_5HO_8 \cdot 4H_2O$), hematite (α-Fe_2O_3) and goethite. Further Weber and DiGiano (1996) reported that the Freundlich equation better described sorption data for environmental samples as compared to the Langmuir equation. This was attributed to the varying composition and surface matrix types (i.e. amorphous, condensed, crystalline) of environmental samples resulting in a varied distribution of reaction energies (Weber and DiGiano, 1996). Therefore, the Freundlich isotherms were selected to describe P sorption onto HFOs.

4.4.2 Desorption Results

P adsorption on chemical solids has been reported to result from chemisorption where phosphate ions replace hydroxide ions (Briggs, 1996) and hence desorption was expected to be negligible. However, batch desorption tests were conducted to evaluate this hypothesis. Preliminary desorption tests conducted with different concentrations of HFO solids showed that the final soluble P concentrations at the end of the tests were higher than the initial soluble P concentrations at the beginning of the tests indicating that desorption occurred. However, comparisons of the final soluble P concentrations between tests (i.e. with different HFO concentrations) showed that the concentrations were similar. Different soluble P concentrations were expected if desorption was the active mechanism. Therefore it was hypothesized that the differences in soluble P concentrations from the beginning to the end of the tests were not due to desorption but rather chemical equilibrium between the soluble P and sorbed P. To assess if desorption did occur, differences in the amount of P associated with the solids were calculated and compared. This calculation gave an indication of whether or not there was a significant difference in the amount of P sorbed onto the solids at the beginning of the test compared to

the end of the desorption test. Any differences in the amount of P sorbed from the beginning to the end of the test was deemed to be a result of desorption of P from the solids.

A conceptual schematic of the batch reaction vessel and HFO sample was developed to describe the calculation of changes in P in the batch desorption tests (Figure 4-4). The batch tests were conducted by adding HFO samples from the SBRs to natural synthetic water (See Section 4.3.4). From Figure 4-4 it can be seen that the resulting solution of HFO sample and natural synthetic water contained two types of P: P associated with the liquid phase ($P_{liquid,}$ mg/L) and P associated with the solid phase ($P_{solid,}$ mg/L). P_{liquid} accounted for soluble P while P_{solid} accounted for co-precipitated and sorbed P. The concentration of soluble P in the HFO sample was measured. The natural synthetic water contained no P. The initial soluble P concentration at the start of the batch test ($P_{liquid,i,}$ mg/L) was thus calculated using the soluble P concentration in the HFO sample and accounting for the dilution of the HFO sample with natural synthetic water. P_{solid} was not measured but was calculated by conducting a P balance on the HFO sample. The HFO samples from the SBRs were fed from the flash mix tank. The difference between the P concentration in the flash feed and the soluble P concentration in the

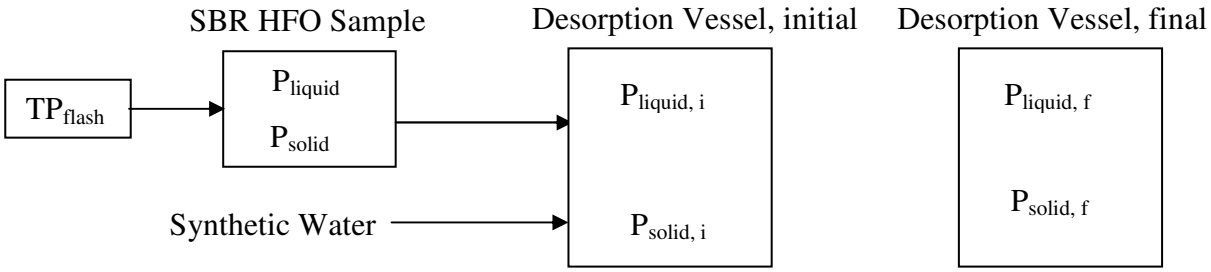

Figure 4-4: Schematic of Desorption Vessel and HFO sample

HFO sample indicated the amount of P that was taken up by the solids. The concentration of total P in the flash tank (TP_{flash}, mg/L) that fed the SBRs was measured. Hence, the concentration of P associated with the solids at the start of the batch test ($P_{solid,i}$, mg/L) was calculated by subtracting the concentration of P in the liquid phase from the concentration of TP in the flash feed (Equation 4-4).

$$P_{solid,i} = TP_{flash} - P_{liquid,i} \qquad \text{(Equation 4-4)}$$

At the end of the batch test a final soluble P concentration was measured. Therefore the final concentration of P associated with the solids ($P_{solid,f}$, mg/L) was calculated by subtracting the concentration of P in the liquid phase at the end of the test ($P_{liquid,f}$, mg/L) from the concentration of TP in the flash feed (Equation 4-5).

$$P_{solid,f} = TP_{flash} - P_{liquid,f} \quad \text{(Equation 4-5)}$$

Table 4-5 summarizes the means and standard deviations (std) of the calculated concentrations of P associated with the solids and the percent difference between initial and final concentrations for each SBR.

Table 4-5: Desorption summary

Sample	$P_{solid,i}$ (mg P/L) mean ± std	$P_{solid,f}$ (mg P/L) mean ± std	% Difference mean ± std
A	3.4 ± 7.4E-5	3.35 ± 1.1E-2	1.3 ± 3.3E-1
B	3.4 ± 1.2E-4	3.36 ± 4.8E-4	0.9 ± 1.7E-2
C	3.4 ± 1.6E-4	3.34 ± 1.3E-4	1.6 ± 4.5E-1
D	3.4 ± 7.8E-6	3.33 ± 2.8E-3	1.8 ± 8.3E-2

The initial and final concentrations of P associated with the HFO solids (Table 4-5) differed by less than 2% in each SBR and hence desorption was considered to be negligible in these tests. Therefore, the results support the hypothesis that the mechanism of P adsorption was chemisorption. Hence, the sorption isotherms should only be used to describe the loading of P onto solids. Subsequent dynamic modelling exercises will consider the lack of reversibility when describing the dynamic removal of P by HFO solids.

4.5 Sorption Model Development and Results

4.5.1 Model Development

The results presented in Chapter 3 indicated that the HFO solids aged as they were retained in the SBRs. Hence, the SBRs mixed liquors contained mixture of solids of differing properties (i.e. fresh and aged solids). Assuming that the aging of solids was kinetically limited it was hypothesized that the relative proportion of fresh and aged solids was a function of SRT. The higher SRT reactors would be expected to have a larger fraction of aged solids in comparison to fresh solids while the younger SRT reactors would have a larger fraction of fresh solids.

Since the composition of the solids in the SBRs could not be directly measured a model was developed to reflect sorption of P onto this mixture. The model was consistent with the general approach of Hauduc et al. (2013), integrating three types of HFO solids: high HFO, low HFO and old HFO, to describe P adsorption on HFO (Figure 4-1). High HFO have an open structure and high specific surface area while low HFO have a more compact structure and less available binding sites (Hauduc et al., 2013). The aging process involved high HFO aging to produce low HFO and low HFO aging to provide old HFO; old HFO were assumed to have no active surface sites and only contribute to the solids mass (Hauduc et al., 2013). It was hypothesized that the transformation of the solids with age would be proportional to the SRT such that the relative fraction of each type of HFO in the SBRs would increase or decrease with SRT as illustrated in Figure 4-5. Aging of High HFO to produce low HFO would decrease the proportion of High HFO with SRT and increase the proportion of low HFO. However, aging also transforms low HFO to old HFO so some of the HFO produced will also decrease with SRT while the fraction of old HFO increases with SRT. It was expected that the information on speciation of solids as a function of SRT would also provide indication of which conversion (i.e. High to Low or Low to Old) was rate limiting in the overall conversion of high HFO to old HFO.

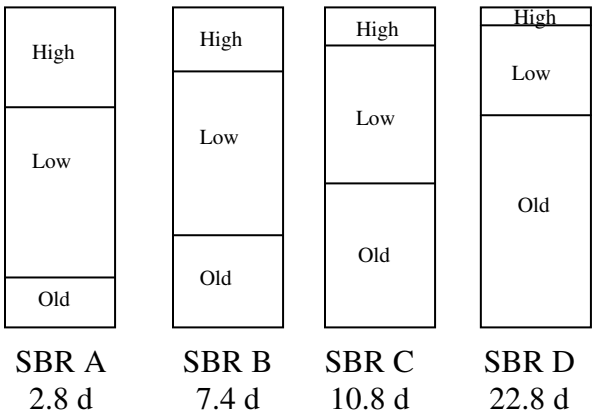

Figure 4-5: Conceptual Schematic of HFO fractions

The adsorption data collected were pooled together and used simultaneously to estimate the amount of each solid type that was present in a sample by matching the observed adsorption

isotherms. The total mass of solids (M_t) in each adsorption test was modeled as the sum of the masses of the 3 types of solids:

$$M_t = f_1 M_t + f_2 M_t + f_3 M_t \quad \text{(Equation 4-6)}$$

where,

$$f_1 = \frac{M_1}{M_t}, f_2 = \frac{M_2}{M_t}, f_3 = \frac{M_3}{M_t}$$

M_1, M_2, and M_3 represented the mass of high HFO, low HFO and old HFO (mg TSS), respectively; and f_1, f_2, and f_3 represented the fractions of high, low and old HFO, respectively. The total mass of P sorbed (X_t) in each sample was modeled as the sum of the contributions from each type of solid:

$$X_t = \sum_{i=1}^{3} X_1 + X_2 + X_3 \quad \text{(Equation 4-7)}$$

Where X_1, X_2 and X_3 represented the masses of P sorbed to each type of HFO solid (mg P). The Freundlich model was employed to describe the amount of sorption of P onto the HFO:

$$q_e = \frac{M_1 K_1 P_e^{1/n_1} + M_2 K_2 P_e^{1/n_2} + M_3 K_3 P_e^{1/n_3}}{M_1 + M_2 + M_3} \quad \text{(Equation 4-8)}$$

where P_e was the soluble P concentration determined after a 24 hour equilibration period in each adsorption test (mg P/L). All the batch adsorption data from all of the reactors were pooled together and used simultaneously to generate q_e values for the model fitting exercise (Appendix B). Hence, the data set contained 71 data points that included replicated tests over a range of P doses.

Some assumptions were made with respect to the distribution of the types of solids (f_1, f_2, f_3) in each reactor and the contribution of the types of solids to the adsorption process. Based on the mixing intensity provided in the flash tank, the flash HFO were assumed to only consist of High HFO (f_1). Therefore for the flash samples f_1 was set to a value of one while f_2 and f_3 were set to zero. Old HFO were defined to have no active sorption sites (Hauduc et al., 2013) and hence the old HFO were assumed to not participate in the sorption reaction. This was achieved by setting K_3 and $1/n_3$ to zero. Global estimates of K_1, K_2, $1/n_1$, $1/n_2$, f_1, f_2, and f_3 were then obtained by minimizing the root mean square error (RMSE) between experimental q_e values (i.e. q_e calculated from Equation 4-1) and q_e predicted from Equation (4-8) using Excel Solver.

Similar responses were obtained for the nonlinear regression model using several initial guesses for the estimates of K_1, K_2, $1/n_1$, $1/n_2$, f_1, f_2, and f_3 for each SBR thereby providing confidence in methodology to obtain the best possible parameter values.

4.5.2 Model Results and Discussion

The performance of the model was initially assessed with respect to the quality of the fit. This included an analysis of the observed and predicted values. The uncertainty was then addressed by examining the uncertainty of the fit parameters (i.e. SE on K_1, K_2, $1/n_1$, $1/n_2$ and the solids fractions). A Monte Carlo procedure was used to determine the parameter confidence intervals for the non-linear regression model according to the method outlined by Lambert et al. (2012). The method by Lambert et al. (2012) involved fitting the predictive model (Equation 8) to the observed q_e values using Excel Solver to obtain the initial best fit parameters and the RMSE of the fit. The RMSE was then used to generate a set of random numbers, assuming a normal distribution with a mean of zero and a standard deviation equal to the RMSE, which were added to the predicted data. The predictive model (Equation 4-8) was then applied to multiple random data sets simultaneously to generate multiple values (n = 96) of best fit parameters which were statistically analyzed to obtain the mean, SE and 95% CIs.

Figure 4-6 illustrates the observed and predicted values determined from the Monte Carlo procedure. Since a broad range of P_e values were estimated the observed and predicted data at the lower concentrations ranges could not be visualized simultaneously. Therefore, the observed and predicted values are shown in Figure 4-6 using the overall data set and the data at the lower ranges. Figure 4-6 includes all 71 data points separated out for each SBR. Table 4-6 summarizes the estimated model parameters, the solids fractions and measures of model fit. The estimated parameters were determined to be non-normally distributed with the exception of K_1, K_2, and $1/n_1$ which were determined to follow a normal distribution. Therefore, non-normally distributed estimates were described in Table 4-6 using the median values along with the 95% CI around the median value while normally distributed estimates were described using the mean and 95% CI around the mean.

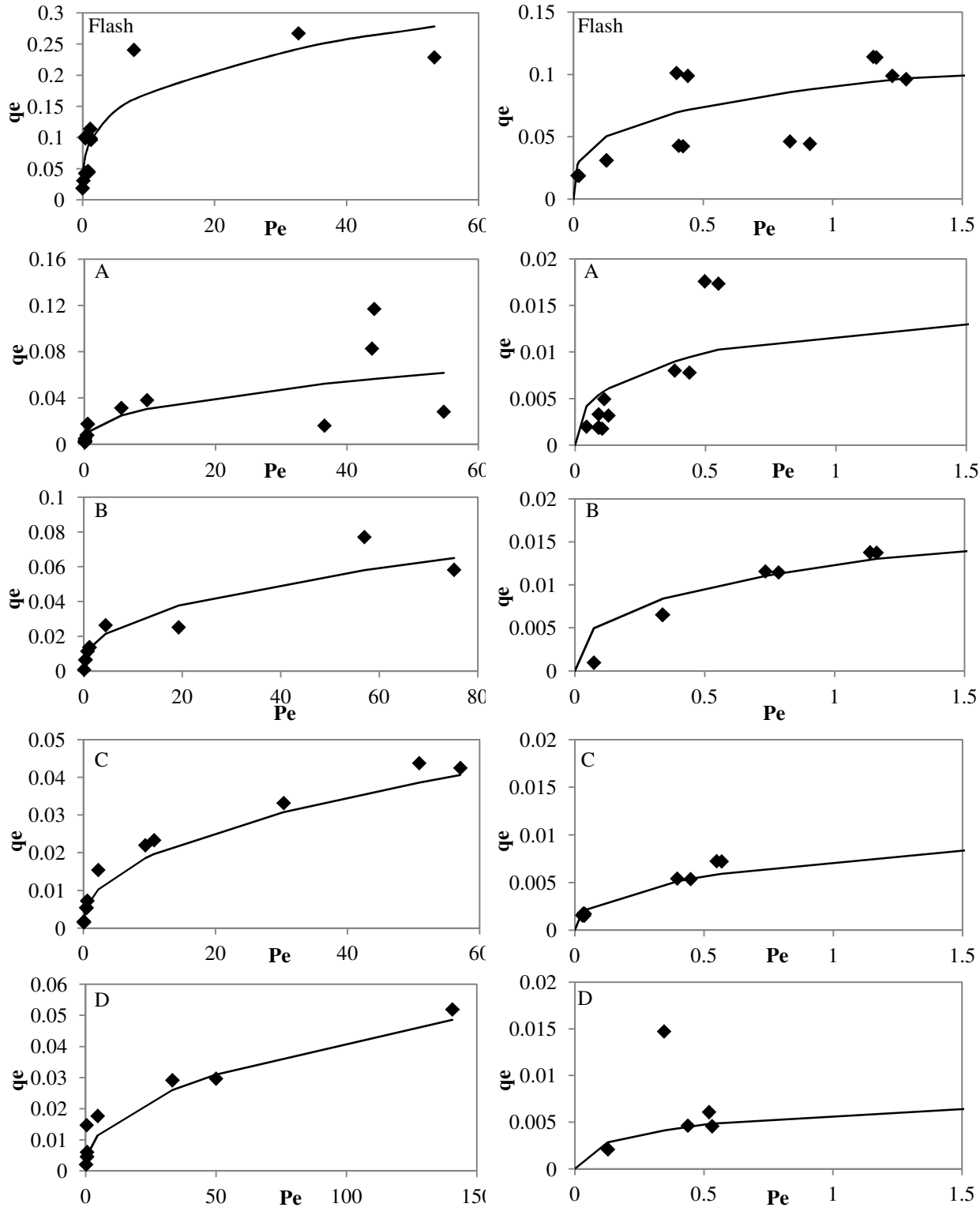

Figure 4-6: Observed vs. Predicted Equilibrium Adsorption. The left hand side shows the entire data set. The right hand side shows the low range data. ♦ observed data – predicted data

Table 4-6: Adsorption model parameter estimates. Estimates based on Monte Carlo procedure by Lambert et al. (2012).

Parameters	Mean x10^3	Lower 95% CI	Upper 95% CI
K_1	90	89	92
K_2	12	11	13
$1/n_1$	280	278	288
Parameters	**Median x10^3**	**Lower 95% CI**	**Upper 95% CI**
$1/n_2$	490	470	530
SBR A			
f_1	81	71	110
f_2	420	400	440
f_3	480	460	490
SBR B			
f_1	84	72	100
f_2	360	340	380
f_3	530	530	550
SBR C			
f_1	37	21	56
f_2	330	310	340
f_3	630	610	640
SBR D			
f_1	33	14	56
f_2	250	240	260
f_3	700	690	720

From Figure 4-6 it can be seen that the calibrated model was able to reasonably represent the observed data in each reactor in both the lower and higher concentration ranges. The estimated values of the model parameters were then examined to obtain insight into the mechanisms responsible for P adsorption. From Table 4-6 it can be seen that the estimated value of K_1 was much higher than K_2 indicating that more adsorption occurred onto the High HFO as compared to the Low HFO. These results supported the expected performance of each of these solid fractions since Low HFO were expected to have fewer sorption sites then High HFO and thus were expected to contribute less to P adsorption.

The solids fractions in the SBRs were compared using the nonparametric Mann Whitney test. Within each SBR, all of the solids fractions were found to be statistically different. The Old HFO represented the highest fraction of HFO and High HFO represented the smallest fraction. Comparing the fractions of High HFO between reactors, the fractions in SBR A and B were

higher than in SBR C and D. However, there were no differences between estimates from SBRs A and B and between SBRs C and D. These results were consistent with the statistical trends in effluent quality found in Chapter 3 where SBR A and B had statistically higher P removal than SBRs C and D. The fractions of Low and Old HFO were found to be different in each SBR.

Figure 4-7 further illustrates the relationship between solids fractions and SRT. Figure 4-7 shows that the trends in the solids fraction in the SBRs were consistent with the previously described conceptual model. The fraction of High HFO decreased at higher SRT. This was expected since higher SRT systems contain a larger proportion of aged solids. The fraction of Low HFO also decreased with SRT. This corresponded to the adsorption capacities that decreased with increasing SRT. The fraction of Old HFO increased with SRT which was consistent with the adsorption capacities that decreased with increasing SRT.

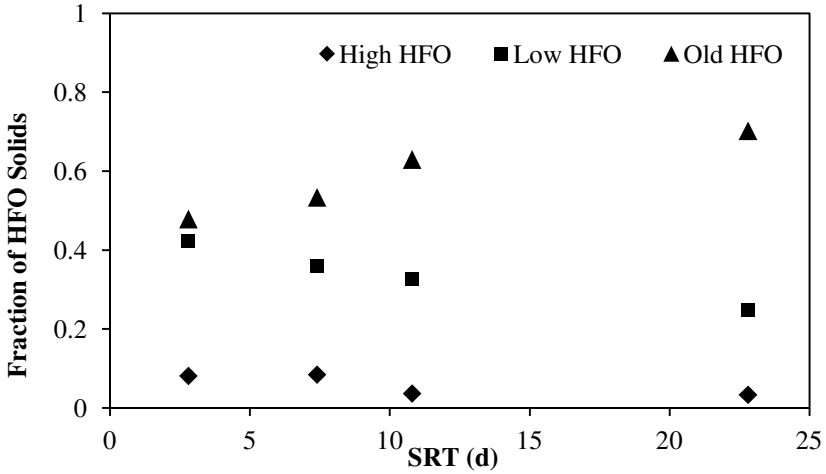

Figure 4-7: Fraction of HFO solids vs. SRT.

Insight into the rates of transformation of the solids from High to Low and Low to Old can also be inferred from the results presented in Figure 4-7. It is hypothesized that low HFO was produced from aging of High HFO and subsequently transformed by aging to produce Old HFO. Since the Low HFO fraction decreased with SRT, it would appear that the rate of transformation of Low HFO into Old HFO was greater than the rate of production of Low HFO

by aging of High HFO. Therefore, it was concluded that transformation of High HFO into Low HFO was the rate limiting step in the overall transformation of high HFO to old HFO.

In order to understand how the different fractions of HFO contributed to overall P adsorption, the mass of P sorbed onto each fraction of HFO was determined for each SBR solid using a P_e value of 0.1 mg P/L and the average TSS concentrations for each SBR as the estimates of M_t. Figure 4-8 summarizes the amount of P sorbed onto the High and Low HFO in each SBR. From Figure 4-8, it can be seen that the mass of P sorbed on the High HFO was consistently higher for all SBRs. Hence, High HFO contributed more to P sorption than Low HFO in each SBR despite the relatively low fraction that high HFO contributed to the overall SBR solids. These results imply that the majority of P uptake observed in the SBRs and in the batch sorption tests was a function of the fresh solid contribution from the flash mix tank rather than the aged solids in the reactor.

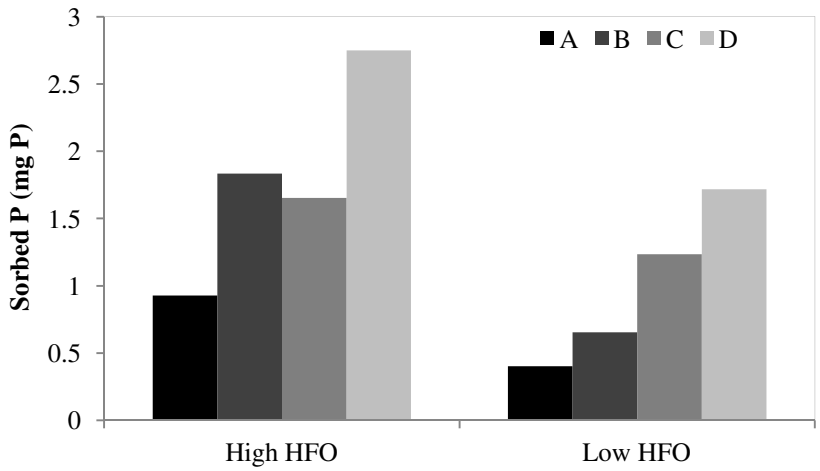

Figure 4-8: Mass of P sorbed onto High and Low HFO in each SBR.

4.6 Conclusions

The sorption of soluble P onto HFO solids of different ages was explored. The conclusions of this study are:

- Fresh HFO have a higher sorption capacity in comparison to aged (2.8, 7.4, 10.8 and 22.8 day) HFO.

- P adsorption onto HFO solids was determined to be best described by the Freundlich isotherm.
- P desorption from HFO solids was negligible supporting chemisorption as the mechanism of P adsorption.

A model was developed to characterize the fractions of HFO solids (i.e. High, Low and Old) that existed at different solids ages, their relative contributions to adsorption and the relationship between HFO solid type and SRT. The model adequately described the adsorption behaviour of soluble P onto HFO solids of different ages. From the model it was determined that:

- The fractions of High and Low HFO decrease with SRT while the fractions of Old HFO increase with SRT.
- The rate of transformation of High HFO into Low HFO appears to be lower than the rate of transformation of Low HFO into Old HFO.
- High HFO contributed more to P sorption than Low HFO in each SBR implying that the fresh flash solids were more responsible for the observed P uptake in the SBRs in comparison to the aged SBR solids.

CHAPTER 5

5. THE EFFECT OF SOLIDS RESIDENCE TIME ON TRANSIENT RESPONSES IN CHEMICAL P REMOVAL

5.1 Overview

The impact of SRT on the dynamics of P removal by HFO solids under 3 different conditions (i.e. uptake during the react cycle of an SBR when operated under steady state and dynamic conditions and in batch tests with preformed solids) was characterized. The results showed that P removal in the SBRs and batch sorption tests was characterized by an initial period of fast removal followed by a period of slower removal until pseudo-equilibrium was reached. The initial rate of removal (i.e. change in the soluble P concentration with respect to time) increased with increasing influent P concentrations. These results were attributed to a larger concentration gradient between the soluble and sorbed phase concentrations leading to a greater initial rate of change. The performance of the SBRs in terms of the equilibrium soluble P achieved at low P loadings (i.e. 3.4 and 6.4 mg P/L; 2.6 and 1.4 mol P/mol Fe) under both transient and steady state operation were consistent with the results reported in Chapter 3. The low SRT (i.e. less than 22.8-26.6 days) SBRs (i.e. A through C) achieved lower soluble P concentrations than the high SRT (i.e. 22.8- 26.6 days) SBR (i.e. SBR D). However, under transient operation SBR D provided the highest P removal at high P loadings (i.e. 16.1 and 82 mg P/L; 0.5 and 0.1 mol P/mol Fe). A model was developed to describe the overall dynamic behaviour of P sorption onto HFO floc. The model was found to provide a good description of P removal in the SBRs and batch tests. Differences in process conditions between tests (i.e. mixing) were reflected in the estimates of the rate coefficients (k). It was found that over a range of SRTs (i.e. 2.8 - 26.6 days) the same rate coefficient could be used to describe P adsorption onto HFO floc. Discrepancies in the estimates of k were attributed to the inconsistent behavior of SBR D at elevated loadings.

5.2 Introduction

Characterization and modelling of the physical and chemical processes involved in attaining extremely low P concentrations with hydrous ferric oxides (HFO) has been the focus of recent

research (Smith et al., 2008a; Szabó et al., 2008; Newcombe et al., 2008b; Weng et al., 2012; Mao et al., 2012; Hauduc et al., 2013). Models that characterize the interactions between P and metal salts have been developed by Ferguson and King (1977), Luedecke et al. (1989), Briggs (1996), WEF (1998), Smith et al. (2008a) and Hauduc et al. (2013). The models that have been developed have improved the ability to predict residual PO_4^{3-} concentrations when extremely low P concentrations are targeted, however they do not address the impacts of aging and solids residence time on removal kinetics. The model limitations stem from the lack of information on the effects of aging of chemical precipitates and the role of solids contact times at solids residence times typical of wastewater solids on P removal (Benisch et al., 2013). In particular there is limited dynamic information related to the impact of aging on the rates at which P adsorbs. There is also limited information on the kinetics of removal.

The kinetics of P removal onto HFO has also been studied by Szabó et al. (2008), Mao et al. (2012) and Zeng et al. (2004). Szabó et al. (2008) studied P removal as a result of co-precipitation and adsorption following ferric chloride addition and due to adsorption onto preformed HFO flocs while Mao et al. (2012) and Zeng et al. (2004) studied the kinetics of P adsorption onto preformed HFO flocs. The kinetics of P removal were characterized by an initial fast removal occurring in under one minute (i.e. instantaneous removal) followed by a much slower subsequent uptake (i.e. hours or days) (Szabó et al., 2008). Mao et al. (2012) showed that the adsorption of dissolved P onto fresh HFO reached pseudo-equilibrium in the first hour.

Empirical models such as the Elovich, first-order, second-order, power function, intraparticle diffusion, and parabolic diffusion models have been employed to describe adsorption kinetics (Table 5-1). Zeng et al. (2004) showed that the Elovich equation provided satisfactory fitting of the kinetic data of P adsorption onto iron oxide tailings. These findings were consistent with the P sorption kinetics observed by Sparks (1989) and Chein and Clayton (1980) in soils. However, application of these models (Table 5-1) is limited to the fitting of experimental results with limited application to continuous flow reactor systems. Further research into the application of sorption kinetics into wastewater systems which are transient and dynamic in nature is required to better describe P sorption behaviour.

Table 5-1: Kinetic Models (adapted from Yu et al., 2012 and Zeng et al., 2004)

Model Name	Model Equation
First Order	$\log(q_{e,exp} - q) = logq_{e,cal} - \frac{k_1 t}{2.303}$
Second Order	$\frac{t}{q} = \frac{1}{k_2 q_{e,cal^2}} + \frac{t}{q_{e,cal}}$
Intra-particle diffusion	$q = k_d t^{0.5} + D$
Power function	$q = at^{b_a}$
Parabolic Diffusion	$\frac{q}{t} = a + \frac{b_a}{t^{1/2}}$

The objective of this work was to characterize the impact of SRT on the dynamics (i.e. change of concentration with respect to time) of P removal under steady state and transient conditions. Samples were obtained from lab scale continuous flow sequencing batch reactors (SBRs) using synthetic natural water under: (1) steady state operation at high and low influent P concentrations and, (2) transient operation when influent P was stepped up for one feed cycle. Dynamic batch sorption measurements were carried out with HFO samples obtained from the lab scale SBRs during steady state operation under low influent P concentrations. A model to describe the overall dynamic behaviour of P sorption onto HFO floc was developed and employed.

5.3 Approach

5.3.1 Experimental Set-up

Dynamic experiments were conducted in four (reactor A, B, C and D) continuously operating SBRs located at Environment Canada's Wastewater Technology Centre (Burlington, Ontario). Each SBR was operated at one of four SRTs. A schematic of the lab scale system is shown in Figure 5-1. Dynamic tests were conducted when the SBRs were operating at a steady state (under high and low influent P concentrations) and under transient conditions. Additional batch adsorption dynamic testing was conducted with SBR samples that were collected during the steady state operation phase under low influent P concentrations.

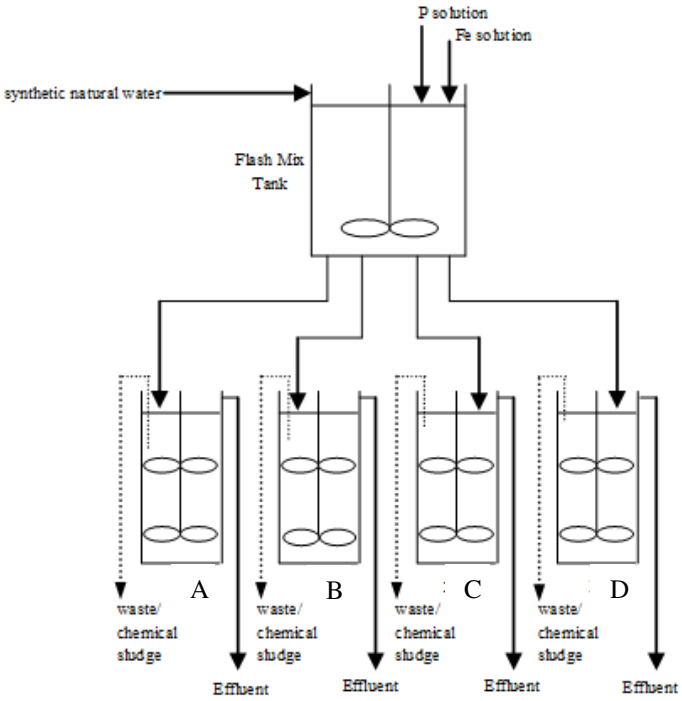

Figure 5-1: Simplified Process Schematic

The SBRs were fed from a common flash mix tank that was fed with a synthetic natural water adapted from a recipe by Environment Canada (1990). The recipe (Table 5-2) was modified to provide an alkalinity typical of wastewater and to include phosphate. A volume of stock phosphate solution was introduced into the flash mix tank via a fluid metering (FMI) pump. Stock phosphate solution (1 g PO_4^{3-}/L) was prepared by dissolving KH_2PO_4 in Milli-Q water. Phosphate concentrations under steady state and transient testing are provided. All chemicals used were reagent grade or better. All solutions were prepared with ultra pure water (Milli-Q, 18 MΩ).

The synthetic feed water in the flash tank was dosed with a stock iron solution (Mean: 16.1 mg Fe/L; 95% CI 13.3-19.0 mg Fe/L) under rapid mixing and was subsequently transferred into each of the SBRs. The stock iron solution (1 g Fe/L) was prepared by dissolving $FeCl_3 \cdot 6H_2O$ in Milli-Q water. The resulting iron: P ratios listed in order of increasing influent P dose were 2.6, 1.4, 0.5, and 0.1 mol Fe/mol P. The SBRs were equipped with pH control, aeration, and mechanical mixing and allowed to react (flocculate), waste, settle and decant. Table 5-3 summarizes the specific design parameters of the flash mix tank and the SBRs. SRT was

controlled by adjusting the waste volumes weekly based on effluent and reactor solid concentrations, on the basis of the dynamic SRT model described by Takács et al. (2008).

Table 5-2: Synthetic natural water recipe

Constituent	Concentration (mg/L)
sodium bicarbonate ($NaHCO_3$)	384
calcium sulfate di-hydrate ($CaSO_4.2H_2O$)	120
magnesium sulfate ($MgSO_4$)	120
potassium chloride (KCl)	8
phosphate (PO_4^{3-})	**Steady State Phase**
High influent P concentration	Mean: 6.4 mg P/L, 95% CI: 6.2-6.6 mg P/L
Low influent P concentration	Mean: 3.4 mg P/L, 95% CI: 2.35-4.51 mg P/L
Transient Phase – One time doses	6.4 mg P/L
	16.1 mg P/L
	82 mg P/L
Alkalinity	268.2 ± 9.8 mg/L as $CaCO_3$
pH	7.6-8.0

Table 5-3: Process Design Parameters

Design Parameter	Flash Mix Tank
Volume (L)	12
Mixing (rpm)	350
Velocity Gradient (G) (s^{-1})	310
HRT	<2 minutes
Design Parameters	**SBRs**
Volume (L)	2.5
Feed Volume (L/cycle)	1.5
Decant Volume (L/cycle)	1.5
Mixing (rpm)	20
Airflow (mL/min)	> 80
pH	6.9 ± 0.1 (adjustments made with 0.1 M NaOH and 0.1 M H_2SO_4)
SRT (d)	Low Influent P: 2.8 (A), 7.4 (B), 10.8 (C), 22.8 (D)
	High Influent P: 3.1 (A), 6.9 (B), 14.3 (C), 26.6 (D)
HRT (h)	10
SBR sequence times	Feed (2mins), React (4.5hrs), Settle (1.25hrs), Decant (13mins)
SBR cycle times	4 cycles/day (6 hours each)

5.3.2 Experimental Plan

The objective of the testing was to explore the time varying responses of chemical P removal under different process conditions (i.e. during steady state operation of the SBRs, during transient operation of the SBRs, and during batch adsorption experiments). Under steady state and transient operation of the SBRs the dynamic experiments were carried out after the influent

P concentration in the flash mix tank had been reacted with the iron dose. Therefore, the dynamic experiments under these process conditions accounted for the residual adsorption of P in the SBRs and not the co-precipitation of P in the flash mix tank. In a wastewater treatment plant removal under both of these process conditions is indicative of Fe addition in a rapid mix tank prior to the aeration basin and the subsequent removal provided by both the freshly dosed HFO and existing HFO solids in the aeration basin. Steady state operation of the SBRs provided information on P removal indicative of a constant influent P loading condition. Dynamic testing during the steady state operation of the SBRs provided a baseline for comparison purposes. As such, the effects of process conditions on P removal could be determined and compared. Transient operation (i.e. non-steady state operation) of the SBRs provided information on how the SBRs and hence P removal proceeded in response to a variable influent P loading. In contrast, batch adsorption experiments provided information on the adsorption of P onto preformed solids. In a wastewater treatment plant this would be indicative of Fe dosing after the aeration basin such that the influent P is contacted with recycled chemical solids in the aeration basin. The batch adsorption experiments facilitated an assessment of whether removal in the SBRs could be predicted from batch testing.

5.3.2.1 Test Procedure – Steady State Operation

Grab samples were collected periodically from the SBRs during the react, settle, and decant phase to characterize the dynamics of P removal while the SBRs were operating at a steady state condition (under high and low influent P concentrations). The first sample was taken from the flash mix tank while its contents were draining into the SBRs. This was considered time zero. Samples were immediately centrifuged (Sorvall ST 16 Centrifuge Series, Thermo Scientific) prior to filtration through a 0.45 μm nitrocellulose membrane filter (Whatman Millipore). Samples were analyzed for soluble P.

5.3.2.2 Test Procedure – Batch Adsorption Experiments

During steady state operation at low influent P concentrations HFO floc were collected for batch adsorption testing. HFO sampling involved taking a grab sample from the respective SBR during the react phase or from the flash mix tank while its contents were draining into the SBRs. HFO samples were analyzed for soluble P and TSS prior to adsorption testing. The

samples that were quantified for soluble P analysis were filtered immediately through a 0.45 μm nitrocellulose membrane filter (Whatman Millipore).

Batch dynamic adsorption experiments were carried out in a temperature controlled benchtop shaker (MaxQ™ 4000 Benchtop Orbital Shaker, Thermo Scientific) at 20°C. A volume of sample containing HFO was added to a polyethylene container and the pH was adjusted to 6.9. A pH controller was used to maintain the pH at 6.9 ± 0.03 throughout the experiment through addition of either 0.1 M H_2SO_4 or 0.1 M NaOH. The rate of stirring was consistent at 150 rpm, which was determined to provide just enough mixing to keep the flocs in suspension. At time zero, a volume of the P stock solution was dosed into the batch adsorption vessel. Table 5-4 lists all the P dosing concentrations tested for each type of HFO sample along with the HFO solid concentrations. Samples were taken for P analysis at various time intervals over a 6 hour timeframe and a final sample was taken after 24 hours. A 24 hour equilibration time has been reported to achieve equilibrium in phosphate adsorption studies (Li and Stanforth, 2000). Data confirming the 24 hour equilibrium time will be shown with the sorption results below. Drawn samples were filtered immediately through a 0.45 μm nitrocellulose membrane filter (Whatman Millipore) and analyzed for soluble P.

Table 5-4: Summary of P Dosing and HFO sample properties

Sample	P Doses (mg/L)	HFO Sample TSS (mg/L)
Flash	3, 3, 2, 2, 1, 1, 0.5, 0.5	29 ± 7
SBR A	4, 4, 2.5, 2.5, 1, 1, 0.5, 0.5	251 ± 55
SBR B	8, 8, 4, 4, 2, 2, 0.5, 0.5	465 ± 86
SBR C	8, 8, 6, 6, 2, 2, 1, 1	968 ± 165
SBR D	12, 8, 8, 4	1854 ± 249

5.3.2.3 Test Procedure – Transient Operation

The transient operation of the SBRs involved stepping up the concentration of P in the SBRs from steady state under low influent P concentrations by changing the influent P concentration of the synthetic water in the flash mix tank over one SBR cycle (Table 5-2). Following the step-up operation, the inputs into the SBR were returned to the original dosing conditions for all subsequent cycles until steady state concentrations of P were recovered (i.e. loading was stepped down to the original low influent P concentration). Once all effluent P concentrations

were close to their respective steady state values the next dose of influent P concentration was administered.

Dynamic sampling for soluble P involved taking grab samples from the SBRs at various time intervals during the react, settle and decant phase. The first sample at time zero was taken from the flash tank while its contents were draining into the SBRs. Samples were immediately centrifuged (Sorvall ST 16 Centrifuge Series, Thermo Scientific) prior to filtration through a 0.45 μm nitrocellulose membrane filter (Whatman Millipore). Since relatively high influent P dose concentrations were used (Table 5-2) all P samples required dilution prior to analysis.

5.3.3 Sample Analysis

All soluble P and TSS samples were collected and analyzed in duplicate. Soluble P concentrations were determined with the optimized ascorbic acid method (detection limit of 10 μg P/L) (Gilmore et al., 2009). A UV-Vis spectrophotometer (UV-1700, Shimadzu Corporation, Kyoto, Japan) with a 10 cm path length was used. Concentrations above 0.1 mg/L were analyzed according to Standard Method 4500-P.E (Standard Methods, 2005) with a 1 cm path length. All glassware and plasticware used were acid washed in a 10% v/v nitric acid solution overnight and rinsed with Milli-Q water. TSS concentrations were determined according to Standard Method 2540D (Standard Methods, 2005).

5.4 Results and Discussion

5.4.1 Steady State Operation

Dynamic experiments with the SBRs operating under steady state conditions were conducted to characterize the rate at which P was taken up during the react phase. Figure 5-2 illustrates the soluble P concentration versus time in the SBRs during steady state operation under low influent P concentrations (i.e. 3.4 mg P/L). The SRTs in the SBRs were 2.8 days (A), 7.4 days (B), 10.8 days (C) and 22.8 days (D). Figure 5-3 shows the changes in soluble P concentration with respect to time in the SBRs during steady state operation under high influent P concentrations (i.e. 6.4 mg/L). The SRTs in the SBRs during the high P concentration operation were 3.1 days (A), 6.9 days (B), 14.3 days (C) and 26.6 days (D). The initial soluble

P concentration in each of the reactors at time zero (Figures 5.2 and 5.3) was estimated on the basis of a mass balance as described in Equation (5-1):

$$P_i = \frac{P_{flash} \times V_{flashfeed}}{V} + P_b \qquad \text{(Equation 5-1)}$$

where P_{flash} is the soluble P concentration in the flash tank effluent (mg/L), $V_{flashfeed}$ is the volume of feed from the flash tank entering the SBRs (L), V is the volume in the SBRs (L) and P_b is the background concentration in the SBR corresponding to the final soluble P concentration in the SBR from the previous cycle (mg/L). Equation (1) accounted for the dilution of the measured soluble P concentration in the flash effluent upon entering the SBRs as well as the background concentration of soluble P in the SBRs. Both Figure 5-2 and 5-3 illustrate the observed data as well as a model simulation. The observed data will be discussed first while subsequent discussion will address the model simulation (Section 5.5).

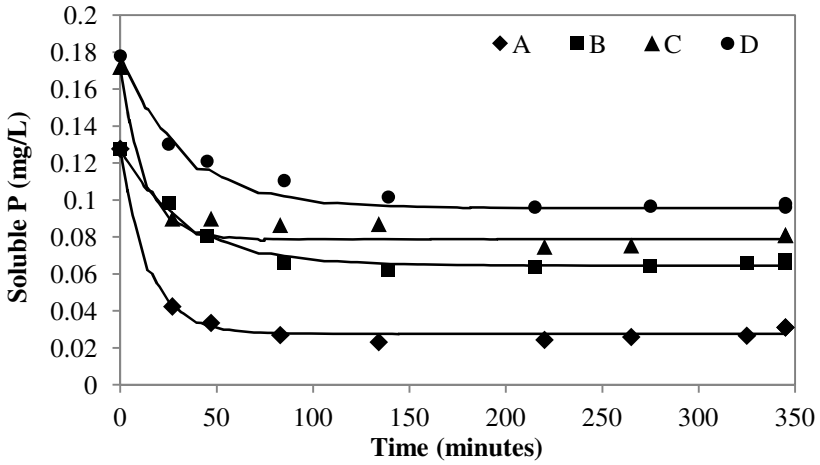

Figure 5-2: Soluble P versus time in SBRs under low influent concentrations (3.4 mg P/L).

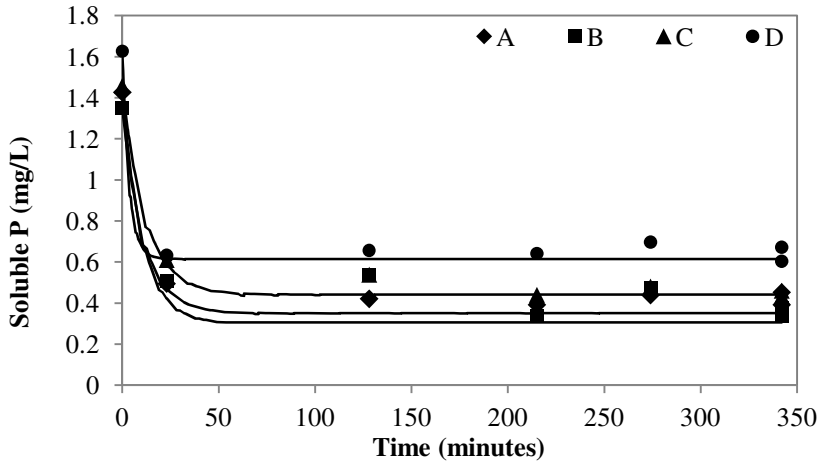

Figure 5-3: Soluble P versus time in SBRs under high influent concentrations (6.4 mg P/L).

The results presented in Chapter 3 indicated that the majority of P removal occurred instantaneously in the flash mix tank as a result of co-precipitation, while subsequent uptake in the SBRs was much smaller and attributed to slower adsorption/surface complexation reactions. From Figures 5-2 and 5-3, it can be seen that the removal of P in the SBRs was characterized by an initial fast removal in the first 25 minutes followed by a slower removal over time until approximately 100 minutes. Pseudo-equilibrium was reached after approximately 100 minutes. These results are consistent with the sorption kinetics observed by Szabó et al. (2008), Mao et al. (2012) and Zeng et al. (2004). However, in the current study pseudo-equilibrium was reached after a longer period of time (i.e. 100 minutes) in comparison to the 60 minutes observed by Mao et al. (2012).

In addition to the transient responses that will be subsequently described the data presented in Figures 5-2 and 5-3 provided insight into the final effluent properties of the SBRs. Performance was evaluated based on the equilibrium concentration of soluble P achieved in each SBR. Under low influent P concentrations (Figure 5-2) the performance of the SBRs increased with decreasing SRT where SBR A achieved the lowest final soluble P concentration. The dynamic performance results for SBR A were consistent with the effluent soluble P concentrations achieved under previous steady state testing in Chapter 3, however, the final concentrations in SBR B through D were higher than the results summarized in

Chapter 3. Under high influent P concentrations (Figure 5-3) SBRs A through C achieved the lowest soluble P concentrations in comparison to SBR D. These results were consistent with the effluent soluble P concentrations reported under steady state testing in Chapter 3. The modest differences between the results summarized in Chapter 3 and those presented in Figures 5-2 and 5-3 were attributed to the fact that the former values represented results that were compiled over a long timeframe while the latter values represented results from a single day of testing.

In order to characterize the rates of P removal (r_p, mg/L/min) a finite difference approximation was used (Equation 5-2):

$$r_p = \frac{dP}{dt} \cong \frac{\Delta P}{\Delta t} = \frac{P_j - P_{j+1}}{t_{j+1} - t_j} \qquad \text{(Equation 5-2)}$$

where j+1 corresponded to one time step ahead of the current time step j. The change in soluble P concentration with respect to time corresponded to the rate of removal of P as a result of the mechanism of adsorption. Adsorption is a concentration gradient driven liquid-solid mass transfer phenomena (Metcalf & Eddy, 2003). The kinetics of adsorption typically consists of three steps: (1) diffusion of the adsorbate (i.e. soluble P) through a fluid film (i.e. boundary layer) surrounding the adsorbent (i.e. HFO) particle, (2) diffusion into the particle (intraparticle/pore), and (3) adsorption onto the surface site (Teng and Low, 2012; Chorover and Brusseau, 2008; Metcalf & Eddy, 2003; Watson, 1999). Figures 5-4 and 5-5 illustrate the rates at which soluble P decreased with respect to time as determined from Equation (5-2) in each SBR under low and high influent P concentration respectively.

From both Figures 5-4 and 5-5 it can be seen that the initial rates of removal were generally much higher in comparison to subsequent values. An exception was observed in SBR B under low influent P concentrations where the rate of removal appeared to steadily decline with respect to time. Under low influent P concentrations, the initial rates were similar for SBR A and C and higher in comparison to the initial rates for SBR B and D. After 50 minutes, the final rates were similar in all the SBRs. Under high influent P concentrations, both the initial and final rates were similar in all the SBRs. A comparison of the rates under low (Figure 5-4) and high (Figure 5-5) influent P concentrations showed that the initial rate of removal was greater

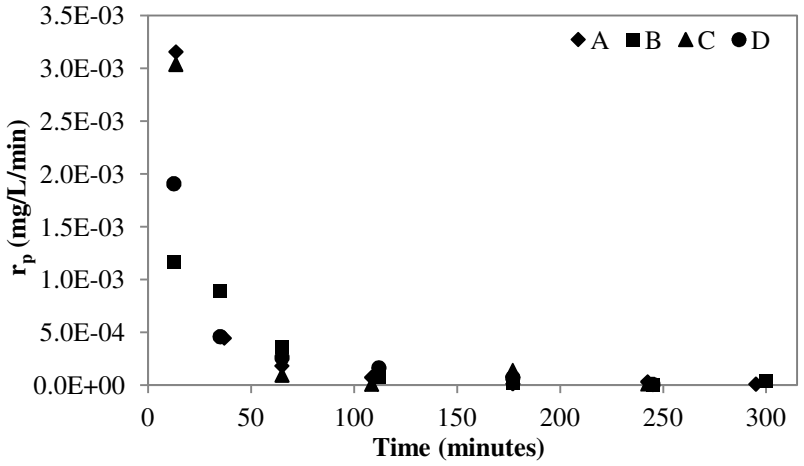

Figure 5-4: The rate of change of soluble P with respect to time in the SBRs under low influent concentrations (3.4 mg P/L).

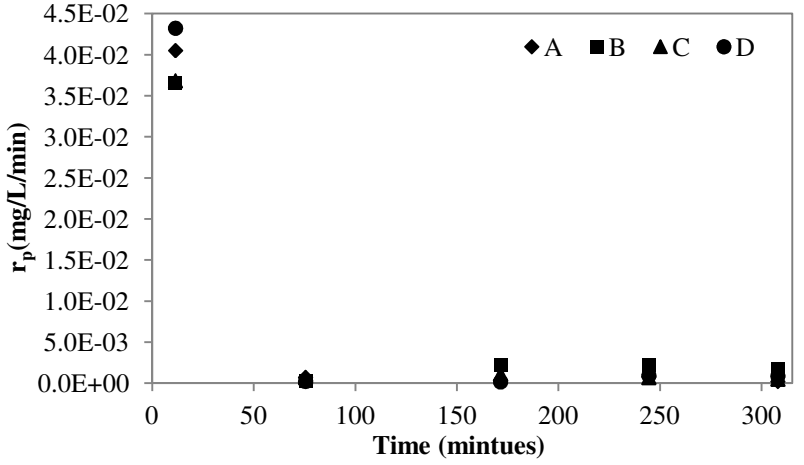

Figure 5-5: The rate of change of soluble P with respect to time in the SBRs under high influent concentrations (6.4 mg P/L).

under high influent P concentrations. This was attributed to a larger concentration gradient between the soluble and the sorbed phase concentrations at higher initial soluble P concentrations. Hence, with a larger gradient, the rate of mass transfer of P was higher. The final rates of removal were small but similar under high and low influent P concentrations. A comparison of the intermediate rates was not possible since the decline in concentration with respect to time was not captured in the results illustrated in Figure 5-5 due to experimental limitation.

5.4.2 Transient Operation

Transient studies were conducted to understand how systems respond to varying P loading. Figure 5-6 illustrates the soluble P concentrations versus time in each SBR (SRT: 2.8 (A), 7.4 (B), 10.8 (C) and 22.8 (D) days) during the transient study phase. The transient study phase involved changing the influent process conditions from a steady state under low influent P concentrations. Influent P doses of 6.4 mg P/L, 16.1 mg P/L and 82 mg P/L were tested. The initial P concentrations were calculated with Equation (5-1).

From Figure 5-6 (a) (dose of 6.4 mg P/L) it can be seen that the removals in SBRs A through C were characterized by an initial fast removal in the first 20 minutes followed by a much slower removal until approximately 80 minutes, reaching pseudo equilibrium after approximately 80 minutes. In SBR D a period of initial fast removal was also observed in the first 20 minutes and pseudo equilibrium was reached after 20 minutes. From Figure 5-6 (b) with a dose of 16 mg P/L the removals in SBR A through C were also characterized by an initial fast removal in the first 20 minutes followed by a much slower removal until approximately 126 minutes, reaching pseudo equilibrium after 126. In SBR D a period of initial fast removal was observed in the first 20 minutes and pseudo equilibrium was reached after 50 minutes. From Figure 5-6 (c) with a dose of 82 mg P/L the initial removal in the first 20 minutes in SBR D was fast and was followed by a slower removal reaching pseudo-equilibrium after 150 minutes. However, the initial removal in the remaining SBRs was slower reaching pseudo-equilibrium after 150 minutes. Based on these results it was evident that the timeframe over which the soluble P concentration declined increased with increasing influent P concentrations. Equilibrium was achieved faster in SBR D and this was likely due to the higher concentration of solids in this reactor (see Chapter 3). Further studies on the effect of solids concentration on P removal are required to verify this conclusion.

The overall removal of P in each of the SBRs after the transient doses was also evaluated. In comparison to the constant loading steady state results under low influent P concentrations (Figure 5-2) the transient results at elevated loadings showed decreased removals in the SBRs. These results were consistent with the decreased removal efficiency of P with increasing

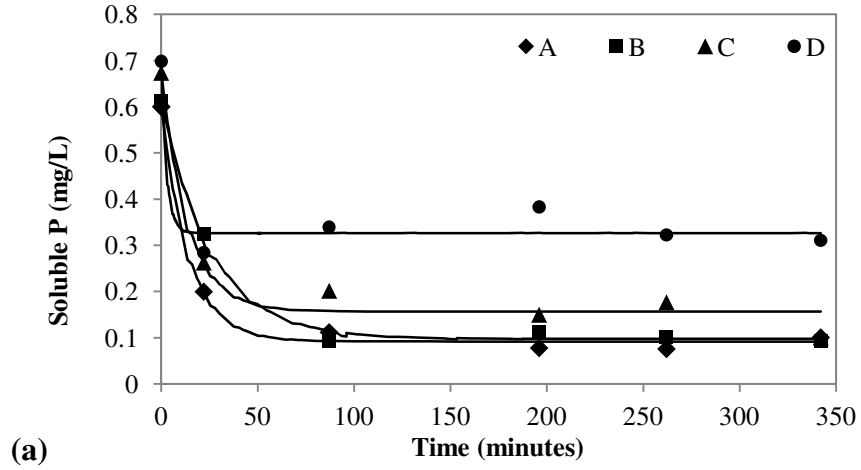

(a)

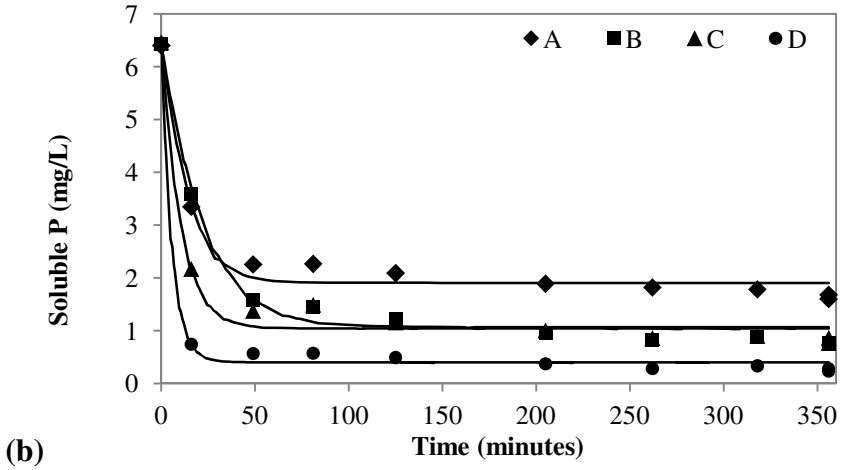

(b)

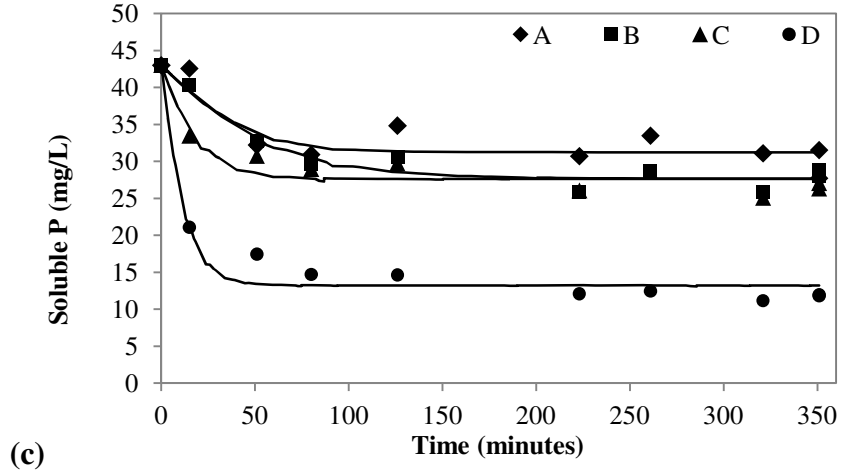

(c)

Figure 5-6: Soluble P versus time in SBRs with (a) 6.4 mg P/L dose, (b) 16.1 mg P/L dose, (c) 82 mg P/L dose

influent P concentrations observed by Szabó et al. (2008). With a 6.4 mg P/L dose (Figure 5-6 a), SBR D demonstrated the lowest removal. These results were consistent with the results observed under steady state operation with both high and low influent P concentrations (Figures 5-2 and 5-3). However with doses of 16.1 and 82 mg P/L (Figures 5-6 b and c), SBR D demonstrated the highest removal when compared with the other SBRs. These results were not consistent with the results observed with steady state operation. Based on the previous studies (Chapter 3 and 4) SBR D was expected to have the lowest removals as a result of the floc morphology (i.e. small surface area and fewer sorption sites) and the reduced quantity of fresh HFO solids that were found to be responsible for a majority of removal in the SBRs. The behaviour of SBR D under elevated influent P concentrations requires further investigation to determine why the behavior switched from that observed under lower loading conditions.

The rates at which the soluble P concentration changed with respect to time in each SBR were calculated with Equation (5-2). Figure 5-7 illustrates the rate of change of soluble P for each dose applied to the SBRs. From Figure 5-7 (a) with a 6.4 mg P/L dose, the initial rates were similar for all the SBRs with the exception of SBR B which had a lower rate. With the 16.1 mg P/L dose (Figure 5-7 b), the initial rates declined with declining SRT in the SBRs while the initial rate in SBR A and B was similar. With an 82 mg P/L dose (Figure 5-7 c), the initial rates also declined with the declining SRT of the SBRs. After 50 minutes, the final rates of removal were small but similar in all the SBRs for the 6.4 and 16.1 mg P/L dose conditions. However, in comparison, the final rates of removal with the 82 mg P/L dose (i.e. after 50 minutes) were similar in all the SBR but generally higher. This was attributed to the higher P loading and thus larger concentration gradient leading to higher rates with this high P dose.

From Figure 5-7 it can also be seen that the initial rates of change were higher than the subsequent rates for doses of 6.4 and 16.1 mg P/L. These results were consistent with the rates observed under steady state operation. However, from Figure 5-7 (c) it can be seen that with an 82 mg P/L dose, the initial rates were only higher than the later ones for SBR D and C. In SBRs A and B the rates did not substantially change with time indicating that P uptake was limited. This may have resulted from the HFO floc reaching their adsorption capacity early in these reactors (i.e. the difference in the sorbed and soluble P concentration was low resulting in

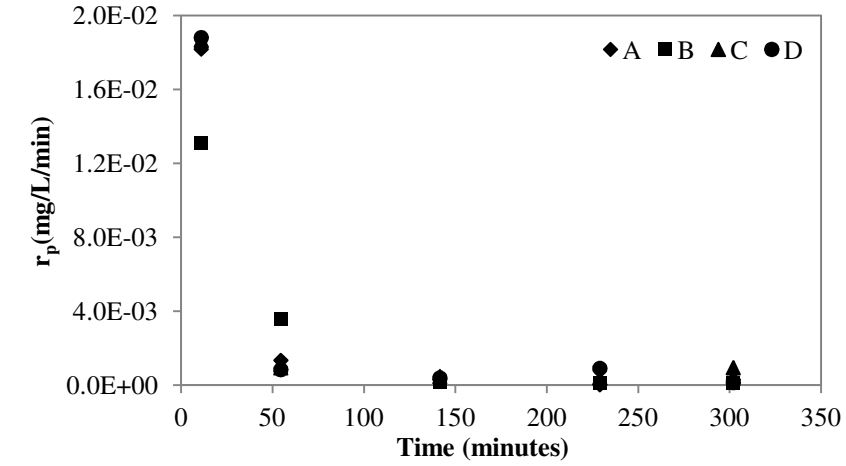

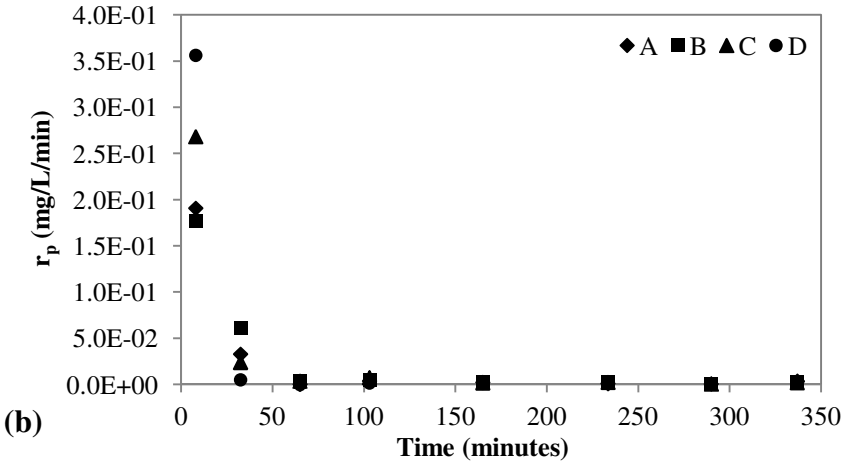

(b)

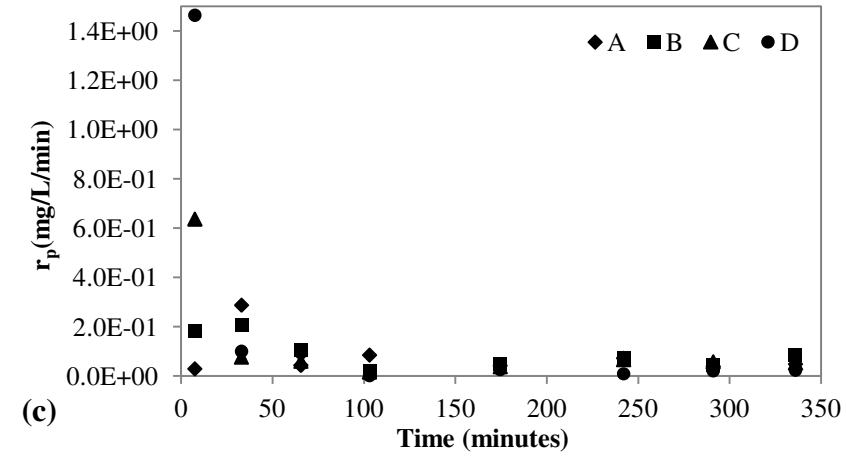

(c)

Figure 5-7: The rate of change of soluble P with respect to time in the SBRs with (a) 6.4 mg P/L dose, (b) 16.1 mg P/L dose, (c) 82 mg P/L dose

low or negligible adsorption). Comparing the initial rates between doses indicated that the initial rate of removal increased with increasing soluble P concentrations. These results were consistent with the initial rates observed under steady state dosing conditions. At higher influent P concentrations the differences between the soluble and sorbed phase concentrations were high resulting in a larger rate of mass transfer from the soluble phase to the sorbed phase.

5.4.3 Batch Adsorption Dynamics

Batch adsorption tests were employed to provide insight into the adsorption dynamics of soluble P onto preformed solids. Figure 5-8 illustrates the results of the P adsorption onto HFO solids from each reactor. The figure legends correspond to the various P doses that were tested with each solid type as described in Table 5-4. The HFO concentrations observed in each reactor were also summarized in Table 5-4. Due to limitation of the experimental method, the initial P concentrations could not be measured and therefore the first sample taken after the P dose was used as the starting concentration (i.e. time 0). Hence, Figure 5-8 illustrates the subsequent removal observed after an initial instantaneous uptake.

From Figure 5-8 it can be seen that the overall trends for the batch sorption kinetics were similar for each HFO sample tested i.e. sorption was characterized by an initial rapid decline followed by a period of slower removal over time until pseudo equilibrium was reached. The samples that had a lower P dose were found to reach pseudo equilibrium faster (i.e. at 250 minutes) than the samples with a higher P dose. These results were consistent with the trends observed under transient conditions (Figure 5-8) where the timeframe over which the decline in residual P occurred increased with increasing influent P concentrations. Confirmation of the 24 hour equilibration time was also observed from the results presented in Figure 5-8. In the majority of the samples tested, differences in removal between 250 minutes and 24 hours were not observed.

The removal of P by each solid type was evaluated based on the results provided in Figure 5-8. Generally, a comparison between solid types indicated that as the SRT of the solids increased, the removal achieved increased. For example, when comparing the final P concentrations after 24 hours, a P dose of 3 mg/L with the flash solids resulted in a final concentration between 1.2

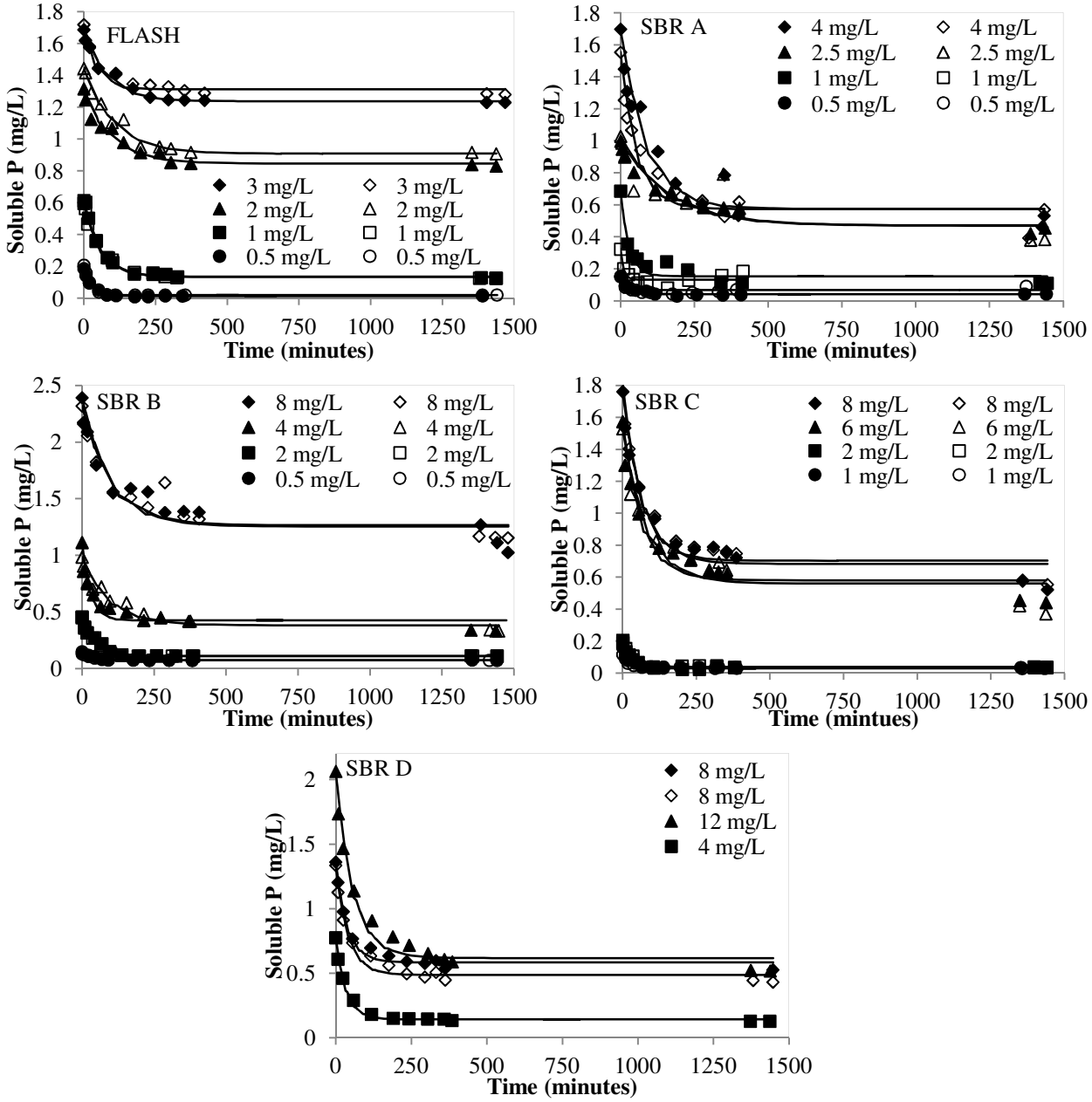

Figure 5-8: Soluble P versus time as a function of P dose in batch sorption tests. Open markers represent replicate tests.

and 1.3 mg/L while a higher P dose of 4 mg/L with SBR A solids resulted in a lower final concentration between 0.5 and 0.6 mg/L. Further, a P dose of 8 mg/L with both SBR B and C solids resulted in a higher final P concentration (i.e. between 1.0 and 1.3 mg/L) in SBR B and a lower concentration (i.e. between 0.5 and 0.6 mg/L) in SBR C. At an even higher SRT, a P dose of 12 mg/L with SBR D solids resulted in a final concentration comparable to that achieved in SBR C with a dose of 8 mg/L (i.e. approximately 0.5 mg/L). These results were

likely due to the fact that the solids concentration increased with SRT (Table 5-4). As the solids concentration increased a much higher P loading was required to provide a similar HFO:P ratio in each test. Hence at similar P doses, the P loading was higher in the lower SRT systems leading to decreased removals.

Information regarding the reproducibility of the batch testing method was also provided in Figure 5-8. A comparison of replicate samples (i.e. closed versus open markers) for a particular P dose showed that the trends in P removal with respect to time were either closely or directly aligned in duplicate samples. For example, with a 1 mg/L P dose in the Flash solids differences between replicate samples are indistinguishable while with a 2 mg/L P dose replicate data followed each other very closely and differences were small. Hence, the results indicated that duplicate samples showed good reproducibility.

The rates at which the soluble P concentration changed with respect to time were calculated with Equation (5-2). Figure 5-9 illustrates the rate of change of soluble P. With the exception of SBR D, the dynamics of P removal onto each solid type was evaluated using four different doses of P. The P doses increased with the SRT of the solids as a result of increasing solids concentrations (Table 5-4). Generally, two “high” P doses and two “low” P doses were evaluated with each solid type. Since a broad range of P doses were employed (Table 5-4) the data at the lower concentration ranges could not be visualized simultaneously. Therefore, the rate values for each solid type shown in Figure 5-9 were separated into two graphs illustrating the “high” P doses on the left and the “low” P doses on the right. Also, since the changes in P concentration were minimal after 400 minutes (Figure 5-8), the timeframe for visualizing the rate data was truncated to 400 minutes for easier visualization of the decline in the rates. From Figure 5-9 it can be seen that the initial rates of removal were generally higher than the subsequent rates. The initial rate of removal increased with increasing P dose. Both of these results were consistent with the results observed under steady state and transient operation. Therefore, the dynamics of P removal onto preformed flocs appeared to behave similarly to the dynamics of P removal onto steady state dosed and transient dosed solids.

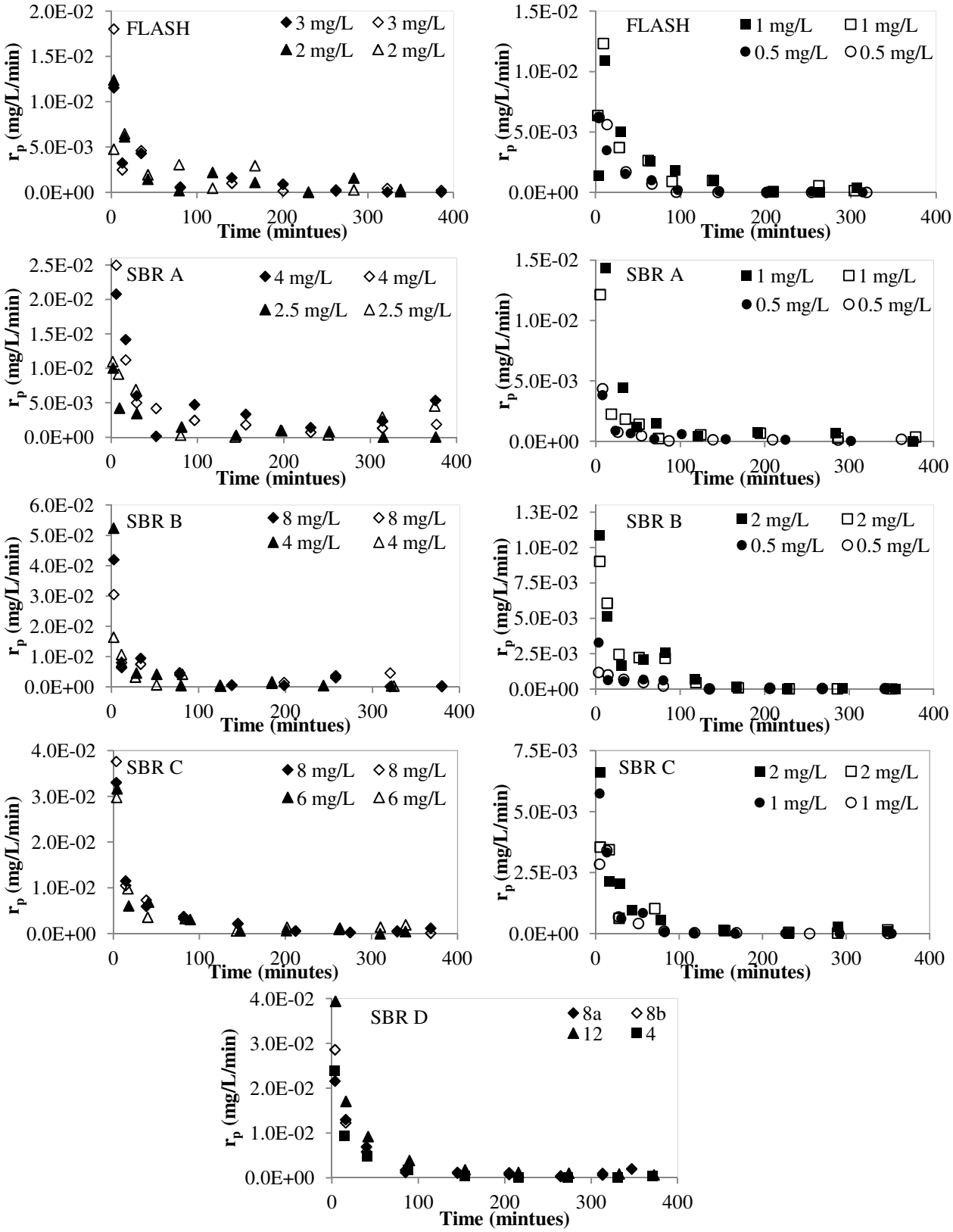

Figure 5-9: The rate of change of soluble P with respect to time in batch sorption tests under high (left) and low (right) P doses.

5.5 Kinetic Model Development and Results

5.5.1 Model Development

The dynamic experiments provided data that described the adsorption of P onto three types of HFO solids: (1) steady state dosed solids, (2) transient dosed solid, and (3) batch preformed solids. Model development focused on the rates of adsorption of soluble P onto previously formed solids. It was hypothesized that the observed rate of removal of soluble P was controlled by the mass transfer of soluble P (P; mg/L) to sorbed P (q; mg P/mg TSS) and that the solid phase P concentration was in equilibrium with the liquid phase P concentration at the liquid-solid interface. In Chapter 4, it was shown that the equilibrium adsorption behaviour of P onto HFO flocs was best described by the Freundlich isotherm. Hence, mass balances on soluble P and sorbed P were assembled for a batch reactor to generate Equations (5-3) and (5-4) that are coupled:

$$\frac{dP}{dt} = -kP + k\left(\frac{q}{K}\right)^n \qquad \text{(Equation 5-3)}$$

$$\frac{dq}{dt} = k\frac{P}{C_s} - \frac{k}{C_s}\left(\frac{q}{K}\right)^n \qquad \text{(Equation 5-4)}$$

where P is the liquid phase concentration of soluble P (mg P/L), q is the sorbed phase concentration (mg P/mg TSS), C_s is the concentration of HFO (mg/L TSS), k is the rate coefficient (1/t), t corresponds to time (minutes), K is a Freundlich constant which indicates the sorption capacity at a specific solution-phase concentration (Weber and DiGiano, 1996), and n is the inverse of the Freundlich constant 1/n which represented a joint measure of the cumulative magnitude and diversity of energies associated with a particular adsorption reaction (Weber and DiGiano, 1996). Derivations of Equations (5-3) and (5-4) are provided in Appendix C.

Calibration of the model denoted by Equations (5-3) and (5-4) was conducted with Matlab by fitting the model to the observed dynamics. In the calibration of the model the values of C_s, n, K, and t were considered as known values. For characterization of the dynamic results under steady state and transient conditions, C_s was quantified by the steady state TSS concentration (mg/L TSS) observed in each reactor as reported in Chapter 3. For characterization of the batch

sorption test results, the HFO concentration (C_s) was quantified using the measured TSS concentration in each batch test (Chapter 4). The values for K and 1/n corresponded to the best fit estimates for these parameters in each reactor that were reported in Chapter 4. The solution of Equations (5-3) and (5-4) required estimates of the initial values of P and q at time zero. For the steady state and transient SBR tests, the initial soluble P concentration corresponded to the estimate of P_i determined from Equation (5-1). For the batch sorption tests, the initial soluble P concentration corresponded to the concentration of the first sample taken after dosing with a dose of P. The initial value of the sorbed phase concentration (i.e. q_i) was treated as an unknown parameter along with the rate constant k. Estimates of q_i and k were determined by solving the coupled ordinary differential equations (Equations 5-3 and 5-4) using non-linear regression with Matlab. A value for k and q_i was determined for each SBR under each dynamic experiment conducted.

It should be noted that the model was developed assuming a reversible reaction between the soluble phase and sorbed phase P concentrations. It was previously noted in Chapter 4 that the model would not account for desorption since P desorption was determined to be negligible. However, the model was developed using mass transfer fundamentals which describe adsorption as a concentration gradient driven process between the soluble and sorbed phases. Therefore, the application of this model should be limited to describing adsorption phenomena only. The model was able to be used in this way since the application was limited to describing the adsorption data sets only. The mass transfer model only accounted for external mass transfer as defined by the concentration gradient between the soluble phase and the sorbed phase. Intraparticle diffusion of P into the HFO floc was not included as it was expected to have minor influence over the experimental timeframe employed (Mao et al., 2012).

The model was developed using the individual Freundlich isotherms reported in Chapter 4 to describe the adsorption of P onto HFO floc. The individual isotherms were used since they provided parameter estimates specific to each SBR. However, it should be noted that the model was also tested using the HFO model generated in Chapter 4 to describe sorption behaviour. The results provided by the HFO model were found to be similar to the results provided by the individual isotherms.

5.5.2 Model Results and Discussion

The performance of the model was initially assessed with respect to the quality of the fit. This included an analysis of the observed and predicted values. The uncertainty was then addressed by examining the uncertainty of the fit parameters (i.e. SE on k and q_i). Confidence intervals for each of the parameters were determined with Monte Carlo simulation (Motulsky and Christopoulos, 2004) in Matlab. The Monte Carlo simulation involved obtaining the best fit estimates of q_i and k, adding random noise to each of these estimates, refitting the model to these random estimates, and repeating the process 1000 times. The generated data sets for k and q_i were statistically analyzed to obtain the mean and the 95% confidence intervals. The distributions were assumed to be normally distributed. The 95% confidence interval was represented by the 2.5 and 97.5 percentiles. The mean parameter estimates along with the 95% CIs around the estimates are subsequently described.

Figures 5-2, 5-3 and 5-6 present the observed and predicted responses under steady state and transient operation. The predicted values for each SBR and each dynamic test were generated using the mean parameter estimates of k and q_i determined for each individual experiment from the Monte Carlo simulation. From Figures 5-2, 5-3 and 5-6, it can be seen that the P concentrations in the SBRs were well represented by the calibrated model. Any deviations in the fit of the calibrated model were attributed to the variability in the observed data. Hence, it was concluded that the model was able to describe the transient P responses in the SBRs under all conditions. In practice, these conditions would be similar to the subsequent removal observed in an aeration basin after Fe addition in a separate flash mix tank under both constant (i.e. steady state) and variable (i.e. transient) P loading conditions.

Figure 5-8 presents the observed and predicted responses for the batch testing. From Figure 5-8 it can be seen that the P concentration in the batch experiments were well represented by the calibrated model at the lower P doses however, the model tended to over predict the final equilibrium P concentrations at the higher P doses for each HFO type. It was suspected that the differences in operating conditions (i.e. mixing intensity and ratio of P removed/mass of HFO solids) and solid types (i.e. preformed versus steady state and transient dosed solids) between

the batch reactors and the SBRs may have attributed to the differences in the model performance. It was concluded that care should be taken when using the batch results as indicators of P removal conditions in the SBRs.

The estimated values of the model parameters were examined to obtain insight into the rates of P adsorption. Figures 5-10 and 5-11 illustrate the mean estimates of k and q_i determined from the Monte Carlo analysis of the dynamic tests in the SBRs under steady state and transient conditions. From Figure 5-10 it can be seen that the rate constant appeared to be similar in SBRs A through C under all the test conditions with the exception of the 82 mg P/L transient dose. A P loading of 82 mg P/L is highly unlikely to be observed in practice and hence the inconsistent results from this test condition were not deemed to be practically problematic. The95% confidence intervals of the estimates also suggested that the values were consistent due to overlap (i.e. with the exception of one or more samples). The k values for SBR D appeared to be different than those for the other SBRs. These results were attributed to the inconsistency in the performance of SBR D under the various test conditions which required further investigation.

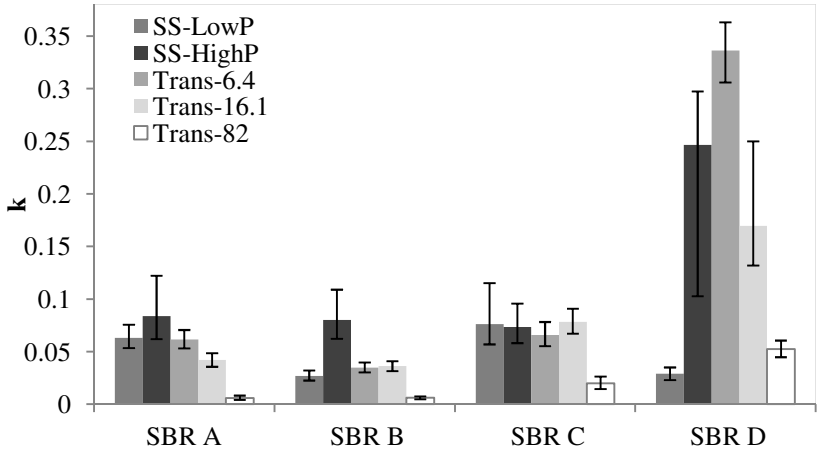

Figure 5-10: Best fit estimates for k (rate constant) under steady state (SS) and transient (Trans) testing. Error bars correspond to 95% confidence intervals.

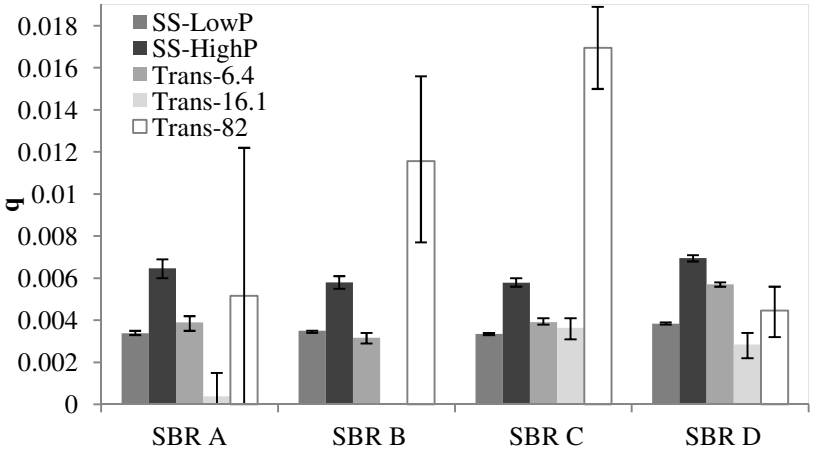

Figure 5-11: Best fit estimates for q_i (initial sorbed phase concentration) under steady state (SS) and transient (Trans) testing. Error bars correspond to 95% confidence intervals.

The rate coefficient is theoretically a function of the fluid film/boundary layer thickness which is affected by mixing (Chorover and Brusseau, 2008). Mixing conditions were constant in each SBR and were provided by both mechanical mixers and aeration (Table 5-3). Hence, based on mixing conditions differences in the rate coefficients were not expected in the SBRs. Thus it was concluded that over a range of SRTs (i.e. 2.8 - 26.6 days), the same rate coefficient could be used to describe P adsorption onto HFO floc.

From Figure 5-11 it can be seen that in the absence of a few outlying results (i.e. the 82 mg P/L transient dose results for SBR B and C, and the 16.1 mg P/L transient does results from SBR A and B) it could be concluded that the values of q_i were generally similar for the SBRs and the various test conditions. These results were consistent with the results from Chapter 4 where the adsorption capacity could not be differentiated between the SBRs. Since the SBRs performed similarly in terms of adsorption (Chapter 4) it would seem reasonable that they also would have similar initial sorbed phase concentrations. However, it should be noted that there was not as much overlap between the estimates of q_i as the k estimates. The 95% confidence intervals around the transient 82 mgP/L dose data were large indicating that there was substantial variability in the fit of q_i to these data sets. Again, since an 82 mg P/L dose is not typical in practice the results from this test condition were deemed to have less practical significance.

The results suggest that the mechanisms controlling P uptake with the high dose were different than those that were controlling the low P doses.

The trends in k and q_i illustrated in Figures 5-10 and 5-11 suggested that there may have been some correlation between these two parameter estimates. Therefore an investigation into the relationship between k and q_i was conducted. To determine if there was any relationship between k and q_i the correlation between these two parameters was calculated using the Pearson correlation coefficient. For each individual experiment, the Monte Carlo generated data sets were used to calculate the Pearson correlation coefficient. The correlation between k and q_i was found to be low under each individual experiment (i.e. generally less than 0.4). These data are summarized in Appendix E. Therefore, based on the low estimates of correlation it was concluded that the model parameters were independent.

Table 5-5 summarizes the range of estimates for k and q_i for each type of HFO solid from the batch sorption tests determined through Monte Carlo analysis. The parameter estimates for each P dose along with the 95% CIs of the estimates are summarized in Appendix D. From Table 5-5, it can be seen that the rate constants were similar for each reactor. There is also overlap between the minimum and maximum values that supports the hypothesis that the values of k were similar. As mentioned previously the rate coefficient is affected by the mixing conditions. In the batch tests, mixing was provided by a shaker table and the speed of mixing was constant in each test (Section 5.3.2.2). Hence, differences in k were not expected.

Table 5-5: Batch sorption model parameter ranges.

Rate Constant (k)	**Flash**	**SBR A**	**SBR B**	**SBR C**	**SBR D**
Average	0.015	0.03	0.017	0.026	0.02
Minimum	0.004	0.004	0.007	0.01	0.015
Maximum	0.04	0.09	0.03	0.05	0.028
Initial Sorbed Phase Concentration (q_i)	**Flash**	**SBR A**	**SBR B**	**SBR C**	**SBR D**
Average	0.052	0.0064	0.006	0.0045	0.0059
Minimum	0.02	0.004	0.0034	0.0022	0.0041
Maximum	0.077	0.0091	0.01	0.0069	0.0068

A comparison of the batch rate coefficients (Table 5-5) to the steady state and transiently dosed coefficients (Figure 5-10) indicated that the values of k were lower in the batch tests. These

differences may be attributed to differences in mixing conditions (Chorover and Brusseau, 2008). Mixing in the SBRs was more turbulent due to aeration in comparison to the swirling provided by the shaker table for the batch tests. Since the thickness of the boundary layer decreases with the extent of mixing (Chorover and Brusseau, 2008) diffusion across the layer was expected to be faster in the SBRs thus leading to a higher rate coefficient in comparison to the batch tests. Therefore, it can be concluded that the model was able to describe differences in operating conditions (i.e. mixing) as reflected by the predicted rate coefficients.

Based on the values of q_i presented in Table 5-5, q_i appeared to be similar for the SBRs which was supported by overlapping minimum and maximum values however q_i was much larger in the Flash samples. The ranges of the q_i values in the SBRs were consistent with the ranges determined from the steady state and transiently dosed solids (Figure 5-11). This was expected since the solids were extracted from the SBRs (Section 5.3.2.2). The inconsistency in the value of q_i from the flash tank versus the SBRs may be attributed to aging phenomena since fresh HFO solids are generally confounded by aging effects making quantitative interpretation more difficult (Lijklema, 1980; Smith et al., 2008a; Mao et al., 2012).

The trends in k and q_i illustrated in Appendix D suggested that there may have been some correlation between these two parameter estimates. For example, the values of k were generally found to be low under "high" P doses and high under "low" P doses (see Section 5.4.3 for definition of "high" and "low" P doses under batch testing). The values of q_i followed the exact opposite trend (i.e. generally high under "high" P doses and low under "low" P doses). To determine if there was any relationship between k and q_i for the batch tests the correlation between the parameters was calculated using the Pearson correlation coefficient. For each individual experiment, the Monte Carlo generated data sets were used to calculate the Pearson correlation coefficient. The correlation between k and q_i was found to be low under each individual experiment (i.e. generally less than 0.4). The data are summarized in Appendix E. Therefore, it was concluded that the parameter estimates were independent under batch testing.

Overall, the calibrated model was found to be applicable to situations where the solids have been already formed and the fate of any additional soluble P is being predicted. The model

provided a good fit to the observed data. The model was able to reflect differences in process conditions (i.e. mixing) between experiments conducted in the SBRs and those in batch tests as was reflected in the values of the rate coefficients. The parameter results also suggested that the same rate coefficient could be used to describe P adsorption onto HFO flocs of different ages (i.e. 2.8-26.6 days). Discrepancies in these estimates were attributed to the inconsistent behavior of SBR D at elevated loadings. Estimates of k and q_i were found to be independent.

The model developed in this study described the behavior of phosphate in an abiotic system. In real wastewater systems, P removal can be expected to be reduced due to competition from organics (Szabó et al., 2008; Mao et al., 2012; Weng et al., 2013). The model describes relatively slow removal processes that result from adsorption. It is anticipated that this model can be combined with existing equilibrium models such as Biowin (EnviroSim, 2007) or the most recent model developed by Hauduc et al. (2013) to improve the ability of these models to describe adsorption of P onto HFO floc when low P concentrations are targeted.

5.6 Conclusions

In this study the interactions between SRT and the dynamics of P removal onto three different solid types (i.e. steady state dosed solids, transient dosed solids, preformed batch solids) were explored and the following conclusions were arrived at:

- P removal in the SBRs and batch sorption tests was characterized by an initial period of fast removal followed by a period of slower removal until pseudo-equilibrium was reached.
- The initial rate of removal (i.e. change in the soluble P concentration with respect to time) increased with increasing influent P concentrations. These results were attributed to a larger concentration gradient between the soluble and sorbed phase concentrations leading to a greater initial rate of change.
- Inconsistencies in the behaviour of SBR D that had the longest SRT (i.e. between 22.8 and 26.6 days) under steady state and transient operation lead to the recommendation that further work be conducted to investigate the behaviour of SBR D under different influent P concentrations and to determine the effect of solids concentration on P removal.

A model was developed to describe the overall dynamic behaviour of P sorption onto HFO floc. The model was found to provide a good description of P removal in the SBRs and batch testing. The model was able to reflect differences in process conditions (i.e. mixing) between experiments conducted in the SBRs and those in batch tests. This was reflected in the estimated values of the rate coefficients between the batch tests and SBRs. From the model parameter estimates it was found that the same rate coefficient could be used to describe P adsorption onto HFO flocs of different ages (i.e. 2.8-26.6 days). Discrepancies in these estimates were attributed to the inconsistent behavior of SBR D at elevated loadings. Estimates of k and q_i were found to be independent.

CHAPTER 6

6. CONCLUSIONS AND RECOMMENDATIONS

6.1 General Conclusions

This research provided a comprehensive understanding of the effects of SRT on chemical P removal in co-precipitation systems. Based on this research the following general conclusions can be made:

1. **P removal was affected by the solids age (i.e. SRT).** Aging as a function of SRT lead to the compaction of HFO flocs leading to a lower surface area and fewer surface sites for binding. As such, lower SRT systems produced higher P removal while higher SRT systems were characterized by lower P removal. The extent of removal achieved as a function of SRT was dependent on the influent P concentration.

2. **Fresh HFO were responsible for the majority of P removal.** Fresh HFO were characterized as having an open structure and a high specific surface area for sorption. In addition to SEM analysis, this was confirmed through batch sorption studies that showed that fresh HFO had a higher sorption capacity in comparison to aged HFO. Mathematical modeling showed that the fresh solid contribution from the flash mix tank was responsible for the majority of the P uptake observed in the SBRs and batch sorption tests rather than the aged solids in the reactor.

3. **The dynamics of P adsorption onto HFO floc was characterized by two phases of removal.** The change in soluble P concentration with respect to time under different process conditions (i.e. during steady state and transient operation of the SBRs and during batch testing) was characterized by an initial period of fast removal followed by a period of slower removal with respect to time until pseudo equilibrium was established.

4. **Sorption rate coefficients can be used over a range of SRTs.** The calibrated sorption rate coefficients were found to be similar for the SBRs under all test conditions indicating that

the rate coefficient was not affected by SRT. These results were confirmed with batch tests where the rate coefficients describing sorption onto SBR solids were similar for all batch test conditions. The consistency in rate coefficients was attributed to the fixed mixing conditions in the SBRs (i.e. mechanical mixing and aeration) and the batch samples (i.e. mechanic shaking).

6.2 Specific Conclusions

The specific conclusions from this study are summarized as follows:

P Removal under Steady State Conditions

In this study the majority of P removal occurred in the flash tank (94% under low influent P concentrations (3.4 mg P/L); 83% under high influent P concentrations (6.4 mg P/L)) with an additional smaller fraction of removal in the SBRs (additional 3.3 – 4.8% removal under low influent P concentrations; 5.5 - 8.8% under high influent P concentrations). Overall, soluble P uptake was found to be higher in the lower SRT systems: $\leq$ 7.4 days under low influent P concentrations and SRTs $\leq$ 14.3 days under high influent P concentrations. In the SBR react cycle alone, P removals (based on initial P concentrations in the SBR) were between 60-80% under low influent P concentrations and 47-56% under high influent P concentrations.

The amount of sorbed P (mg P/mg TSS) was found to decrease with SRT providing evidence that aging changed floc morphology. Differences in floc morphology (i.e. open vs. compact floc structure) between flash solids and SBR aged solids were evident based on SEM analysis. However, differences in particle size distributions could not be differentiated supporting the hypothesis that changes in floc morphology are more responsible for differences in P removal than floc size.

P Removal in Batch Sorption Studies

The results of batch sorption studies characterizing the sorption of soluble P onto HFO solids of different ages indicated that Fresh HFO have a higher sorption capacity in comparison to aged (2.8, 7.4, 10.8 and 22.8 day) HFO. P desorption from HFO solids was found to be

negligible supporting chemisorption as the mechanism of P adsorption. Mathematically, P adsorption onto HFO solids was determined to be best described by the Freundlich isotherm.

An equilibrium sorption model was developed to describe the contribution of different classes of HFO solids (i.e. High, Low or Old) to adsorption. High, Low and Old HFO were characterized as having high specific surface area for sorption, low specific surface area for sorption, and no adsorption capacity, respectively. The model was found to adequately describe P adsorption onto HFO solids of different ages. Modelling also showed that the fractions of High and Low HFO decreased with SRT, the fractions of Old HFO increased with SRT, the rate of transformation of High HFO into Low HFO was lower than the rate of transformation of Low HFO into Old HFO, and the High HFO contributed more to P sorption than Low HFO in each SBR implying that the fresh flash solids were more responsible for the observed P uptake in the SBRs in comparison to the aged SBR solids.

The dynamics of P removal

In this study it was confirmed that P removal in the SBRs and batch sorption tests was characterized by an initial fast period of removal followed by a period of slower removal until pseudo-equilibrium was reached. The initial rate of removal (i.e. change in the soluble P concentration with respect to time) increased with increasing influent P concentrations. These results were attributed to a larger concentration gradient between the soluble and sorbed phase concentrations leading to a greater initial rate of change. The performance of the SBRs in terms of the equilibrium soluble P achieved at low P loadings (i.e. 3.4 and 6.4 mg P/L) under both transient and steady state operation were consistent with the results reported in Chapter 3. The low SRT (i.e. less than 22.8-26.6 days) SBRs (i.e. A through C) achieved higher P removal in comparison to the high SRT (i.e. 22.8- 26.6 days) SBR (i.e. SBR D). However, under transient operation SBR D provided the highest P removal at high P loadings (i.e. 16.1 and 82 mg P/L).

A model was developed to describe the dynamic behaviour of P sorption onto three different solid types (i.e. steady state dosed SBR solids, transient dosed SBR solids, and preformed batch solids). Overall, the calibrated model was found to provide a good description of P removal in the SBRs and batch testing. The model was able to reflect differences in process

conditions (i.e. mixing) between experiments conducted in the SBRs and those in batch tests. This was reflected in the estimated values of the rate coefficients between the batch tests and SBRs. It was found that the same rate coefficient could be used to describe P adsorption onto HFO flocs of different ages (i.e. 2.8-26.6 days). Discrepancies in these estimates were attributed to the inconsistent behavior of SBR D at elevated loadings.

6.3 Recommendations for Future Work

The following recommendations are suggested for future chemical P removal studies with Fe salts.

There was some uncertainty as to which parameter (TSS or Fe) would provide a better estimate of the concentration of HFO solids in the reactor for the purposes of normalization. TSS concentrations may be biased as the mass of TSS will increase with increasing P concentrations as a result of the added mass that P provides to the solids. The Fe concentrations were considered to provide a measure of the generated HFO since all of the dosed Fe was expected to precipitate into the HFO (i.e. residual soluble Fe concentrations are negligible). However, this estimate would be low since the contribution of hydroxide to HFO was ignored. For future studies detailed characterization of HFO mass should be performed.

The residual soluble P samples from the flash tank effluent (P_{flash}) were filtered immediately after Fe dosing and therefore the time frame for removal (i.e. contact time) was limited to the HRT in the rapid mix tank. Much lower residual P concentrations were observed if the samples were left for a longer period of time prior to filtration. Treatment plants that have been recently designed and upgraded to meet ultra low TP limits including the Spokane County Regional Water Reclamation Facility (Washington, USA) and the West Camden Sewage Treatment Plant (New South Wales, Australia) have been able to innovatively integrate separate rapid mix tanks to ensure the necessary mixing intensity and contact time are provided for chemical P removal (Johnson et al., 2012; Takács et al., 2011). Therefore, future research to optimize the contact time or HRT necessary to achieve the lowest residual P concentrations at the lowest possible Fe dose in these rapid mix tanks would be beneficial.

It was suspected that the differences in operating conditions (i.e. mixing intensity and ratio of P removed/mass of HFO solids) between the batch reactors and the SBRs may have contributed to the differences in P removal observed between these sample types. For future studies, P adsorption onto HFO should be characterized in the SBRs in-situ. This could have been achieved by turning the Fe dosing off during transient studies.

During transient operation of the SBRs the change in soluble P concentration with respect to time reached pseudo-equilibrium faster in SBR D most likely due to the higher concentration of solids in this reactor (see Chapter 3). Further studies on the effect of solids concentration on P removal are recommended to verify this conclusion.

During transient operation of the SBRs, SBR D demonstrated the lowest removal with a 6.4 mg P/L dose which was consistent with the results observed under steady state operation with both high (3.4 mg P/L) and low (6.4 mg P/L) influent P concentrations. However with doses of 16.1 and 82 mg P/L, SBR D demonstrated the highest removal when compared with the other SBRs. These results were not consistent as SBR D was expected to have the lowest removals as a result of the floc morphology (i.e. small surface area and fewer sorption sites) and the reduced quantity of fresh HFO solids that were found to be responsible for a majority of removal in the SBRs (Chapter 3 and 4). Therefore, further investigation into the behaviour of SBR D under elevated influent P concentrations to determine why the behavior switched from that observed under lower loading conditions is recommended.

A dynamic P model was developed in this study to describe P sorption onto HFO floc. This model was limited to describing P sorption onto HFO flocs at a constant pH. Future studies that aim to integrate the effects of pH, variable water chemistry and the different fraction of HFO solids (i.e. High, Low and Old) on P sorption would be beneficial.

REFERENCES

Benisch, M., deBarbadillo, C., Barnard, J. and Neethling, JB. (2013). Sustainable Operating Practices for Achieving Low Phosphorus Effluents. *Conference Proceedings, Nutrient Removal and Recovery 2013*, WEF/IWA.

Berkheiser, V.E., Street, J.J., Rao, P.S.C. and Yuan, T.L. (1980). Partitioning of inorganic orthophosphate in soil-water systems. *CRC Crit. Rev. Envir. Control*, 10, 179-224.

Briggs T.A. (1996). Dynamic Modelling of Chemical Phosphorous Removal in the Activated Sludge Process, M.Eng. Thesis, School of Graduate Studies, McMaster University, Hamilton, Ontario, Canada.

Caravelli, A.H., De Gregorio, C. and Zaritzky, N.E. (2012). Effect of operating conditions on the chemical phosphorus removal using ferric chloride by evaluating orthophosphate precipitation and sedimentation of formed precipitates in batch and continuous systems. *Chemical Engineering Journal*, 209, 469-477.

Caravelli, A. H., Contreras, E.M., and Zaritzky, N.E. (2010). Phosphorus removal in batch systems using ferric chloride in the presence of activated sludges. *Journal of Hazardous Materials*, 177, 199-208.

Chien, S.H. and Clayton, W.R. (1980). Application of Elovich equation to the kinetics of phosphate release and sorption in soils. *Soil Science Society of America Journal*, 44, 265-268.

Chorover, J. and Brusseau, M.L. (2008). Kinetics of Sorption – Desorption. In S.L Brantley, J.D. Kubicki, White, A.F. (Eds.), *Kinetics of Water – Rock Interaction* (pp. 109-149). New York, NY: Springer.

Davis, J.A. and Leckie, J.O. (1980). Surface-ionization and complexation at the oxide-water interface. III. Adsorption of anions. *Journal of Colloid and Interface Science*, 74, 32-43.

de Haas, D.W., Wentzel, M.C., and Ekama, G.A. (2001). The use of simultaneous chemical precipitation in modified activated sludge systems exhibiting biological excess phosphate removal. Part 6: Modelling of simultaneous chemical-biological P removal- Review of existing models. *Water SA*, 27(2), 135-150.

Department of Fisheries and Oceans Canada (DFO). (2010). Protecting the Health of Canada's Lakes, Experimental Lakes Area. Retrieved from http://www.dfo-mpo.gc.ca/regions/CENTRAL/pub/ela-rle/index-eng.htm

Dzombak, D.A. and Morel, F. (1990). Surface Complexation Modeling: Hydrous Ferric Oxide. New York, NY: Wiley.

Eleuterio, L. and Neethling, J.B. (2009). Low Phophorus Analytical Measurement Study. *Proceedings from Nutrient Removal 2009 Conference*, Water Environment Federation, 1050-1077.

Environment Canada (1990). Environmental Protection Series. Biological Test Method: Acute Lethality Test Using Daphnia ssp. Retrieved from http://publications.gc.ca/collections/collection_2013/ec/En49-24-1-11-eng.pdf

Environmental Literacy Council (ELC). (2002). Phosphorus Cycle. Retrieved from http://www.enviroliteracy.org/article.php/480.php

EnviroSim (2007). BioWin Tutorial and Examples: Process Models Used in Biowin. Retrieved from http://www.softfactory.fr/download/biowin/modelsusedinbiowin.pdf

Falk, M.W., Liu, H., Hauser, D.W. and Neethling, JB. (2012). Achieving Less than 0.050 mgP/L Reliably with Active Chemical Sludge. *Conference Proceedings, WEFTEC 2012*, Water Environment Federation, 6960-6969.

Ferguson, J.F., King, T. (1977). A Model for Aluminum Phosphate Precipitation. *Journal Water Pollution Control Federation*, 49(4), 646-658.

Fluid Imaging Technologies. (2012). FlowCAM Manual, Version 3.2. Fluid Imaging Technologies: Yarmouth, Maine. Retrieved from http://uic.umn.edu/sites/uic.umn.edu/files/FlowCAM%20Manual%20for%20Visual%20Spreadsheet%20Version%20%203-1.2.2%20June%202012.pdf

Geelhoed, J.S., Hiemstra, T., and Van Riemsdijk, W.H. (1997). Phosphate and sulfate adsorption on goethite: Single anion and competitive adsorption. *Geochimica et Cosmochimica Acta*, 61(12), 2389-2396.

Gillberg, L., Nilsson, D., Åkesson, M. (1996). The Influence of pH when Precipitating Orthophosphate with Aluminum and Iron Salts, In H.H. Hahn, E. Hoffmann and H. Ødegaard (Eds.), *Chemical Water and Wastewater Treatment IV. – Proceedings of the 7th Gothenburg Symposium Edinburgh 1996*. New York, NY: Springer-Verlag Berlin Heidelberg.

Gilmore, R.L. (2009). Laboratory Studies in Chemically Mediated Phosphorus Removal. Thesis submitted to the Department of Geography and Environmental Science, Wilfrid Laurier University.

Golberg, S. (1985). Chemical modelling of anion complexation on goethite using the constant capacitance model. *Soil Science Society of America Journal*, 50, 1154-1157.

Gu, A.Z., Liu, L., Neethling, J.B., Stensel, H.D., and Murthy, S. (2011). Treatability and fate of various phosphorus fractions in different wastewater treatment processes. *Water Science & Technology*, 63(4), 804-810.

Gu, A.Z., Nehreen, M., Benisch, M. and Neethling, J.B. (2009). Fractionation and Treatability Assessment of Phosphorus in Wastewater Effluents – Implications on Meeting Stringent Limits. *Conference Proceedings WEFTEC 2009*, Water Environment Federation, p 480-500.

Hauduc, H., Takács, I., Smith, S., Szabó, A., Murthy, S., Daigger, G.T. and Sperandio, M. (2013). A Dynamic Physicochemical Model for Chemical Phosphorus Removal. *Conference Proceedings, Nutrient Removal and Recovery 2013*, WEF/IWA.

Hiemstra, T and Van Riemsdijk, W.H. (1996). A Surface Structural Approach to Ion Adsorption: The Charge Distribution (CD) Model. *Journal of Colloid and Interface Science*, 179, 488-508.

Hingston, F.J. (1981). A Review of Anion Adsorption. In M.A. Anderson and A.H. Rubin (Eds.), *Adsorption of Inorganics at Solid-Liquid Interfaces*. Ann Arbor: Ann Arbor Science

Holtan, H., Kamp-Nielsen, L. and Stuanes, A.O. (1988). Phosphorus in soil, water and sediment: an overview. *Hydrobiologia*, 170, 19-34.

Jenkins, D. and Hermanowicz, S.W. (1991). Principles of Chemical Phosphate Removal, In R. Sedlak (Ed), *Phosphorus and Nitrogen Removal from Municipal Wastewater: Principles and Practice. 2nd ed.* Boca Raton, FL: Lewis Publishers.

Jenkins, D., Ferguson, J.F. and Menar, A.B. (1971). Review Paper, Chemical Processes for Phosphate Removal. *Water Research*, 5, 369-389.

Johnson, B.R. and Daigger, G.T. (2009). Integrated Nutrient Removal Design for Very low Phosphorus Levels. *Water Science & Technology*, 60(9), 2455-2462.

Johnson, B.R., McClymont, A., and Moss, D. (2012). Design to Operation of the 0.05 mg/L Total Phosphorus Greenfield MBR Spokane County Regional Water Reclamation Facility. *Conference Proceedings, WEFTEC 2012*, Water Environment Federation, 370-378.

Johnson, B.R., Spani, C., Menglekoch, M., and Baur, R. (2005). The Reality of Attaining Plant Effluent Phosphorus Limits of less than 0.07 mg P/L, *Conference Proceedings, WEFTEC 2005*, Water Environment Federation, 6112-6124.

Jones, R.D. (2002). Phosphorus Cycling. In Hurst, C.J., Crawford, R.L., Knudsen, G.R., McInerney, M.J. and Stetzenbach, L.D. (Eds.), *Manual of Environmental Microbiology 2nd Edition* (p 450-455). Washington, D.C: ASM Pres.

Kang, S., Choo, K., and Lim, K. (2003). Use of Iron Oxide Particles as Adsorbents to Enhance Phosphorus Removal from Secondary Wastewater Effluent. *Separation Science and Technology*, 38(15), 3853-3874.

Lambert, R.J.W., Mytilinaios, I., Maitland, L. and Brown, A.M. (2012). Monte Carlo simulation of parameter confidence intervals for non-linear regression analysis of biological data using Microsoft Excel. *Computer Methods and Programs in BioMedicine*, 107 (2), 155-163.

Levesque, S., Barnard, J., deBarbadillo, C., and Frias, R. (2010). Numeric Nutrient Criteria on the Horizon Can nutrient removal surpass the limit of technology? *Water Environment & Technology*, 22(4), 26-31.

Li, L. and Stanforth, R. (2000). Distinguishing Adsorption and Surface Precipitation of Phosphate on Goethite (α-FeOOH*). Journal of Colloid and Interface Science*, 230, 12-21.

Lijklema, L. (1980). Interaction of Orthophosphate with Iron(III) and Aluminum Hydroxides. *Environmental Science & Technology*, 14(5), 537-541.

Luedecke, C., Hermanowicz, S.W. and Jenkins, D. (1989). Precipitation of ferric phosphate in activated sludge: a chemical model and its verification. *Water Science & Technology*, 21, 325-337.

Mao, Y., Phan, A.N., Xin, Y. and Waite, T.D. (2012) Effects of pH, floc age and organic compounds on the removal of phosphate by pre-polymerized hydrous ferric oxides. *Separation and Purification Technology*, 91, 38-45.

Mathews, P.G. (2005). Design of experiments with MINITAB. Milwaukee, WI: American Society for Quality, Quality Press.

Metcalf & Eddy. (2003). Wastewater Engineering: Treatment and Reuse. New York, NY: McGraw Hill.

Minister of Justice (2012). Wastewater Systems Effluent Regulations SOR/2012-139. Retrieved from http://laws-lois.justice.gc.ca/eng/regulations/sor-2012-139/index.html

Motulsky, H. and Christopoulos, A. (2004). Fitting Models to Biological Data Using Linear and Nonlinear Regression: A practical guide to curve fitting. Toronto, ON: Oxford University Press, Inc.

Musvoto, E.V., Wentzel, M.C., Loewenthal, R.E., and Ekama, G.A. (2000). Integrated Chemical – Physical Processes Modelling – I. Development of a Kinetic-Based Model for Mixed Weak Acid/Base Systems. *Water Resources*, 34(6), 1857-1867.

National Institute of Standards and Technology (NIST). (2001). NIST Standard Reference Database 46. Gaithersburg, Maryland, U.S.A.

Neethling, J.B. et al. (2008). Low P Concentration Measurements, Water Environment Research Foundation, Retrieved from http://www.werf.org/nutrients/

Neethling, J.B., Benisch, M., Clark, D. and Gu, A. (2007). Phosphorus Speciation Provides Direction to Produce 10ug/L. *Conference Proceedings, Nutrient Removal 2007*, *Water Environment Federation*, 1517-1526.

Neethling, J.B., Clark, D., Pramanik, A., Stensel, H.D., Sadino, J., and Tsuchihashi, R. (2010). WERF Nutrient Challenge Investigates limits of nutrient removal technologies. *Water Science & Technology*, 61(4), 945-953.

Newcombe, R.L., Rule, R.A., Hart, B.K. and Moller, G. (2008a). Phosphorus Removal from Municipal Wastewater by Hydrous Ferric Oxide Reactive Filtration and Coupled Chemically Enhanced Secondary Treatment: Part I-Performance. *Water Environment Research*, 80(3), 238-247.

Newcombe, R.L., Strawn, D.G., Grant, T.M., Childers, S.E. and Moller, G. (2008b). Phosphorus Removal from Municipal Wastewater by Hydrous Ferric Oxide Reactive Filtration and Coupled Chemical Enhanced Secondary Treatment: Part II-Mechanism. *Water Environment Research*, 80(3), 248-256.

Office of the Auditor General of Canada (OAG). (2007). OAG. *Case Study 1.3.5. – Phosphorus in Lake Erie: Do we need a new plan*. In: 2001 October Report of the Commissioner of the Environment and Sustainable Development. Retrieved from http://www.oag-bvg.gc.ca/internet/English/att_c101se3-5_e_11698.html

Pierri, E., Tsamouras, D., Dalas, E. (2000). Ferric phosphate precipitation in aqueous media. *Journal of Crystal Growth*, 213, 93-98.

Rietra, R.P.J.J., Hiemstra, T. and Van Riemsdijk, W.H. (2001). Interaction between Calcium and Phosphate Adsorption on Goethite. *Environmental Science & Technology*, 35(16), 3369-3374.

Sagberg, P., Ryrfors, P. and K.G. Berg. (2006). 10 years of operation of an integrated nutrient removal treatment plant: ups and downs. Background and water treatment. *Water Science & Technology*, 53(12), 83-90.

Sheehy, P. and Martz, E. (2012). Doing Monte Carlo Simulation in Minitab Statistical Software. Minitab Inc. Retrieved from http://www.minitab.com/en-us/Published-Articles/Doing-Monte-Carlo-Simulation-in-Minitab-Statistical-Software/

Smith, S., Takács, I., Murthy, S., Daigger, G.T., Szabó, A. (2008a). Phosphate Complexation Model and Its Implications for Chemical Phosphorus Removal. *Water Environment Research*, 80(5), 428-438.

Smith, D.S., Gilmore, R.L., Szabó, A., Takács, I., Murthy, S., Daigger, G.T. (2008b). Chemically Mediated Phosphorus Removal in Low Levels: Analysis and Interpretation of Data. *Water Environment Federation, WEFTEC 08 Conference Proceedings*, 3558-3574.

Smith, D.S., Ferris, F.G. (2001). Proton Binding by Hydrous Ferric Oxide and Aluminum Oxide Surfaces Interpreted Using Fully Optimized Continuous pKa Spectra. *Environmental Science & Technology*, 35(23), 4637-4642.

Sparks, D.L. (1989). Kinetics of soil chemical processes. New York, NY: Academic Press Inc.

Spivakov, B. YA., Maryutina, T.A. and Muntau, H. (1999). Phosphorus Speciation in Water and Sediments. *Pure and Applied Chemistry*, 71(11), 2161-2176.

Standard Methods for the Examination of Water and Wastewater (Standard Methods). (2005). (21st ed.). American Public Health Association, American Water Works Association, and Water Environment Federation, Washington DC, USA.

Stumm, W., Huang, C.P. and Jenkins, S.R. (1970). Specific chemical interactions affecting the stability of dispersed systems. *Croatica Chemica Acta*, 42, 223-224.

Szabó, A., Takács, I., Murthy, S., Daigger, G.T., Licskó, I., Smith, S. (2008). The Significance of Design and Operational Variables in Chemical Phosphorous Removal. *Water Environment Research*, 80(5), 407-416.

Szabó, A., Takács, I., Lisckó, I., Murthy, S., and Daigger, G. (2006). The importance of slow kinetic reactions in simultaneous chemical P removal. *Conference Proceedings WEFTEC 2006*, Water Environment Federation, 4864-4872.

Takács, I., Murthy, S., Smith, S., McGrath, M. (2006a). Chemical Phosphorous Removal to Extremely Low Levels: Experience of Two Plants in the Washington D.C. Area. *Water Science & Technology*, 53(12), 21-28.

Takács, I., Murthy, S. and Fairlamb, P.M. (2006b). Chemical Phosphorus removal model based on equilibrium chemistry. *Water Science & Technology*, 52(10), 549-555.

Takács, I., Stricker, A.-E., Achleitner, S., Barrie, A., Rauch, W. and Murthy, S. (2008). Do you know your sludge age? *Conference Proceedings, WEFTEC 2008*, Water Environment Federation, 3639-3655.

Takács, I., Johnson, B.R., Smith, S., Szabó, A., Murthy, S. (2011). Chemical P Removal – from lab tests through model understanding to full-scale demonstration. *Conference Proceedings, Design Operation and Economics of Large Wastewater Treatment Plants 2011*, IWA.

Teng, T.T and Low, L.W. (2012). Removal of Dyes and Pigments from Industrial Effluents. In S.K. Sharma, and R. Sanghi (Eds.), *Advances in Water Treatment and Pollution Prevention*. (pp. 65-94). New York, NY: Springer

Vadstein, O. (2000). Heterotrophic, planktonic bacteria and cycling of phosphorus. Phosphorus requirements, competitive ability, and food web interactions. In B. Schink (Ed.), *Advances in Microbial Ecology 16th Edition* (p 115-167). New York, NY: Kluwer Academic Plenum Publishers.

Washington State Department of Ecology (2010). Washington State Laws about Phosphorus Information. Retrieved from http://www.ecy.wa.gov/programs/wq/nonpoint/phosphorus/law.html

Water Environment Federation (WEF). (1998). Biological and Chemical Systems for Nutrient Removal. Alexandria, VA: Water Environment Federation.

Watson, J. S. (1999). Separation methods for waste and environmental applications. New York, NY: Marcel Dekker.

Weber, W.J.J., and Digiano, F.A. (1996). Process Dynamics in Environmental Systems. Toronto, ON: John Wiley & Sons, Inc.

Weng, L., Van Riemsdijk, W.H. and Hiemstra, T. (2012). Factors Controlling Phosphate Interaction with Iron Oxides. *Journal of Environmental Quality*, 41, 628-635.

Water Environment Research Foundation (WERF). (2008). Treatment Processes for Low Nitrogen and Phosphorus: Theoretical Performance and Demonstrated Performance Variability, Preliminary Information. Retrieved from http://www.werf.org/c/KnowledgeAreas/NutrientRemoval/ProductsToolsnonWERF/Treatment_Processes.aspx

XCG Consultants Ltd. (2010). Review of Phosphorus Removal at Municipal Sewage Treatment Plants Discharging to the Lake Simcoe Watershed. Retrieved from http://www.weao.org/assets/docs/resources-links/reports/review-of-phosphorus-removal-to-lake-simcoe.pdf

Yu, S., Dong, X., Gong, H., Jiang, H. and Liu, Z. (2012). Adsorption Kinetic and Thermodynamic Studies of Phosphate onto Tantalum Hydroxide. *Water Environment Research*, 84(12), 2115-2122.

Zeng, Le., Li, X. and Liu, J. (2004). Adsorptive removal of phosphate from aqueous solutions using iron oxide tailings. *Water Research*, 38, 1318-1326.

Appendix A Raw Steady State SBR Characteristics under High and Low Influent P

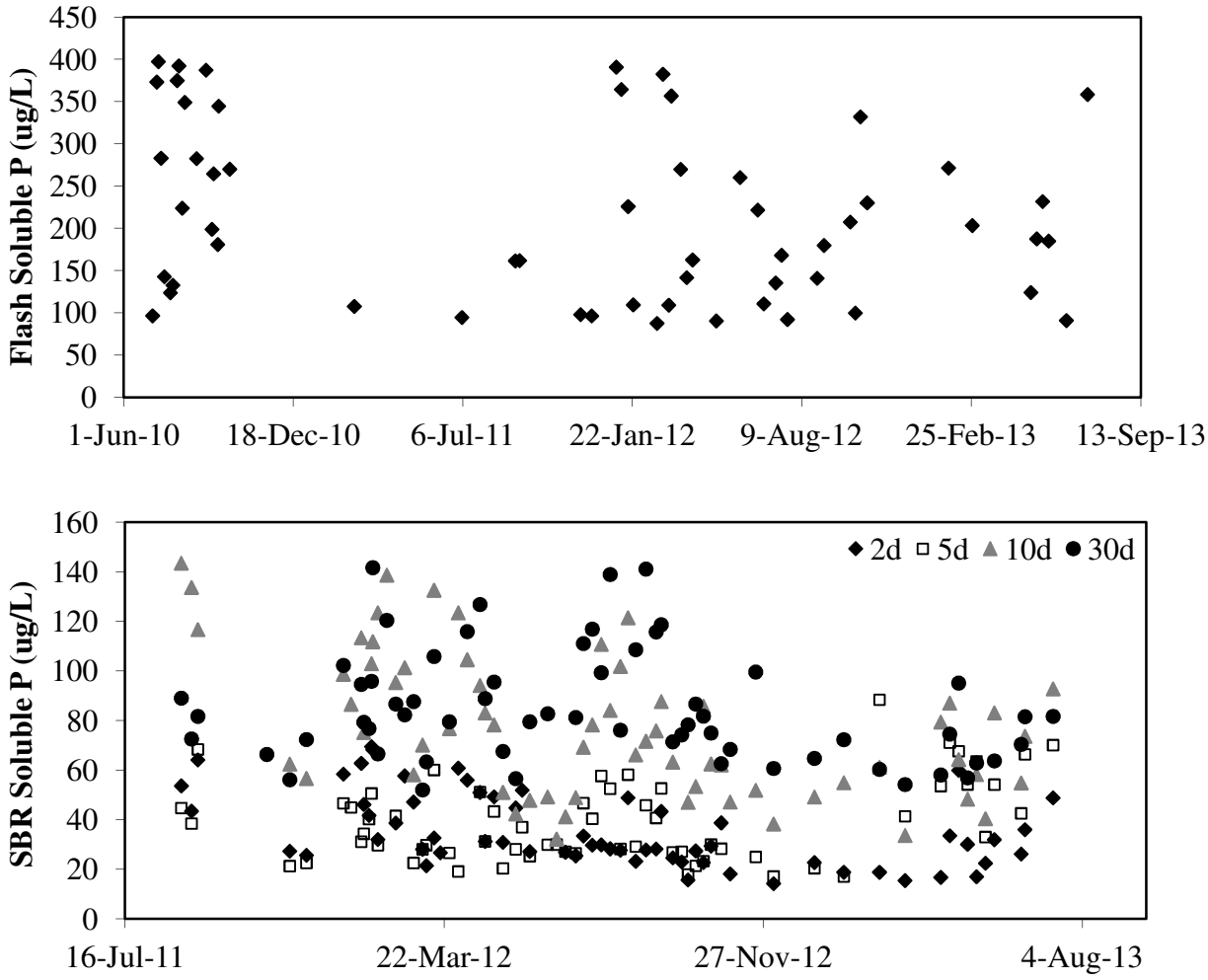

Figure A-1: Raw Soluble P Profiles – Low influent P concentrations

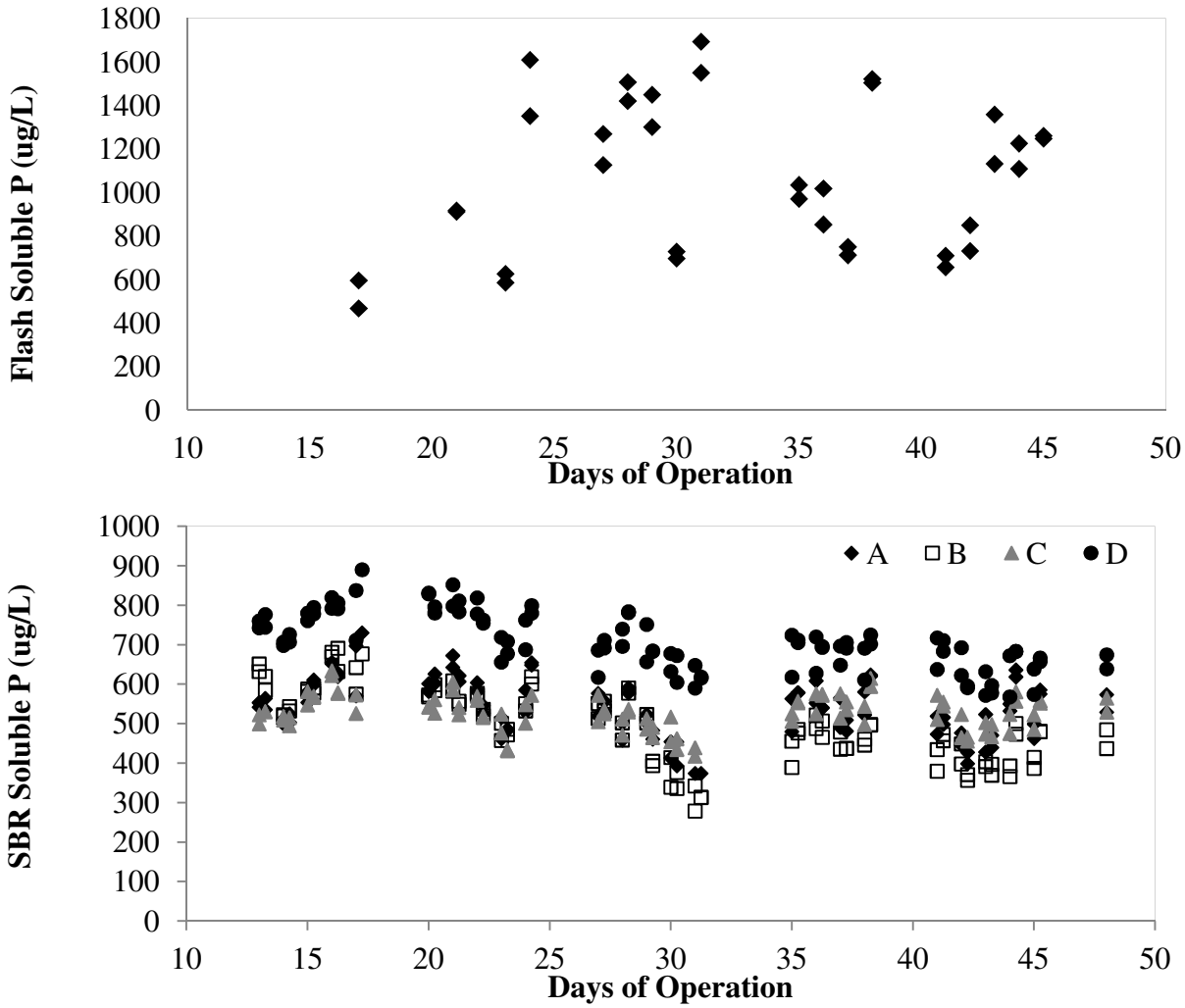

Figure A-2: Raw Soluble P Profiles – High influent P concentrations

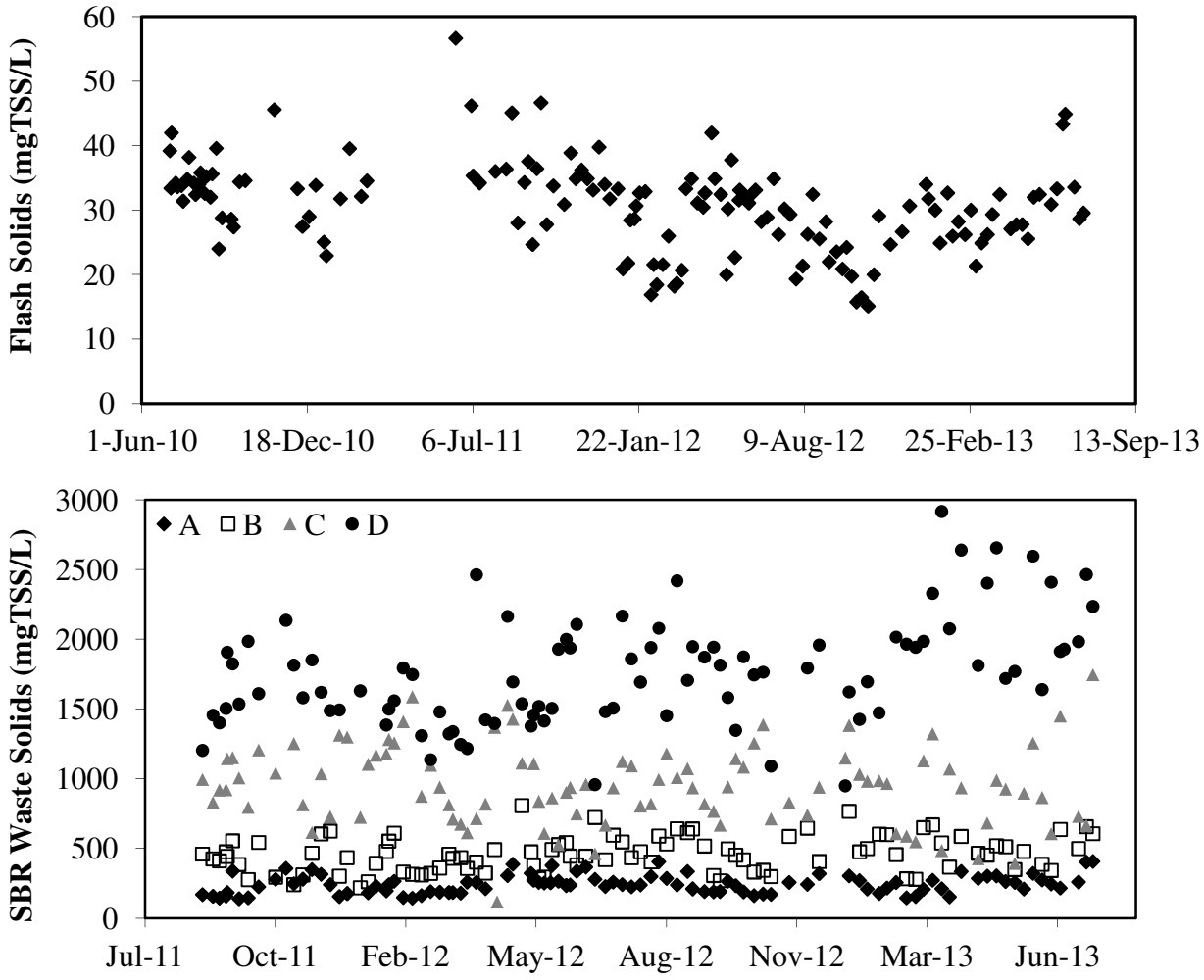

Figure A-3: Raw TSS Profiles - Low influent P concentrations

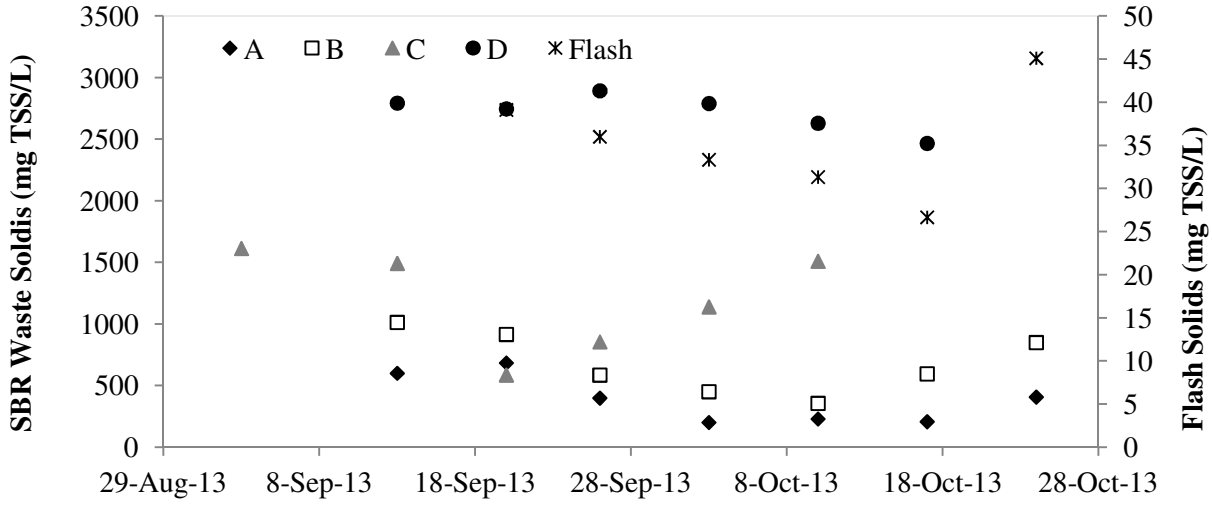

Figure A-4: Raw TSS Profiles – High influent P concentrations

Table A-1: Raw Total P Data (mg P/L)

	Flash	SBR A	SBR B	SBR C	SBR D
Low influent P	4.8	24.5	58.1	109	216
	3.3	26.8	46.5	61.6	192
	3.3	23.3	59.4	83.2	130
	3.4	22.0	53.5	75.2	108
	3.2	15.3	80.8	67.1	150
	2.4	14.3	109	203	313
		30.1	42.4	49.4	
		15.9			
		27.4			
High influent P	6.6	27.8	73.5	167	260
	6.5	28.4	78.1	191	280
	6.5	26.4			
	6.8	26.7			
	6.1				
	6.3				
	6.3				
	6.2				

Table A-2: Raw Fe Data (mg Fe/L)

	Flash	SBR A	SBR B	SBR C	SBR D
Low influent P	18.1	103.0	288	464	998
	17.2	138.0	347	454	777
	14.6	78.5	455	368	848
	14.6	78.3	262	480	813
		70.1	204	248	
		77.6			
		132.0			
High influent P	18.1	82.6	265	567	1000
	17.2	82.3			
	14.6				
	14.6				

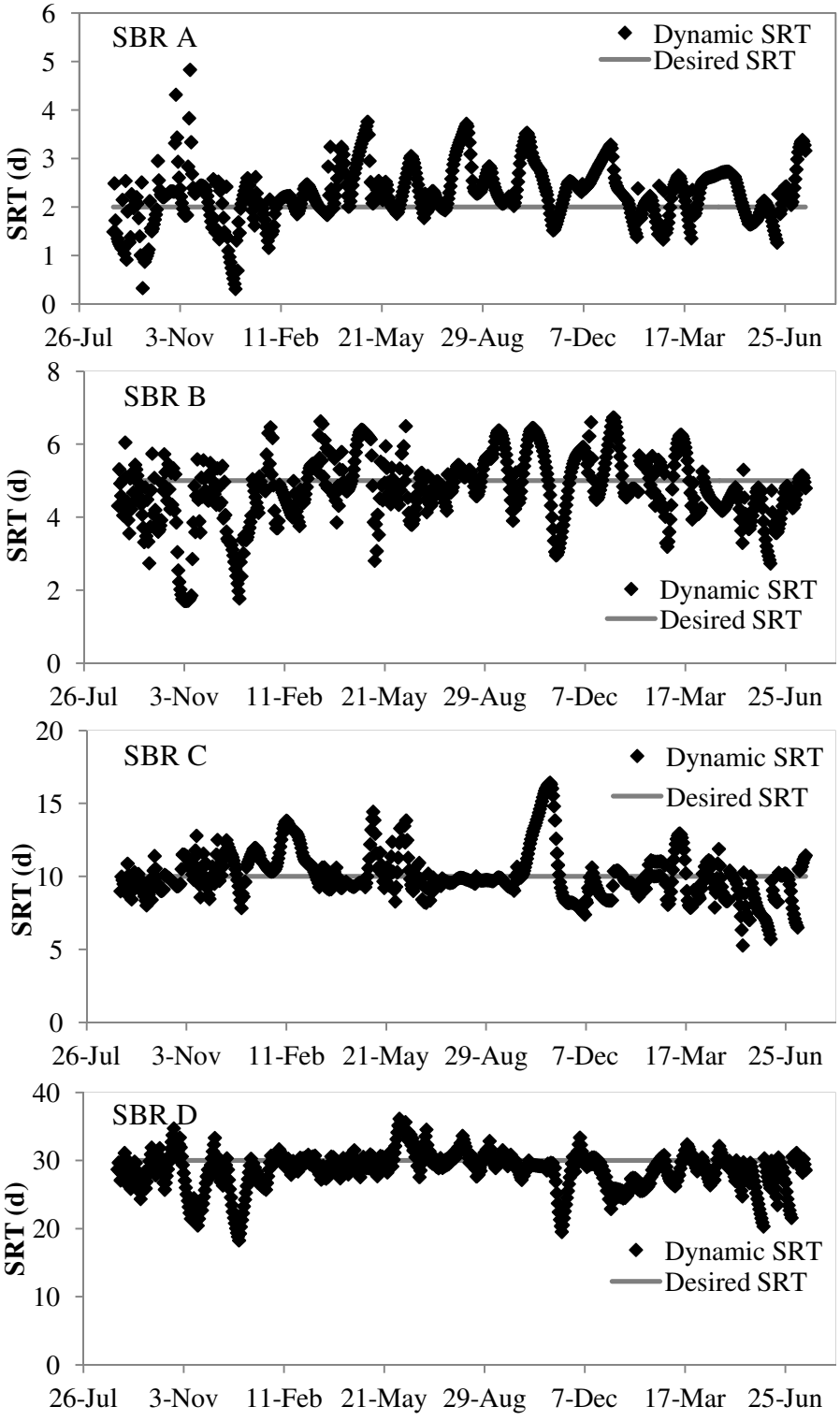

Figure A-5: SRT Profiles – Low influent P concentrations

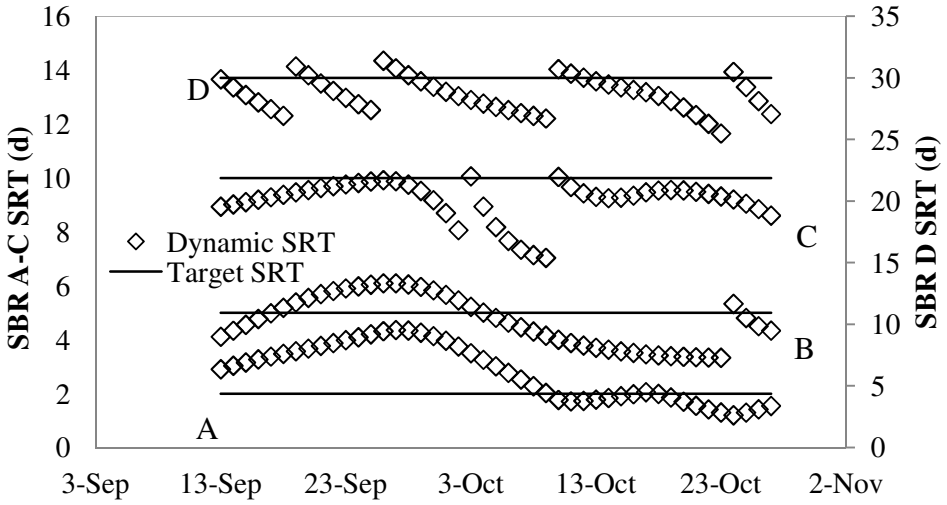

Figure A-6: SRT Profiles – High influent P concentrations

Appendix B Raw Data – Adsorption Test

Table B-1: Adsorption Test Raw Data

P Dose (mg/L)	Test Volume (L)	TSS (mg/L)	Co (mg/L)	Ce (mg/L)
FLASH				
60	0.1	29	60.02	53.31
40	0.1	28	40.26	32.72
16	0.06	34	16.02	7.78
4	0.25	25	4.01	1.17
4	0.25	25	4.01	1.16
3	0.25	20	3.21	1.23
3	0.25	20	3.21	1.28
2	0.2	42	2.78	0.83
2	0.2	42	2.78	0.91
1.6	0.25	30	1.69	0.41
1.6	0.25	30	1.69	0.42
1.6	0.25	19	2.32	0.40
1.6	0.25	19	2.32	0.44
1	0.25	34	1.20	0.13
1	0.25	34	1.20	0.13
0.5	0.25	30	0.58	0.01
0.5	0.25	30	0.58	0.02
SBR A				
64	0.06	332	64.04	54.73
64	0.1	170	64.04	44.14
60	0.1	196	60.02	43.79
40	0.1	216	40.03	36.57
16	0.1	170	16.04	9.55
16	0.06	332	16.04	5.64
4	0.25	203	4.06	0.50
4	0.25	203	4.06	0.55
2.5	0.25	272	2.56	0.44
2.5	0.25	272	2.56	0.38
1	0.5	209	1.15	0.11
1	0.5	317	1.14	0.13
1	0.5	317	1.14	0.09
0.5	0.5	283	0.61	0.04
0.5	0.5	283	0.61	0.10
0.5	0.5	249	0.56	0.09
0.5	0.5	249	0.56	0.09

Table B-1: Adsorption Test Raw Data (Continued)

P Dose (mg/L)	Test Volume (L)	TSS (mg/L)	Co (mg/L)	Ce (mg/L)
SBR B				
96	0.10	357	96.05	75.20
96	0.06	507	96.05	56.99
32	0.06	507	32.05	19.27
16	0.06	440	16.07	4.44
8	0.25	503	8.07	1.14
8	0.25	503	8.07	1.16
6	0.25	460	6.06	0.73
6	0.25	460	6.06	0.78
4	0.25	568	4.04	0.34
4	0.25	568	4.04	0.34
2	0.25	303	4.04	0.34
2	0.25	303	4.04	0.34
0.5	0.25	515	4.04	0.34
0.5	0.25	515	0.57	0.07
SBR C				
96	0.1	917	96.11	57.08
96	0.06	1033	96.11	50.86
60	0.06	897	60.09	30.31
32	0.1	917	32.11	10.68
32	0.06	1033	32.11	9.36
16	0.06	897	16.09	2.23
8	0.25	1045	8.13	0.55
8	0.25	1045	8.13	0.57
6	0.25	1055	6.11	0.45
6	0.25	1055	6.11	0.40
2	0.25	1183	2.10	0.03
2	0.25	1183	2.10	0.04
1	0.25	644	1.03	0.04
1	0.25	644	1.03	0.03
SBR D				
250	0.06	2110	250.18	140.60
96	0.06	1555	96.13	49.96
96	0.06	2155	96.11	33.25
32	0.06	1555	32.13	4.59
32	0.06	2155	32.11	0.35
12	0.2	1905	12.11	0.52
8	0.2	1673	8.18	0.53
8	0.2	1673	8.18	0.44
4	0.2	1905	4.11	0.13

Appendix C Derivation of Model Equations (Chapter 5: Equations 5-3 and 5-4)

Mass Balance

Parameters:

V= volume (L)

P = soluble P concentration (mg P/L)

q = sorbed phase concentration (mg P/mg TSS)

r = reaction rate

t = time

C_s = concentration of HFO (mg TSS/L)

k = rate constant

K = Freundlich constant

1/n = Freundlich constant

Assumptions:

1. Batch Reactors i.e. No inflow our outflow

   Therefore, Accumulation = ± Reactions or $\frac{dMass}{dt} = \frac{d(VP)}{dt} = \pm Vr$

2. reversible reaction, i.e.
   soluble P $\overset{k}{\leftrightarrow}$ sorbed P
3. constant volume

Mass Balance around soluble P concentration:

$$\frac{dP}{dt} = -kP + kP_{sorbed}$$

$$P_{sorbed} = qC_s$$

However, since Freundlich adsorption applies i.e. $q = KP^{1/n}$, then $P_{sorbed} = \left(\frac{q}{K}\right)^n$

Therefore, $\frac{dP}{dt} = -kP + k\left(\frac{q}{K}\right)^n$

Mass Balance around sorbed P concentration:

$$\frac{dP_{sorbed}}{dt} = kP - kP_{sorbed}$$

Substituting in known relationships,

$$C_s \frac{dq}{dt} = kP - k\left(\frac{q}{K}\right)^n$$

Therefore, $\frac{dq}{dt} = \frac{k}{C_s} P - \frac{k}{C_s}\left(\frac{q}{K}\right)^n$

Appendix D Batch Sorption Parameter Estimates

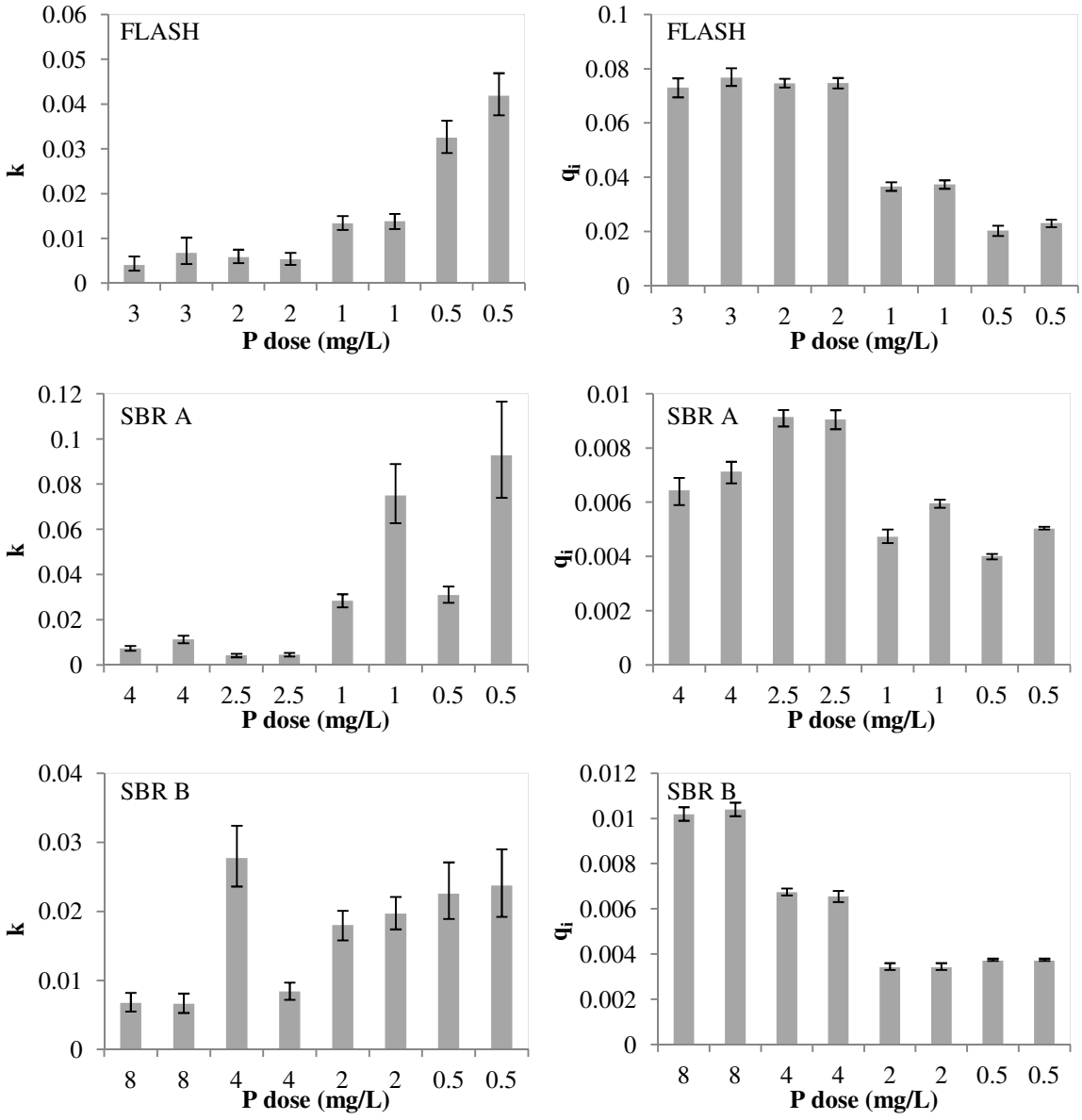

Figure D- 1: Batch sorption model parameter estimates of k and q_i. Error bars correspond to 95% confidence intervals.

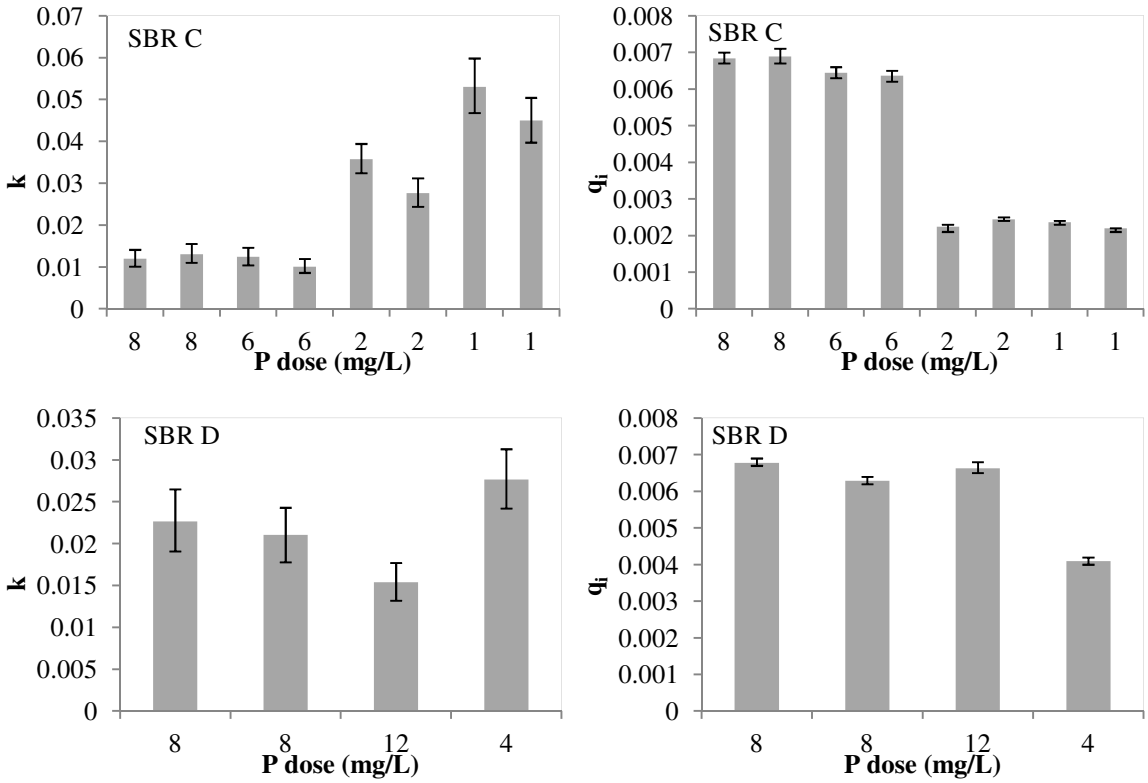

Figure D- 1: Batch sorption model parameter estimates of k and q_i. Error bars correspond to 95% confidence intervals (continued)

Appendix E Correlation Coefficients

Table E-1: Correlation coefficients for steady state and transient data

Test Condition	SBR A	SBR B	SBR C	SBR D
Steady state – low influent P (3.4 mg P/L)	0.35	0.19	0.25	0.33
Steady state – high influent P (6.4 mg P/L)	0.21	0.28	0.22	0.14
Transient – 6.4 mg P/L dose	0.24	0.27	0.35	-0.17
Transient – 16.1 mg P/L dose	-0.32	-	0.03	0.21
Transient – 82 mg P/L dose	-0.42	-0.37	-0.28	-0.14

Table E-2: Correlation coefficients for batch sorption data at various P doses

	3 mg/L	**3 mg/L**	**2 mg/L**	**2 mg/L**	**1 mg/L**	**1 mg/L**	**0.5 mg/L**	**0.5 mg/L**
Flash	-0.27	-0.32	-0.08	0.13	0.23	0.19	0.33	0.21
	4 mg/L	**4 mg/L**	**2.5 mg/L**	**2.5 mg/L**	**1 mg/L**	**1 mg/L**	**0.5 mg/L**	**0.5 mg/L**
SBR A	-0.07	-0.14	0.33	0.39	0.15	0.27	0.25	0.18
	8 mg/L	**8 mg/L**	**4 mg/L**	**4 mg/L**	**2 mg/L**	**2 mg/L**	**0.5 mg/L**	**0.5 mg/L**
SBR B	0.13	0.18	0.12	0.36	0.19	0.14	0.22	0.28
	8 mg/L	**8 mg/L**	**6 mg/L**	**6 mg/L**	**2 mg/L**	**2 mg/L**	**1 mg/L**	**1 mg/L**
SBR C	0.21	0.22	0.35	0.42	0.26	0.27	0.15	0.18
	8 mg/L	**8 mg/L**	**12 mg/L**	**4 mg/L**				
SBR D	0.24	0.19	0.26	0.28				